Microstructure, Mechanical, and Tribological Evaluation of Carbide-Based Wear-Resistant Coatings for Aerospace Applications

Oluwadamilola Ogunmola

A Thesis
In the Department
of
Chemical and Materials Engineering

Presented in Partial Fulfilment of the
Requirements for the Degree of
Master of Applied Science (MASc.), Chemical Engineering

at

Concordia University
Montréal, Québec, Canada

December 2024

CONCORDIA UNIVERSITY

School of Graduate Studies

This is to certify that the thesis prepared

By: **Oluwadamilola Ogunmola**

Entitled: **Microstructure, mechanical, and tribological evaluation of carbide-based wear-resistant coatings for aerospace applications**

and submitted in partial fulfillment of the requirements for the degree of

Master of Applied Science (Chemical Engineering)

complies with the regulations of the University and meets the accepted standard with respect to originality and quality.

Signed by the final examining committee:

____Chair
Dr. Sixu Deng

____Examiner
Dr. Moussa Tembely

____Supervisor
Dr. Christian Moreau

____Supervisor
Dr. Pantcho Stoyanov

Approved by____
Alex De Visscher, Chair
Department of Chemical and Materials Engineering

December, 2024 ____
Mourad Debbabi, Dean
Gina Cody School of Engineering and Computer Science

Abstract

Microstructure, mechanical, and tribological evaluation of carbide-based wear-resistant coatings for aerospace applications

Oluwadamilola Ogunmola

Thermally sprayed tribological coatings are extensively employed in aerospace applications to address critical issues including corrosion, erosion, oxidation, abrasive wear, and fatigue under different service conditions. Besides addressing these difficulties, these coatings are essential for improving the efficiency of gas turbine engines, thereby decreasing fuel consumption and emissions.

High Velocity Air-Fuel (HVAF) thermal spraying has become a promising method for producing carbide-based tribological coatings, offering significant advantages over other techniques such as Air Plasma Spray (APS) process. Its higher particle velocity and lower flame temperature result in denser coatings with reduced oxide content and enhanced hardness. These properties make HVAF an ideal method for developing advanced coatings that can effectively resist surface degradation caused by wear, corrosion, and erosion, even under extreme temperatures.

The objective of our research work is to investigate the tribological properties of thermally sprayed carbide-based coatings deposited by plasma spray and high velocity air fuel deposition processes. This work consists of two research studies, the first emphasize the influence of deposition processes (i.e., APS and HVAF) and binder content (i.e., pure carbide and cemented carbide) on the microstructural, mechanical, and tribological behavior of chromium carbide-based coatings at room temperature and 450 °C. The second study is a preliminary work that evaluates the microstructure of pure silicon carbide coatings deposited by suspension plasma spraying process.

The tribological test was performed using a ball-on-flat tribometer and the wear profiles were obtained using a laser confocal microscope. The *Ex-situ* characterization of the as-deposited coatings were performed using scanning electron microscopy (SEM), energy dispersive spectroscopy (EDS), X-ray diffraction (XRD), image analysis, and the Vickers microhardness test was performed on the cross-sections of the coatings at room temperature. The HVAF sprayed Cr_3C_2-25NiCr coating deposited with the 4L4 nozzle exhibits the lowest friction and improved wear resistance compared to all the tested APS coatings at room temperature and 450°C. Moreover, the second study has demonstrated that pure SiC coatings can be produced using suspension plasma spray (SPS) process and open pathway for future development of ceramic materials which are prone to decomposition.

Acknowledgement

My heartfelt and unfeigned gratitude to God Almighty, my creator and my source of inspiration. Who gave me the profound grace to start and finish well despite the numerous challenges faced, Amen.

I would like to express my deepest appreciation to my supervisors, Dr. Pantcho Stoyanov and Dr. Christian Moreau, for granting me the opportunity to work under their tutelage. The success of this project is a direct result of their unwavering support, expert guidance, and inspiring mentorship. I am also sincerely thankful to Dr. Ali Dolatabadi, Dr. Richard R. Chromik, Dr. Amit Roy, Dr. Fadhel Ben Ettouil, Dr. Bruno de Castilho, and Dr. Alejandra I. Encalada for their valuable collaborations, insightful feedback, and mentorship throughout the course of this research.

A special thanks goes to the members of the Thermal Spray Laboratory research group for their expertise and support during my experiments. I am also grateful for the technical assistance provided by Dr. Dmytro Kevorkov, which was integral to the success of the experimental work. Additionally, I extend my appreciation to Concordia University for offering the platform and resources that enabled me to carry out this research effectively.

The authors thankfully acknowledge the financial support provided by the Natural Sciences and Engineering Research Council of Canada (NSERC) through the Alliance Grants program (ALLRP 571542 - 21) and by the Fonds de recherche du Québec – Nature et technologies (FRQNT) under the NOVA program.

Finally, I would like to express my heartfelt thanks to my wife, parents, and siblings for their constant encouragement and support during my academic journey.

Contribution of Authors

This thesis consists of one manuscript currently under review, while the other manuscript is ready for submission. I am the principal author of both, with my supervisors, Dr. Pantcho Stoyanov and Dr. Christian Moreau, serving as co-authors in collaboration with others. As the principal author, I was responsible for the experimental work and technical report writing, while my supervisors provided valuable analytical insights and guidance throughout the project. I also wish to recognize the efforts of the co-authors involved in the development of these article manuscripts:

- Chapter 3: **Oluwadamilola Ogunmola**, Amit Roy, Ben Ettouil F, Alejandra I. Encalada, Richard R. Chromik, Ali Dolatabadi, Christian Moreau, Pantcho Stoyanov. Microstructural, mechanical, and tribological evaluation of chromium carbide-based coatings deposited by APS and HVAF processes.

Oluwadamilola Ogunmola conducted in-depth literature review, developing the conceptual framework, designing the methodology, carrying out the experiments, performing the analysis, drafting the original manuscript, and revising the final version. Ben Ettouil F. contributed to optimizing the spraying parameters and depositing the coatings. Richard Chromik and Alejandra I. Encalada handled the Raman testing and SEM analysis. Amit Roy provided a critical review of the manuscript and addressed the issues in the original draft. Ali Dolatabadi, Christian Moreau, and Pantcho Stoyanov contributed to the conceptualization, provided guidance, helped interpret the results, and reviewed the manuscript.

- Chapter 4: **Oluwadamilola Ogunmola**, Amit Roy, Bruno. de Castilho, Ben Ettouil F, Pantcho Stoyanov, Christian Moreau, Suspension plasma spraying of pure silicon carbide coatings.

Oluwadamilola Ogunmola conducted in-depth literature review, developing the conceptual framework, designing the methodology, carrying out the experiments, performing the analysis, drafting the original manuscript, and revising the final version. Ben Ettouil F. contributed to optimizing the spraying parameters and depositing the coatings. Bruno de Castilho handled the Raman test and SEM analysis. Amit Roy provided a critical review of the manuscript and addressing the issues in the original draft. Pantcho Stoyanov and Christian Moreau contributed to the conceptualization, provided guidance, helped interpret the results, and reviewed the manuscript.

Table of Contents

List of Figures

List of Tables

Abbreviations

APS – Atmospheric Plasma Spraying

CVD – Chemical Vapor Deposition

COF – Coefficient of Friction

EDS – Electron Dispersive Spectroscopy

HVAF – High Velocity Air Fuel

HVOF – High Velocity Oxygen Fuel

HVOLF – High Velocity Oxygen Liquid-Fuel

HP – High Power

LP – Low Power

PVD – Physical Vapor Deposition

SPS - Suspension Plasma Spraying

SEM – Scanning Electron Microscopy

XRD – X-ray Diffraction

Organization of Thesis

I. Chapter 1 presents the introduction along with the motivation and scope of the thesis.

II. Chapter 2 presents background information on the concepts of tribology and thermal spray processes. Additionally, the existing literature review on tribological coatings with emphasis on chromium and silicon carbide-based coatings were discussed in detail.

III. Chapter 3 presents the comparative study of chromium carbide coatings: microstructural, mechanical and tribological properties using APS and HVAF processes

IV. Chapter 4 presents the suspension plasma spraying of pure silicon carbide coatings.

V. Chapter 5 highlights the overall conclusions and the future work on thermally sprayed carbide-based coatings.

Chapter

1. INTRODUCTION & SCOPE

In this chapter…

*The motivation and brief introduction to the thesis is presented with its objectives***.**

1.1 Introduction

Engineering machines such as gas turbine engines are used in numerous industries including aviation, power generation, and marine applications for generating power in large-scale quantity [1]. In the aviation industry, several components of the jet engine including compressor, combustion system, turbine, and exhaust work in synergy to convert fuel chemical energy into kinetic energy that are later utilized for generation of thrust to drive modern commercial aircraft [2]–[4]. Basically, the air introduced into the system is transformed into compressed air by the compressor and thereafter transferred to the combustion chamber at a speed of 160 km/h where it is heated together with fuel at a temperature of 1300 °C to form a pressurized gas. The gas is expanded and converted into rotational kinetic energy to drive the turbine blades [1].

Recently, gas turbines have been increasingly employed across three main categories, including peak load (with less than 10% utilization), base load (approaching 100% utilization), and intermediate load operations [5]. The utilization of jet engines is projected to rise in the coming years [6]. However, the aerospace industry is constantly faced with challenges related to the risk of jet engine failures, which severely impact the service life, safety, and cost associated with component replacement [7]. The frequent start-stop cycles under base load conditions lead to substantial relative motion between interacting components, resulting in wear issues [2]. Specifically, components such as combustion liner, transition piece, turbine blade, and turbine ring experience continual friction due to constant interfacial contact during operation [8]. The interaction results in high contact pressure and rise in temperature which lead to fretting wear. The fretting wear induces significant fretting damage such as crack initiation as well as interfacial degradation to the component which affects the safety, economy, and service life [9]. Furthermore, the relative motion between the interacting surfaces at elevated temperatures results in considerable material degradation due to friction and wear [10]. While hot-section components are exposed to extreme temperatures ranging from 1000 °C to 1300 °C, frictional contact or external heat sources are the main causes of temperature rise in the cold section of the gas turbine engines. The temperature rise alters the mechanical properties of critical components, leading to decreased abrasion resistance [11]. Other challenges faced are constant demand for sustainable solutions to CO_2 emissions, noise, maintenance costs, and operational safety [7]. Therefore, efforts to improve the efficiency, reliability, and longevity of gas turbine components will be a key objectives for the aviation industry as demand for more sustainable and cost-effective power generation solutions grows [6].

Surface engineering is an established technology for protecting and extending the lifespan of engineering components used in nuclear power plants, automobiles, offshore structures, and aerospace industries [12]–[18]. Moreover, this technology makes it possible to improve the mechanical properties, corrosion and wear resistance of metallic components that are susceptible to surface degradation when subjected to aggressive service conditions [14]. Generally, friction and wear are renowned mechanisms that lead to the degradation of engineering components, thereby limiting their durability and overall performance [19]. Tribological coatings are utilized to mitigate the damage posed by friction and wear mechanisms [20], [21]. An ideal tribological coating possess good adhesion properties with the base metal, high hardness and toughness, thermal stability and sufficient shear strength to resist contact pressures [22]. In the aerospace industry, coatings are applied to improve the performance and extend lifetime of gas turbine engine components such as gears, blade, bearings, dynamic seals and static seals [23]. Soft coatings such as copper and nickel of hardness less than 10 GPa provides resistance against friction occurring at the sliding interface which contribute to undesirable subsurface cracking and subsequent wear damage, while hard coatings such as carbide, oxides, nitrides, and diamonds possess hardness above 10 GPa and offer resistances against abrasion, erosion, and impact wear prevents ploughing of materials both on a macro and micro scale [22], [24].

Several deposition methods such as vapor deposition (physical and chemical), electrodeposition processes and thermal spraying, etc. are used for fabrication of tribological coatings that can be tailored towards a specific application [25]. Electrodeposition techniques such as electroless and electrophoretic process are the most economical process. However, the process is not environment friendly due to release of highly toxic by-products [26]. While PVD offers superior coating properties, the high-vacuum environment requirements lead to operational complexity and high cost. This requirement can also compromise the size and shape of parts that can be coated. Moreover, PVD process has low deposition rate resulting low coating thickness and longer processing time. Chemical vapor deposition offers moderate equipment cost and higher deposition rate compared to PVD, making it more suitable for applications requiring thicker coatings in less time. However, the precursor gas mixture and the required maintenance such as cleaning and neutralization of the output gases increases the overall cost of the process [27]. Thermal spray techniques have significantly expanded the range of surface modification and coating technologies available today. This method has evolved into a reliable and cost-effective solution for depositing thick coatings across a wide variety of feedstock materials and substrates. In the aerospace industry, thermal spray coatings have proven to be indispensable, playing a crucial role in modern manufacturing and maintenance processes [28]. Numerous techniques exist for the development of tribological coatings, researchers and engineers are currently exploring innovative approaches to enhance their performance and versatility.

Carbide-based coatings are currently used in aerospace applications as protective materials to prevent the degradation of critical components within the gas turbine. These coatings are applied to turbine blades, vanes, and other components in jet engines to protect them from wear caused by high-speed particles and corrosive environments [29]. Furthermore, the coatings subsequently extend the lifetime of the coated components while significantly reducing maintenance cost. Carbide-based coatings provide better wear, erosion, and corrosion resistance than other coating materials such oxide-based or nitride-based materials [30]. Generally, thermally sprayed tungsten carbide-based coatings are usually the most preferred and widely used wear resistant coatings for gas turbine components due to its attractive properties such as high hardness, high wear resistance and fracture toughness, high elasticity, chemical inertness and low friction making them suitable for anti-wear applications [7]. These hard particles are sprayed as cermet by co-deposition with binders such as Cr, Ni or Co. The binder phase provides the required toughness, while the hard WC particles phase improved the wear resistant property [31], [32]. WC-Co coatings has been employed for repair of gas turbine shafts, aircraft landing gear and certain jet engine components [33]. However, the use of tungsten carbide-based coatings at high temperatures above 500 ºC is limited due to low oxidation resistance of the hard WC particles [31]. This is why their application is limited in high-temperature environments. Thus, there is need for the development of viable alternatives that can reduce the overall wear rate of critical components of gas turbine engines and operate efficiently under extreme conditions.

Chromium carbide-based coatings are gradually emerging as a better alternative to replace tungsten carbide-based coatings for wear resistance application due to their high hardness and excellent tribological properties in harsh environments [34]. Chromium carbide-based coating offers an improved erosion, corrosion and oxidation resistance making them suitable for use at elevated temperatures up to 900°C [35]. Recent research has shown that Cr_3C_2-based coatings with nickel chromium (NiCr) as metal matrix binder offer high corrosion and oxidation resistance [36], low friction coefficient and better wear resistance than thermally sprayed WC-Co coatings [37], [38]. Additionally, the coefficient of thermal expansion of chromium carbide-based coatings (10.3×10^{-6} °C^{-1}) is close to that of steel (11.4×10^{-6} °C^{-1}) and nickel (12.8×10^{-6} °C^{-1}) that makes up the base of high temperature alloys [39]. This minimizes stress generated by thermal expansion mismatch during thermal cycling [40]. Since the demand for chromium carbide-based coatings for extreme environment is increasing exponentially, the potential benefits of thermally sprayed chromium carbide-based coatings can help address numerous challenges associated with wear of critical components in jet engines [30].

Silicon carbide (SiC) is a highly promising candidate for high temperature structural applications due to its outstanding properties, including high strength, hardness, thermal conductivity, abrasion resistance, chemical stability, and oxidation resistance [41]–[43]. The ceramic coating offer exceptional tribological characteristics and have been utilized to enhance the wear resistance and durability of aerospace moving components such as gas turbine blades, seals, and turbocharger rotors in extreme environments [43], [44]. SiC coatings have been fabricated by traditional methods such as physical or chemical vapor deposition [45], magnetron sputtering [46], and laser-assisted deposition [47]. However, studies have demonstrated that thermal spray methods like suspension plasma spray (SPS) [48], and suspension high-velocity oxy-fuel (S-HVOF) [44], are more cost-effective routes for producing dense SiC-based coatings with high deposition rates. Ultimately, the choice of method used to deposit carbide-based coatings depends on the specific application requirements, including the thickness and properties of the coating, base material considerations, and equipment availability.

1.2 Thesis objectives

The main objective of this research work is to develop the next generation thermally sprayed carbide-based coatings that can operate effectively over long periods of time and consequently, improving tribological performance in harsh environments. The following sub-objectives have been identified for this thesis:

- Examine the effect of deposition processes, spray parameters, and binder content on the microstructure of the carbide-based coatings.
- Evaluate the friction and wear resistance performance of carbide-based coatings at room and elevated temperatures.
- Perform analysis of the worn surfaces to interpret the interfacial processes of carbide-based coatings in various environments.
- Provide recommendations to the aerospace research community regarding the design strategy for development of carbide-based coatings.

References

[1] B. Zohuri and P. McDaniel, “Gas Turbine Working Principals,” in *Combined Cycle Driven Efficiency for Next Generation Nuclear Power Plants: An Innovative Design Approach*, Cham: Springer International Publishing, pp. 149–174, 2018.

[2] W. A. Sirignano and F. Liu, “Performance Increases for Gas-Turbine Engines Through Combustion Inside the Turbine,” *J. Propuls. Power*, vol. 15, pp. 111–118, 1999, https://api.semanticscholar.org/CorpusID:120555434.

[3] A. Poullikkas, “An overview of current and future sustainable gas turbine technologies,” *Renew. Sustain. Energy Rev.*, vol. 9, no. 5, pp. 409–443, 2005, doi: https://doi.org/10.1016/j.rser.2004.05.009.

[4] M. T. Schobeiri, “Introduction, Gas Turbines, Applications, Types,” in *Gas Turbine Design, Components and System Design Integration: Second Revised and Enhanced Edition*, Cham: Springer International Publishing, 2019, pp. 1–32.

[5] P. A. Pilavachi, “Power generation with gas turbine systems and combined heat and power,” *Appl. Therm. Eng.*, vol. 20, no. 15, pp. 1421–1429, 2000, doi: https://doi.org/10.1016/S1359-4311(00)00016-8.

[6] I. I. Enagi, K. A. Al-attab, and Z. A. Zainal, “Liquid biofuels utilization for gas turbines: A review,” *Renew. Sustain. Energy Rev.*, vol. 90, pp. 43–55, 2018, doi: https://doi.org/10.1016/j.rser.2018.03.006.

[7] D. Dzhurinskiy, A. Babu, P. Pathak, A. Elkin, S. Dautov, and P. Shornikov, “Microstructure and wear properties of atmospheric plasma-sprayed Cr3C2-NiCr composite coatings,” *Surf. Coatings Technol.*, vol. 428, p. 127904, 2021, doi: https://doi.org/10.1016/j.surfcoat.2021.127904.

[8] H. L. Bernstein, “Materials Issues For Users Of Gas Turbines.,” 1998. https://api.semanticscholar.org/CorpusID:17100621.

[9] M. Lavella, “Contact Properties and Wear Behaviour of Nickel Based Superalloy René 80,” *Metals (Basel).*, vol. 6, no. 7, 2016, doi: 10.3390/met6070159.

[10] I. M. Allam, “Solid lubricants for applications at elevated temperatures,” *J. Mater. Sci.*, vol. 26, no. 15, pp. 3977–3984, 1991, doi: 10.1007/BF00553478.

[11] P. J. Blau, “Elevated-temperature tribology of metallic materials,” *Tribol. Int.*, vol. 43, no. 7, pp. 1203–1208, 2010, doi: https://doi.org/10.1016/j.triboint.2010.01.003.

[12] F. Rubino, D. Merino, A. T. Silvestri, C. Munez, and P. Poza, “Mechanical properties optimization of Cr3C2-NiCr coatings produced by compact plasma spray process,” *Surf. Coatings Technol.*, vol. 465, p. 129570, 2023, doi: https://doi.org/10.1016/j.surfcoat.2023.129570.

[13] T. Burakowski and T. Wierzchon, *Surface Engineering of Metals*. CRC Press, 1998.

[14] M. Ramezani, Z. Ripin, T. Pasang, and C.-P. Jiang, “Surface Engineering of Metals: Techniques, Characterizations and Applications,” *Metals (Basel).*, vol. 13, p. 1299, 2023, doi: 10.3390/met13071299.

[15] J. R. Davis, “Surface Engineering for Corrosion and Wear Resistance,” 2001.

https://api.semanticscholar.org/CorpusID:106545388.

[16] G. Shi *et al.*, “Effect of surface modification on friction characteristics of sliding bearings: A review,” *Tribol. Int.*, vol. 177, p. 107937, 2023, doi: https://doi.org/10.1016/j.triboint.2022.107937.

[17] J. S. Burnell-Gray and P. K. Datta, *Surface Engineering Casebook: Solutions to Corrosion and Wear-Related Failures*. Elsevier Science, 1996.

[18] T. Bell, H. Dong, and Y. Sun, “Realising the potential of duplex surface engineering,” *Tribol. Int.*, vol. 31, no. 1, pp. 127–137, 1998, doi: https://doi.org/10.1016/S0301-679X(98)00015-2.

[19] B. Bhushan, *Introduction to tribology–Second edition*. John Wiley & Sons, Ltd, 2013.

[20] S. Rao, S. Kumar, M. Palle, and P. Sriharsha, “A critical review on surface coatings for engineering materials,” *IJMET*, vol. 7, pp. 80–85, 2016.

[21] S. Amin, H. Panchal, and A. Professor, “A Review on Thermal Spray Coating Processes,” *Int. J. Curr. Trends Eng. Res. Sci. J. Impact Factor*, vol. 2, no. 4, pp. 556–563, 2016.

[22] S. Jakovljević and D. Landek, “Special Issue: Tribological Coatings—Properties, Mechanisms, and Applications in Surface Engineering,” *Coatings*, vol. 13, no. 2, 2023, doi: 10.3390/coatings13020451.

[23] K. Holmberg, A. Matthews, and H. Ronkainen, “Coatings tribology - Contact mechanisms and surface design,” *Tribol. Int.*, vol. 31, no. 1–3, pp. 107–120, 1998, doi: 10.1016/S0301-679X(98)00013-9.

[24] K. Holmberg, H. Ronkainen, and A. Matthews, “Tribology of thin coatings,” *Ceram. Int.*, vol. 26, no. 7, pp. 787–795, 2000, doi: 10.1016/S0272-8842(00)00015-8.

[25] K. G. Budinski, *Surface engineering for wear resistance*, no. October. Prentice Hall, 2007.

[26] M. I. Boulos, P. L. Fauchais, and J. V. R. Heberlein, “Fundamentals of Combustion and Thermal Plasmas,” in *Thermal Spray Fundamentals: From Powder to Part*, Cham: Springer International Publishing, 2021, pp. 57–83.

[27] J. D. Majumdar, “Thermal and Cold Spraying Technology in Manufacturing,” in *Handbook of Manufacturing Engineering and Technology*, A. Nee, Ed. London: Springer London, 2013, pp. 1–37.

[28] J. R.C. Tucker, “Introduction to Coating Design and Processing,” *ASM Handbook, Therm. Spray Technol.*, vol. 5A, 2013.

[29] A. Pauzi, M. Ghazali, W. F. H. W Zamri, and A. Rajabi, “Wear Characteristics of Superalloy and Hardface Coatings in Gas Turbine Applications-A Review,” *Metal*, vol. 10, pp. 2–14, 2020, doi: 10.3390/met10091171.

[30] A. R. Govande, A. Chandak, B. R. Sunil, and R. Dumpala, “Carbide-based thermal spray coatings: A review on performance characteristics and post-treatment,” *Int. J. Refract. Met. Hard Mater.*, vol. 103, p. 105772, 2022, doi: https://doi.org/10.1016/j.ijrmhm.2021.105772.

[31] V. B. Voitovich, V. V Sverdel, R. F. Voitovich, and E. I. Golovko, “Oxidation of WC-Co, WC-Ni and WC-Co-Ni hard metals in the temperature range 500–800 °C,” *Int. J. Refract. Met. Hard Mater.*, vol. 14, no. 4, pp. 289–295, 1996, doi: https://doi.org/10.1016/0263-4368(96)00009-1.

[32] Q. Yang, T. Senda, and A. Ohmori, “Effect of carbide grain size on microstructure and sliding wear behavior of HVOF-sprayed WC–12% Co coatings,” *Wear*, vol. 254, no. 1, pp. 23–34, 2003, doi: https://doi.org/10.1016/S0043-1648(02)00294-6.

[33] M. Jafari, M. H. Enayati, M. Salehi, S. M. Nahvi, and C. G. Park, “Microstructural and mechanical characterizations of a novel HVOF-sprayed WC-Co coating deposited from electroless Ni–P coated WC-12Co powders,” *Mater. Sci. Eng. A*, vol. 578, pp. 46–53, 2013, doi: https://doi.org/10.1016/j.msea.2013.04.064.

[34] L. Pawlowski, *The Science and Engineering of Thermal Spray Coatings: Second Edition*. John Wiley & Sons, New York, 2008.

[35] E. Gariboldi, L. Rovatti, N. Lecis, L. Mondora, and G. A. Mondora, “Tribological and mechanical behaviour of Cr3C2–NiCr thermally sprayed coatings after prolonged aging,” *Surf. Coatings Technol.*, vol. 305, pp. 83–92, 2016, doi: https://doi.org/10.1016/j.surfcoat.2016.07.087.

[36] N. Vashishtha, R. K. Khatirkar, and S. G. Sapate, “Tribological behaviour of HVOF sprayed WC-12Co, WC-10Co-4Cr and Cr3C2−25NiCr coatings,” *Tribol. Int.*, vol. 105, pp. 55–68, 2017.

[37] R. Gopi, I. Saravanan, A. Devaraju, and P. Ponnusamy, “Tribological behaviour of thermal sprayed high velocity oxy-fuel coatings on tungsten carbide – A review,” *Mater. Today Proc.*, 2020, [Online]. Available: https://api.semanticscholar.org/CorpusID:225450545.

[38] S. Mahade, A. Mulone, S. Björklund, U. Klement, and S. V Joshi, “Investigating Load-dependent Wear Behavior and Degradation Mechanisms in Cr3C2-NiCr coatings deposited by HVAF and HVOF,” *J. Mater. Res. Technol.*, 2021, https://api.semanticscholar.org/CorpusID:239953533.

[39] V. Matikainen, H. Koivuluoto, and P. Vuoristo, “A study of Cr3C2-based HVOF- and HVAF-sprayed coatings: Abrasion, dry particle erosion and cavitation erosion resistance,” *Wear*, vol. 446–447, p. 203188, 2020, doi: https://doi.org/10.1016/j.wear.2020.203188.

[40] S. Chatha, H. Sidhu, and B. Sidhu, “Characterisation and Corrosion-Erosion Behaviour of Carbide based Thermal Spray Coatings,” *J. Miner. Mater. Charact. Eng.*, vol. 11, 2012, doi: 10.4236/jmmce.2012.116041.

[41] F. Mubarok and N. Espallargas, “Tribological behaviour of thermally sprayed silicon carbide coatings,” *Tribol. Int.*, vol. 85, 2015, doi: 10.1016/j.triboint.2014.11.027.

[42] F. Mubarok and N. Espallargas, “Suspension Plasma Spraying of Sub-micron Silicon Carbide Composite Coatings,” *J. Therm. Spray Technol.*, vol. 24, 2015, doi: 10.1007/s11666-015-0242-2.

[43] J. Mukherjee, S. Chakraborty, S. Chakravarty, A. Ranjan, and P. K. Das, “Mechanical and tribological properties of silicon carbide coating on Inconel alloy from liquid pre-ceramic precursor,” *Ceram. Int.*, vol. 40, no. 5, pp. 6639–6645, 2014, doi: https://doi.org/10.1016/j.ceramint.2013.11.121.

[44] H. Memon, A. Rincón Romero, K. Derelizade, F. Venturi, and T. Hussain, “A new hybrid suspension and solution precursor thermal spray for wear-resistant silicon carbide composite coatings,” *Mater. Des.*, vol. 224, p. 111382, 2022, doi: https://doi.org/10.1016/j.matdes.2022.111382.

[45] M. Soković *et al.*, “Cutting properties of the Al2O3+SiC(w) based tool ceramic reinforced with the PVD and CVD wear resistant coatings,” *J. Mater. Process. Technol.*, vol. 164–165, pp. 924–929, 2005, doi: https://doi.org/10.1016/j.jmatprotec.2005.02.071.

[46] M. Liu *et al.*, “Influence of radio frequency magnetron sputtering parameters on the structure and performance of SiC films,” *Ceram. Int.*, vol. 47, no. 17, pp. 24098–24105, 2021, doi: https://doi.org/10.1016/j.ceramint.2021.05.120.

[47] M. Das, V. K. Balla, D. Basu, S. Bose, and A. Bandyopadhyay, “Laser processing of SiC-particle-reinforced coating on titanium,” *Scr. Mater.*, vol. 63, no. 4, pp. 438–441, 2010, doi: https://doi.org/10.1016/j.scriptamat.2010.04.044.

[48] A. Rincón, Z. Pala, and T. Hussain, “A suspension high velocity oxy-fuel thermal spray manufacturing route for silicon carbide – YAG composite coatings,” *Mater. Lett.*, vol. 281, p. 128601, 2020, doi: https://doi.org/10.1016/j.matlet.2020.128601.

[49] B. N. T. Persson, “History of Tribology,” in *Encyclopedia of Lubricants and Lubrication*, T. Mang, Ed. Berlin, Heidelberg: Springer Berlin Heidelberg, 2014, pp. 791–797.

[50] J. Echávarri, E. de la Guerra, and E. Chacón, “Tribology: A Historical Overview of the Relation Between Theory and Application,” in *A Bridge between Conceptual Frameworks: Sciences, Society and Technology Studies*, R. Pisano, Ed. Dordrecht: Springer Netherlands, 2015, pp. 135–154.

Chapter

2. BASIC CONCEPTS & BACKGROUND

In this chapter…

A brief introduction to the concept of tribology including friction, wear and lubrication were discussed. Also, different types of thermal spraying techniques widely used for depositing tribological coatings have been presented.

2.1 Brief History of Tribology

The term tribology stems from the Greek word "tribos," indicating rubbing or attrition. Tribology was established in 1966 by the British tribologist Peter Jost [1]. It was subsequently defined in 1967 by a committee of the Organization for Economic Cooperation and Development (OECD) in the United Kingdom [2]. The committee made an estimate of the revenues that could be generated by the industry if tribological principles are applied in their operations. Tribology deals with the science and technology of mating surfaces in relative motion. Figure 2.1 illustrates the three main concepts of tribology which include friction, wear and lubrication. During interaction, forces are conveyed, mechanical energy is transformed, and both the physical and chemical properties, including the surface topography of the interacting components, are modified. The impact of surface interactions governs friction, wear, and lubrication characteristics [3].

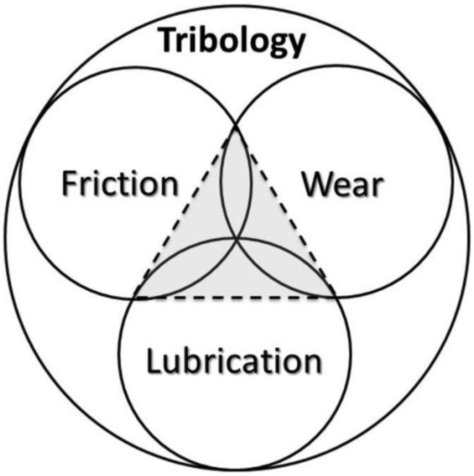

Figure 2.1 Schematic of tribological triangle [4].

Tribology has gained recognition and significant progress in various industries, including aerospace, automotive, and manufacturing [5]. The design of machines may utilize existing knowledge of tribology to enhance their performance and durability [6]. Nowadays, tribologists utilize advanced techniques such as microscopy and modeling to examine the behavior of engineering materials under different operating conditions [2]. Understanding the complex relationships existing between materials, lubricants, and machine operating conditions is essential for minimizing friction and preventing failures associated with tribological phenomena [6]. The objective of tribology research is to minimize losses resulting from friction and wear at all levels of technology and enhance machine efficiency, improve performance, and save maintenance costs. Thus, tribology research will continually evolve as scientists seek innovative methods to enhance machine performance and minimize material wear and friction [7].

2.1.2 Friction

Friction is described as a force that resist the motion of interacting surfaces in contact, and it occurs in the regions adjacent to and between solid surfaces [8]. Moreover, when surfaces in contact move relative to each other, the resulting friction between the interacting surfaces converts kinetic energy into thermal energy. Friction is an important aspect of human life. For instance, friction is required for walking without slipping or falling, between tires and roads, and between mechanical parts that are bolted together. However, friction is undesirable for most industrial machines because it causes energy loss, leading to degradation of the interacting components and reduces the overall efficiency of the machine [9]. Basically, there are two forms of friction which are static and kinetic friction. Static friction opposes the onset of relative motion, while kinetic opposes the continuance of relative motion that was initiated. The coefficient of static friction μs, is usually higher than the coefficient of kinetic friction, μk. However, both static and kinetic COFs depend on a pair of surfaces in contact [10]. According to Fig. 2.2, a tangential force, F_T, is required to initiate the relative motion between two bodies kept in close contact by a normal force F_N. Such force is referred to as friction force which is required to overcome the static friction force, F_f, opposing the motion. The ratio $F_T/F_N = \mu s$ is the coefficient of static friction. However, to maintain the motion of two bodies moving at a given sliding speed, a tangential force is required to counteract the kinetic friction force. In this case, the ratio $F_T/F_N = \mu k$ is the coefficient of kinetic (or dynamic) friction [11].

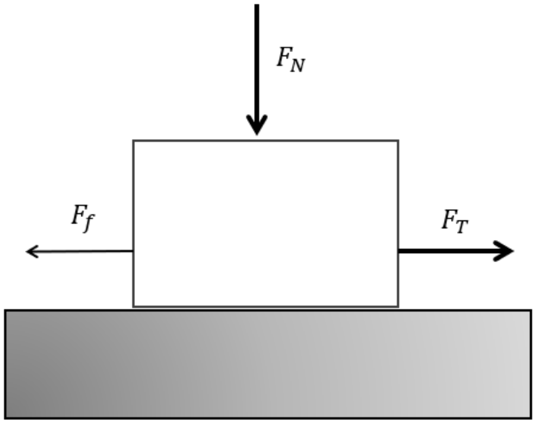

Figure 2.2 Schematics diagram of the forces required to move two bodies in contact, with relevant definition of coefficients of static and kinetic friction adapted from [11].

On the other hand, friction takes place due to energy dissipation at the interface, and may occur by material deformation, asperity interactions, fracture, viscous fluid flow, and interatomic interactions. [12]. Figure 2.3 illustrates different interfacial phenomena that frequently occur in frictional systems.

The friction in two-body abrasion is usually high due to the plowing effect of hard asperities against softer counterparts. In contrast, friction between smooth surfaces is generally lower unless significant adhesion takes place between the interacting pairs, or when the surfaces are roughened by wear. Friction involving third bodies is usually more complex because friction occurs both within the particle layer and at the sliding interfaces. Density gradients and pores may develop in these layers, and their shear strength varies non-linearly with density. In rolling contact and lubricated surfaces, friction is influenced by how fluid is driven towards the sliding interface, the roughness of the mating surface, and the Λ-ratio, which is the ratio of film thickness to the composite surface roughness [11].

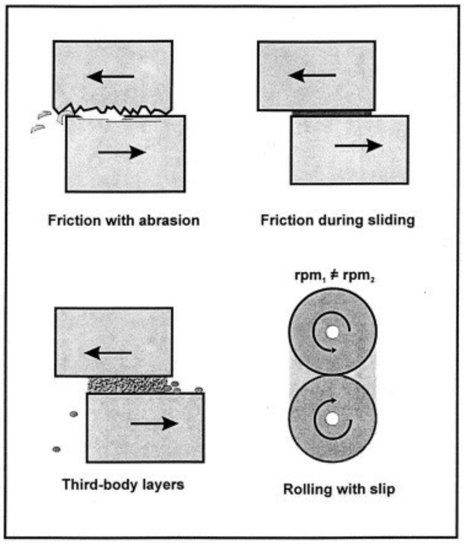

Figure 2.3 Common interfacial conditions in frictional systems. Friction by hard asperities (upper left), smooth sliding with or without an interfacial liquid layer (upper right), friction by sandwiched layer of particles (lower left), and friction under rolling with slip (lower right) [8].

2.1.3 Wear

Wear is another integral part of tribology concept that is intimately linked to frictional processes and may occur when two surfaces move relative to each other. The contact leads to a detrimental removal of material from operating solid surface [13]. The surface damage or material removal could result from one or both of two solid surfaces in relative motion [7]. In most metallic components, wear causes damage such as deformation and cracking, resulting in material removal in form of small wear debris which accumulates with time, often in a linear manner [14]. It is worth mentioning that increased wearing of metallic components could lead to an increase in power loss, oil consumption and the cost of component replacement may increase. Ultimately, it reduces efficiency and the overall performance of the system. Therefore, as much as possible wear events should be minimized [13].

Wear can occur in different form depending on the service conditions it is subjected to, including the type of load or stress level, the environmental temperature, and the properties of the material itself [10]. Figure 2.4 shows the schematics of common types of wear. Adhesive wear occurs on the principles of solid-phase welding of interacting surface atoms [15]. Adhesive wear is a critical type of wear and usually characterized by high friction and wear rates [16]. The wear phenomenon is usually facilitated by clean surfaces, non-oxidizing conditions, and chemical or structural similarities between the sliding surfaces [17]. When two materials interact in relative motion, atoms/particles from the softer material tend to wear away unless the strength of both interacting materials are equal. In this case, both materials undergo wear, with molecules and micro-particles being pulled off each surface. The fragmented particles generated get trapped at the interface and cause even more surface area for atomic adhesion, leading to high wear rate [18]. Adhesive wear can result in increased roughness and protrusions such as bumps above the original surface. In industrial manufacturing, this process is referred to as galling and may lead to delamination of oxidized layer protecting the underlying bulk material, thereby increasing the chances of stronger adhesion [2]. Abrasive wear results from the removal of material by hard asperities sliding against a softer one, digging into it and ploughs numerous grooves [17]. The hard particles may come from the material itself or from counteracting surfaces within the tribo-system [19]. Abrasive wear has two main categories, which includes two-and three-body abrasion. Two-body abrasion is caused by hard protuberances or particles moving with the counterface, while in three-body abrasion is caused by free or loose abrasive particles present as interfacial elements between the mating counterparts [20]. Due to the abovementioned deformation mechanisms, the abrasive particles in a two-body mechanism can cut deeply into the workpiece material, whereas in the case of three-body abrasion, the abrasive grains may take extended time cutting into the material. Therefore, two-body abrasion is considered more severe and results in wear rates which is three times greater than the three-body mechanism under the same loading condition [21]. Fatigue is associated with repeated loading and unloading cycles [22]. Fatigue wear induce surface and subsurface cracks which after a certain number of cycles lead to severe damage, in the form of large fragments and/or large pits, on one or both mating surfaces [2]. Once a crack has been initiated, each loading cycle extends the crack by a small amount, even though the cyclic stress intensity is below the normal strength. The stress could be due to vibration or thermal cycling. Subsurface and surface fatigues are mostly observed during repeated rolling and sliding cycles, respectively [23]. Other wear processes includes corrosion wear which occur due to combined effect of mechanical wear and chemical degradation [24]. Erosion is caused by the impact of solid particles, liquid droplets, or gas [25], while fretting occurs in small-scale oscillatory motion between two surfaces in contact, causing localized wear and surface damage [26].

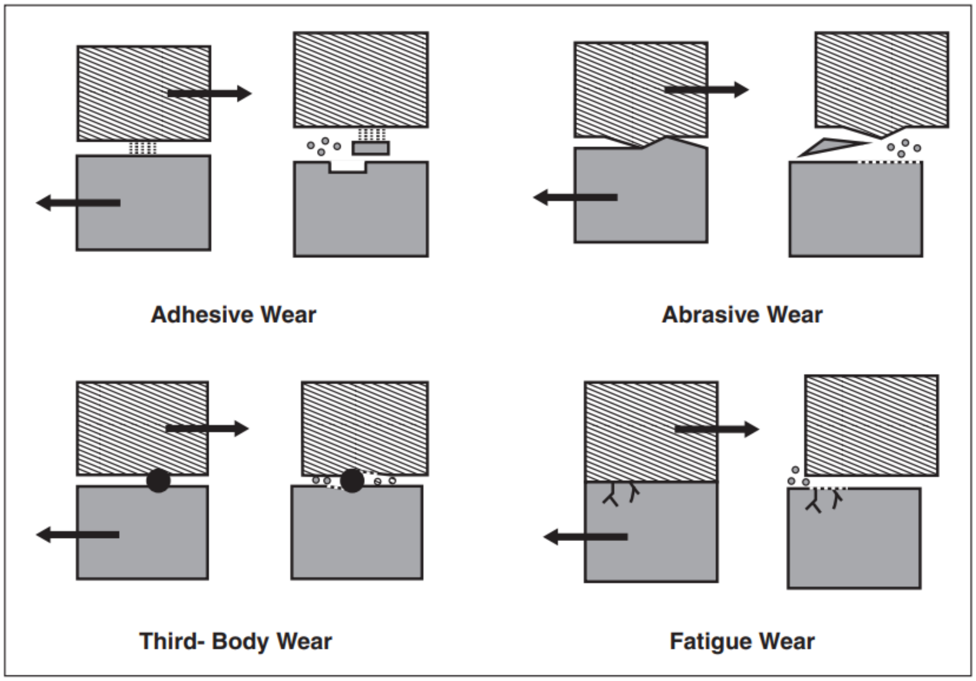

Figure 2.4 Common types of wear damage; adhesive wear (upper left), two-body abrasive wear (upper right), three-body abrasive wear (lower left), and fatigue wear (lower right) [27].

As previously mentioned, wear has been a major problem limiting the performance of engineering components. To reduce wear damage, it is essential to select durable materials with appropriate design and properties to minimize the stresses acting on it, and employ protective coatings or lubricants to minimize the wear rate [28].

2.1.4 Lubrication

Mechanical systems such as bearings, gears and machine components are designed to interact in different ways, such as sliding and rolling in relation to one another [12]. The interaction between the mating surfaces occurs at the real contact area which is influenced by normal load and mechanical properties [16]. The resulting interactions produce high frictional forces that could generate high temperatures and expose the mechanical systems to wear. Lubricants are used to minimize friction (resulting from vibrations) and wear of mechanical systems in relative motion [29]. Lubricants are introduced between the actual surface contact and frictional force inhibiting the surfaces movement, subsequently help to extend the life of mechanical components and reduce energy consumption [30]. Lubricants can exist in the form of liquids such as petroleum or mineral oils, silicone fluids and synthetic esters, while the commonly used solid lubricants includes MoS_2, graphite, hexagonal BN and boric acid H_3BO_3 [29], [30]. Liquid lubricants can be applied on moving parts by hydraulic actions to keep the parts separated. They are selected for application based on the effects of temperature change on the viscosity of the lubricant which is to be kept at minimum. Solid lubricants find application in extreme working conditions where conventional oils failed to work. They have low shear strength, low hardness, high adhesion thermal stability and chemical inertness [17]. However, studies have shown that the operating conditions of many lubricants are limited at low or high temperature, in vacuum or at extreme contact pressure [31]. Moreover, the environmental concerns posed by lubricants further limit their improved tribological applications. For instance, liquid lubricants are composed of 90% oil and 10% additives. The additives present are toxic and not environmentally friendly [32]. These challenges led to the use of wear-resistant materials with good frictional properties and can operate without lubrication [33].

2.2 Thermal Spray Technology

Thermal spray processes involve a set of coating processes where a heat source is used to melt feedstocks in the form of powder, wire or rod form. The molten or semi-molten particles are then projected towards a readily prepared substrate by expanding a process gas. Once the particles impinge on the substrate, they cool and build up, particle by particle, layer by layer, resulting in coating deposit. It is an adaptable procedure for depositing various feedstock materials at high temperature on practically any substrate making it a very robust techniques in providing engineering and design solutions that protect gas turbine components and enhance their overall efficiency [34]. Thermal spray technology provides the opportunity to coat a diverse range of materials without causing substrate distortion or encountering thickness constraints. It offers precision, eco-friendliness, and the capability to effectively repair worn or damaged parts compared to traditional processes such as electroplating, electroless deposition, and physical/chemical coating methods, which have drawbacks such as elevated processing expenses, diminished deposition efficiency, and the generation of environmentally hazardous by-products [35]. Figure 2.5 presents the classification of thermal spray processes based on the source of energy used in generating the high-temperature and high-velocity gas stream.

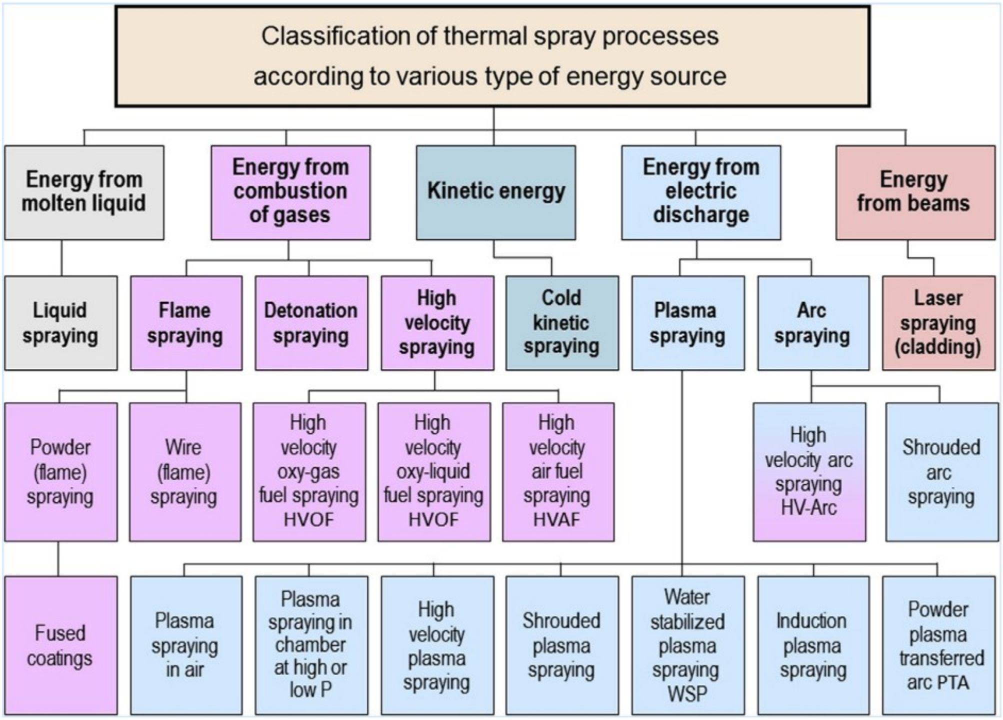

Figure 2.5 Classification of thermal spray coating processes based on the energy source used in the process [36].

This thesis utilized atmospheric plasma spray (APS) and high velocity air fuel (HVAF) processes for the deposition of chromium carbide-based wear resistant coatings. On the other hand, silicon carbide-based coating was deposited by suspension plasma spray (SPS) process. The comparative analysis of each thermal spray process has been described in more detail in the following sub-sections.

2.2.1 Plasma spray process

Plasma spraying (PS) is a versatile thermal spray deposition technique which uses an electrical arc to generate a high temperature (more than 20000 °C) for melting and spraying materials onto a surface. The schematic of a plasma torch is presented in Fig. 2.6. Plasma spray process is a low cost and flexible methods for depositing coatings with high thickness and density from the micro to the macro scale [37]. Moreover, it has advantages of high flame temperature, high energy concentration, high bonding strength, lower dilution of the coating, and high deposition efficiency [38]. Plasma jets are generated by using an inert gas like argon or nitrogen, combined with hydrogen or helium as secondary gases. The gases are heated by the electric arc created between cathode and anode electrodes until it is fully ionized. Thereafter, the material to be deposited is injected into the plasma plume and heated by means of a plasma jet, having high temperature and speed. The molten or partially molten droplets (depend on the grain size powders), are accelerated towards the surface of the pretreated substrate, which deform and deposit the coating on the surface [39].

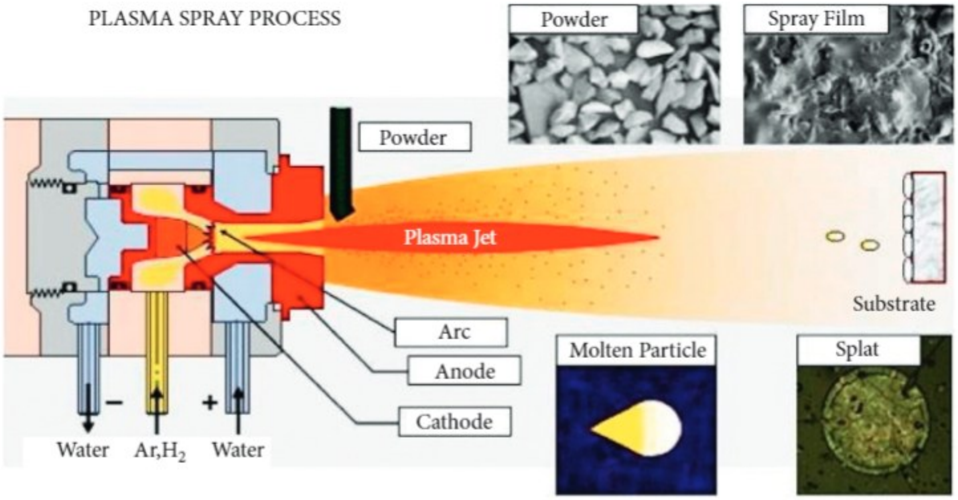

Figure 2.6 Schematic diagram of plasma spray process [40].

Atmospheric plasma spray (APS) is a conventional thermal spray process that has been widely used especially in industries such as aerospace, automotive, and energy for several decades for depositing a wide range of materials, including metals, ceramics, and composites, for enhancing wear resistance, corrosion resistance, thermal barriers, and other surface properties of engineering component. This process allows the deposition of powders with a particle size ranging from 10 to 100 µm to form a lamellae coating microstructure of micrometer thickness and diameter of a few tens to hundreds of micrometers. However, the main drawback is the challenges of processing nanometric particles due to difficulty injecting them into the plasma jet as they tend to form larger aggregates that can block the injection path and nozzle throats [41]. Furthermore, the resulting APS coatings have a characteristic lamellar structure due to successive impingement of molten splats, revealing micro-defects such as un-melted particles, porosity, and weak interlamellar bonding between splats that could deteriorate the coating's functionality and overall service performance [42].

Suspension plasma spray (SPS) is a novel variant of atmospheric plasma spray processes that allows the deposition of sub-micrometric or nanometric particles (between 500 nm to 5 µm) [43]. The process also makes it possible to achieve thin coatings of thickness ranging from 20 to 100 µm with finer microstructural features compared to the APS coatings [43]. The process uses the basic equipment of the conventional process, but the feedstocks is dispersed in a solvent generally water, ethanol or their mixture, at a certain ratio to form a suspension [44]. The prepared suspension is injected into the plasma plume where it undergoes atomization to form very fine solid droplets. The liquid from the droplet evaporates and the fine powder particles can undergo a partial or full melting and may form agglomerates. The melted particles impinge on the surface to form a fine structured coating [45]. The typical SPS coating exhibit a columnar or vertical cracks microstructure, which strongly depends on the spray parameters such as feed rate of liquids, standoff distance, solid loadings of liquid [46]. The injection mode also plays a crucial role in achieving the desired coating structure. Fig. 2.7 shows various injection modes of injecting feedstock slurry. Radial injection allows the injection of the slurry perpendicularly in the direction of the plasma jet by an external injector. However, some suspension droplets/particles may not pass through the plasma jet, leading to less efficient heating and possibly incomplete melting, which can negatively affect the coating quality. Whereas, in axial injection mode, slurries are fed directly into the plasma flow by a co-axial injector, thereby allowing longer residence time in the high-temperature core of the plasma jet, leading to more uniform and complete melting of particles [47].

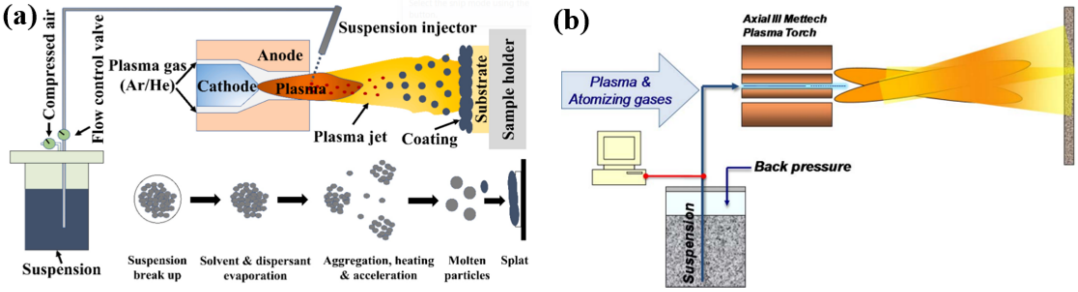

Figure 2.7 Schematic diagram of (a) radial and, (b) axial feeding of feedstock [47].

2.2.2 High-Velocity Air Fuel (HVAF)

HVAF is a thermal spray coating technique that can be employed for producing a dense coating with minimal oxidation. Unlike the high velocity oxygen fuel (HVOF) process, HVAF uses a compressed air instead of oxygen for spraying which reduces the chances of decarburization and decomposition of carbide particles. The relatively low processing temperature in HVAF process also help to retain the solid-state nature of the particles deposited [48].

Figure. 2.8 shows the schematic of HVAF spray process. The process involved burning gaseous fuel and compressed air in the combustion chamber to produce relatively high temperature and pressure. The lower oxygen concentration lowers the combustion temperature but allows the efficient heating and acceleration of the axially injected particles to a supersonic state and then propelled towards the substrate where they undergo plastic deformation and adhere to the surface to form a coating. HVAF particle temperatures are typically lower, and the particle velocities are significantly higher than the conventional HVOF spraying process [49], [50].

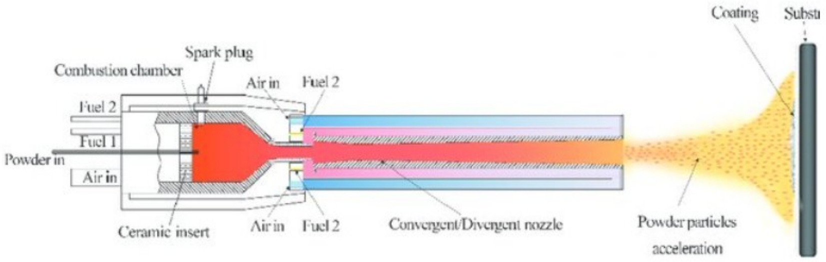

Figure 2.8 Schematic diagram of HVAF spray processes [51].

HVAF technique has some advantages over other combustion spray processes such as high jet velocity and low flame temperature which results in dense coating with low porosity. The oxygen used in HVOF process is replaced by air in the HVAF process which reduces the chances of particle oxidation, resulting in coating with improved phase retention without any crack formation. Moreover, HVAF is a low-cost alternative that can produce dense coatings and higher deposition efficiency compared to the HVOF process.

2.3 Wear resistant coatings

The interfacial contact layer plays a significant role in tribological systems that operate under sliding conditions due to its effects on friction and wear behavior. This layer, which forms the interface between two sliding surfaces has several important effects that impact the overall tribological performance of the system [52].

Generally, the contacting interfaces in gas turbine engines can be classified into clearance control and tribological interfaces. Figure 2.9 shows the contact locations in a gas turbine engine. Clearance control refers to systems, which are located directly in the gas path and includes abradable, abrasives and knife-edge seals. While the tribological interface includes blade root interfaces, bearings, gears, and seals. These contact interfaces are extremely sensitive to wear degradation that could lead to degradation of the moving components and subsequently to failure of the machinery. In addition, premature wear of these components could result in an increased number of engine teardowns, which significantly increases the maintenance costs of an aircraft [53], [54]. However, if the contact area is reduced, low friction would be expected, and this can only be achieve using wear resistant coatings [52].

Wear resistance coatings are employed to protect mechanical parts from catastrophic damage resulting from wear events. These coatings are also utilized for maintaining the optimal performance and durability of structural components [55].

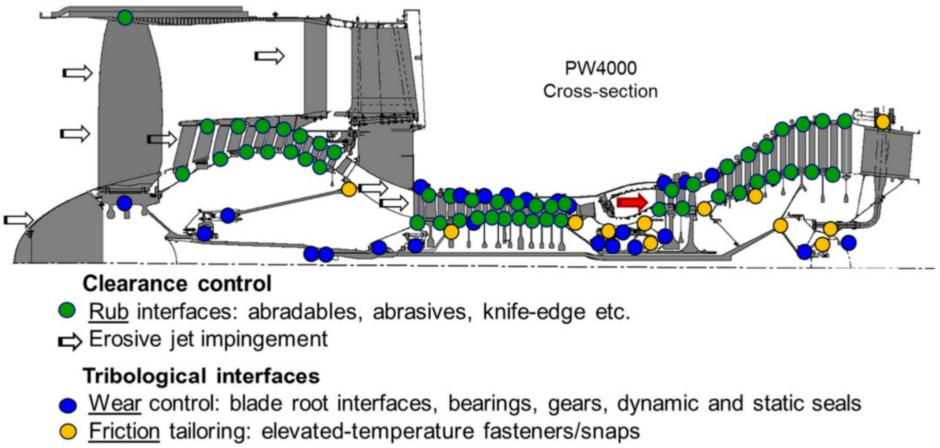

Figure 2.9 Cross-section of the contact locations in a jet engine [54].

Several wear resistant coatings have been employed for many decades in the industries to mitigate wear by applying them to the surface of components and tools to protect them from wear degradation under harsh operating conditions [56]. The common coatings materials that are widely used for wear resistant coating consist mainly of nitrides, borides, carbon-based, oxides and carbides due to their high hardness and wear resistance properties. These materials also offer excellent chemical stability and oxidation resistance making them suitable for specific wear-related challenges in severe environments [57]. This thesis focused mainly on carbide coatings such as chromium-carbide and silicon carbide-based coatings.

2.3.1 Performance of plasma sprayed chromium carbide-based coatings

2.3.1.1 Microstructure and mechanical properties

Plasma sprayed Cr_3C_2-NiCr coatings provides resistance against abrasive wear and a low friction coefficient from room temperature up to 850 °C, due their high thermal stability and oxidation resistance [58]. The microstructures of plasma sprayed carbide coatings are characterized by lamellar microcracks, unmolten particles, weak interfaces and voids between successive splats [59]. Figure 2.10 presents the typical microstructure of plasma sprayed Cr_3C_2-NiCr coating. The coating shows an inhomogeneous microstructure characterized by metallic Ni-Cr matrix (denoted by A) having different grey contrast that are rich in Cr and C from the Cr_3C_2 phase dissolved in the matrix, together with mixed carbide (dark grey regions, denoted by B) interspersed with voids (black regions, denoted by C) carbide particles are distributed within the coating, giving rise to an inhomogeneous microstructure. On the other hand, the high energy level and lower particle velocity of plasma spray methods can cause decarburization of primary Cr_3C_2 phases into secondary phases such as Cr_7C_3 and $Cr_{23}C_6$ phases, and oxidation leading to formation of Cr_2O_3 phases [60]. Rubino *et al*. [61] reported the decomposition of Cr_3C_2 phase into Cr_7C_3 and $Cr_{23}C_6$ phases. The Cr_7C_3 phases are formed by decarburization of Cr_3C_2 while $Cr_{23}C_6$ phases were formed by precipitation mechanism during the cooling process of the deposited splats. However, minimal amount of Cr_2O_3 phases were present in the coating due to spraying in inert environment. Similar study by Marcano *et al*. reported the presence of Cr_7C_3 and Cr_3O_2 phases in vacuum plasma spray Cr_3C_2-NiCr coating, indicating that decarburization and oxidation of primary Cr_3C_2 phase occur [58]. It is worth mentioning that these phases have lower mechanical properties and wear resistance compared to the original Cr_3C_2 phase [62]. Despite this limitation, some available studies have shown that plasma sprayed chromium carbide-based offers improved mechanical performance. Chhabra *et al*. study revealed that plasma sprayed Cr_3C_2-NiCr coatings exhibit higher hardness, higher bond strength, dense and defects free [63]. Mihailo reported the improved microhardness and bond strength of plasma sprayed 75Cr_3C_2-25NiCr coatings and the improved properties was ascribed to the powder feed rate and that the coatings did not show the presence of un-melted powder particles, precipitates, and inter-lamellar pores [62]. Lin *et al*. [64] reported that supersonic plasma sprayed NiCr-Cr_3C_2 coatings exhibited improved properties (micro-hardness, deposition efficiency, bonding strength and elastic modulus) and lower porosity value than HVOF coating.

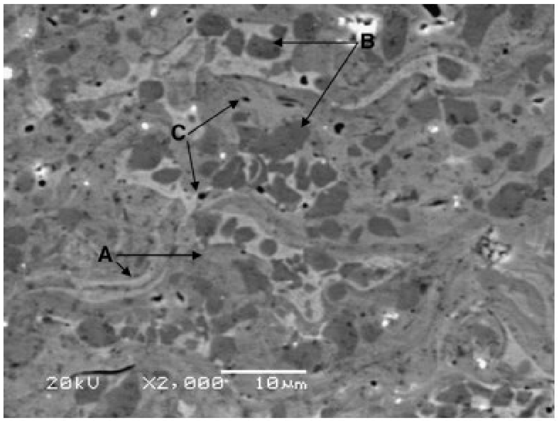

Figure 2.10 Cross-section of vacuum plasma sprayed Cr_3C_2-NiCr coatings [58].

While several studies have shown that plasma sprayed carbide coatings usually undergo decomposition, coating issues such as debonding of carbide grains due to rebounding is comparatively lower in plasma spraying than in other thermal spraying techniques such as high velocity-based spraying processes [65].

2.3.1.2 Friction and wear properties

In general, there are only a few studies that examine the friction and wear performance of plasma sprayed Cr_3C_2-NiCr coatings especially at elevated temperatures. Most of the available studies focus mainly on studying the wear behavior at room temperatures. For instance Yinlong *et al.* [66] reported that plasma Cr_3C_2-NiCr coating exhibit poor wear performance than D-gun Cr_3C_2-NiCr coating. Whereas Mishra *et al*. [67] investigation revealed that plasma sprayed Cr_3C_2-NiCr coatings exhibit lower friction coefficient and higher wear resistance compared to uncoated samples at ambient temperature. The low friction was ascribed to the formation of oxide layer at the sliding interface, which reduced direct contact between surfaces, while the improved wear resistance was linked to the coating's uniform, dense microstructure and increased hardness. Li *et al*. [68] studied the friction and wear behaviour of plasma-sprayed Cr_3C_2-NiCr against TiO_2 coating at different sliding speeds and loads. A decrease in the friction coefficient and increased wear rate of the as-sprayed coatings as the speeds and loads increased, were reported. The wear mechanism identified at lower loading was fatigue wear while plastic deformation and shear fracture dominates at higher loads. Other study by Lin *et al*. [64] compares the wear behavior of NiCr-Cr_3C_2 coatings deposited by supersonic plasma spraying and high velocity oxy-fuel processes. The results according to Fig. 2.11 show that SPS coating friction variation for single curve is relatively smooth compared to that of HVOF coatings.

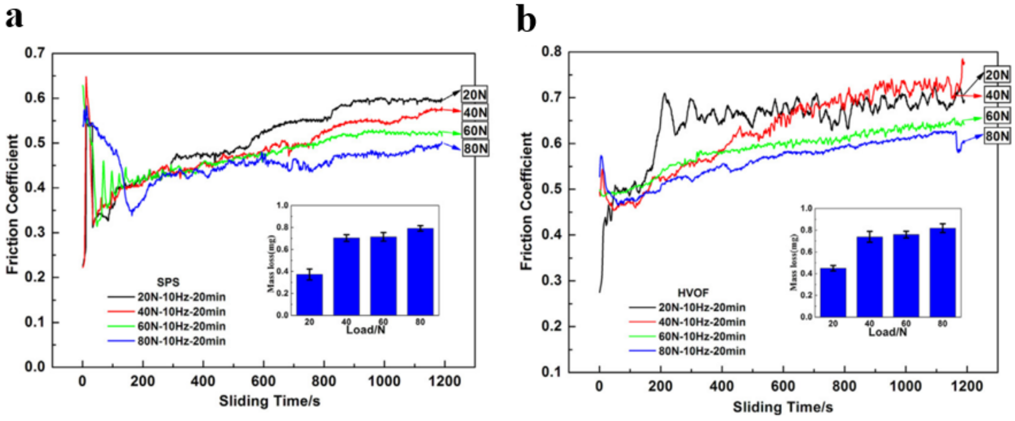

Figure 2.11 Variation of COF against the sliding time under different loads (a) SPS coating (b) HVOF coating [64].

Moreover, the mass loss of SPS coatings is lower than that of HVOF coatings under same applied load. The improved friction and wear properties of SPS coatings were attributed to high hardness and minimal coating defects compared to HVOF coatings. The high temperature wear testing of plasma sprayed Cr_3C_2-NiCr coatings by Pankaj *et al*. [63] revealed that Cr_3C_2-NiCr coatings demonstrated low friction and improved wear resistance at 400°C due to formation of oxide layers which acted as load bearers. However, the increase in the temperature up to 800°C led to increased friction and wear rate due to thermal softening and precipitation of carbides from the top layer of the coating. The results are an indication that the hardness and wear resistance to penetrating abrasive particles of Cr_3C_2-based coatings may decrease at higher temperatures and the oxide layers formed can be removed by micro-cutting, thereby exposing the base materials to wear damage [69].

2.3.2 Performance of HVAF sprayed chromium carbide-based coatings

2.3.2.1 Microstructure and mechanical properties

Chromium carbide-based coatings deposited by high-velocity processes offer superior wear resistance compared to plasma-sprayed coatings, due to the enhanced coating properties achievable with high-velocity techniques [70]. These coatings are widely used in industries for components that require wear protection and corrosion resistance in high-temperature environments [69]. High Velocity Oxy-Fuel (HVOF) processes are commonly employed for Cr_3C_2-based coatings; however, the high temperatures involved in the process cause some decarburization or dissolution or complete melting of Cr_3C_2 grains also takes place. This has led to the increased adoption of the High-Velocity Air-Fuel (HVAF) process, which mitigates the risk of carbide degradation, making it a preferable alternative to traditional HVOF methods [69]. Figure 2.12 presents the microstructure of Cr_3C_2–NiCr coating deposited by HVOF and HVAF processes. The HVOF coating (Fig. 2.12a) undergoes consideration carbide degradation, as shown by the white arrows, while the carbides in HVAF coating (Fig. 2.12b) undergo minimal degradation and individual carbide maintains their original angular morphology. Additionally, the pores produced by HVOF process (Fig. 2.12c) are larger when compared to the HVAF spray coating (Fig. 2.12d). The high porosity content in HVOF process is undesirable for dry unlubricated wear applications, because it can act as active site for crack initiation and propagation under stress, which reduces the coating's wear resistance [71]. The hardness of thermally sprayed coatings strongly depends on the microstructural features, phase constitution and porosity content. Although studies have shown that the fracture toughness of HVOF Cr_3C_2-25NiCr coating are comparable to that spray by HVAF process, but the low porosity content in HVAF Cr_3C_2-NiCr coating facilitate improved hardness than HVOF sprayed coatings [71]. Hardness can be beneficial in minimizing formation of wear debris and reducing adhesion between contacting surfaces under sliding wear conditions, thereby leading to low wear damages [72]. Thus, the proper optimization of thermal spray process parameters plays a key role in ensuring high carbides retention and defects free coatings, resulting in high hardness and perform better against wear and corrosion.

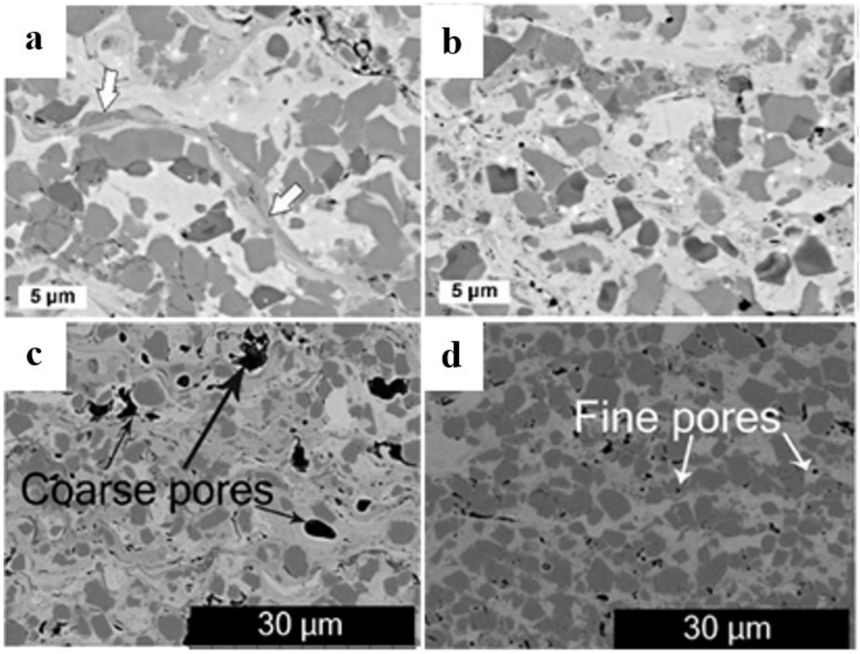

Figure 2.12 Microstructures of chromium carbide-based coating, (a-c) HVOF, (b-d) HVAF [71], [73].

2.3.2.2 Friction and wear properties

Several research on the sliding wear behaviour of HVOF sprayed Cr_3C_2-NiCr coatings has been studied in some detail, but a comprehensive assessment of the sliding wear behaviour of HVAF-sprayed Cr_3C_2-NiCr coatings is still limited [69]. Bolelli *et al*. [48] examined the tribological properties of fine and coarse Cr_3C_2-25Ni20Cr powders deposited by means of HVOF and HVAF processes. It was reported that HVAF coatings exhibit the best wear performance and that fine feedstock powder provides more resistant to wear than the coarse powder due to stronger matrix-carbide cohesion within the lamellae after spraying. Mahade *et al*. [71] study reveals that HVAF Cr_3C_2-NiCr coatings undergo increase COF and low wear resistance at lower load due to delamination of tribo-films, but at higher loading conditions, HVAF coatings demonstrate superior wear performance than HVOF coatings. The same author reported the wear resistance of high velocity air fuel (HVAF) sprayed Cr_3C_2-NiCr coatings by including GNP employing hybrid approach in which Cr_3C_2-NiCr (powder) and graphene nano platelets GNP (suspension) are co-axially injected [74]. It was reported that no decarburized carbide was observed in all the HVAF sprayed coatings. Moreover, the coefficient of friction and specific wear rates were lower for GNP incorporated coatings compared to the coating without GNP. In another study by the same author, pure chromium carbide (Cr_3C_2) suspension was co-deposited with an Inconel-625 (IN-625) powder using HVAF process to deposit improved wear and corrosion resistant coatings. The sliding wear rate results clearly demonstrated improved wear resistance of hybrid coatings compared to the conventional IN-625 coating. The improved wear resistance was attributed to an increased carbide retention by the HVAF process [75]. Matikainen *et al*. [73] studied the high temperature sliding wear behaviour of Cr_3C_2-25NiCr. The results show that the HVAF Cr_3C_2-25NiCr coatings demonstrate the lowest friction coefficient and significantly improved wear resistance than the HVOF Cr_3C_2-25NiCr coatings at 700 °C. The surface state of the wear tracks following sliding test are presented in Fig. 2.13. It can be observed that HVAF sprayed coatings maintained a dense structure without surface cracking which enabled the formation of stable tribo-oxide layer on the wear track, as shown in Fig. 2.13a. Whereas HVOF Cr_3C_2-25NiCr coating exhibited subsurface cracking caused by sinusoidal loading cycles during the wear test, as shown in Fig. 2.13b. Such subsurface cracking promotes the removal of the tribo-oxide layer subjecting the underlying material to oxidation and wear. These studies have also demonstrated that HVAF process can be utilized to fabricate chromium carbide-based coatings with a dense coatings structure, increased carbide retention, and without any subsurface cracking. Moreover, HVAF process can enable the formation of thick oxide layer on the wear track that will provide improved wear and oxidation resistance to critical components in gas turbine engine [69].

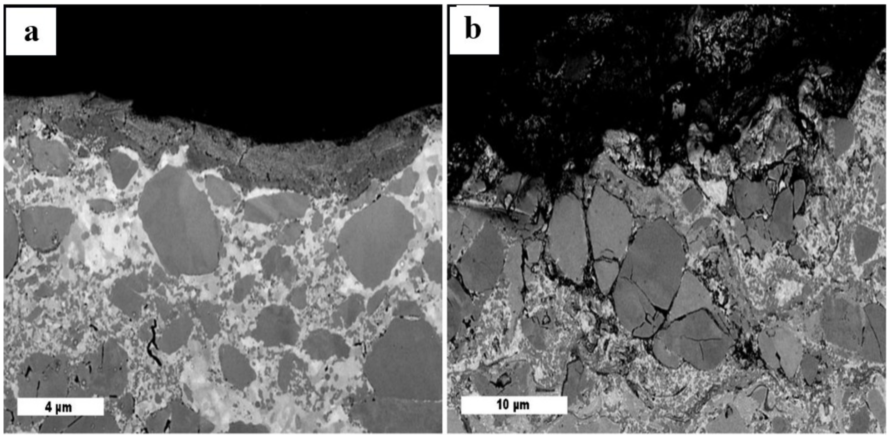

Figure 2.13 SEM of Cr_3C_2-25NiCr coatings wear track deposited by (a) HVAF (b) HVOF [73].

2.3.3 Performance of thermally sprayed silicon carbide-based coatings

2.3.3.1 Microstructure and mechanical properties

Thermal spraying of silicon carbide is extremely difficult due to its tendency to decompose into gas at elevated temperatures. Nowadays, silicon carbides are thermally sprayed as a ceramic matrix composite (CMC) through co-deposition with oxide binders such as Al_2O_3 and Y_2O_3 to minimize oxidation and improve deposition efficiency [76]. Figure 2.14a shows the cross-section of silicon carbide coating containing 30 wt.% of nano-film YAG binder produced by high-frequency pulse detonation (HFPD) method. The coating is characterized by small pores formed during spraying and some grindingpolishing artefacts were visible in the darkest spots region. The higher magnification image of the coating in Fig. 2.14b reveals non-deformed SiC particles (dark grains) embedded in a bright region of YAG binder. The inherent pores in the coating originated from trapped gases which also contributed to a low hardness value of 484 ± 47 $HV_{0.1}$ [77]. Acacio *et al*. [78] produce SiC-YAG coatings by suspension HVOF thermal spray method. The results showed that SiC particles were protected from oxidation by the completely melted YAG, and that the coating contains a low degree of porosity (0.6 ± 0.2%) and higher microhardness values

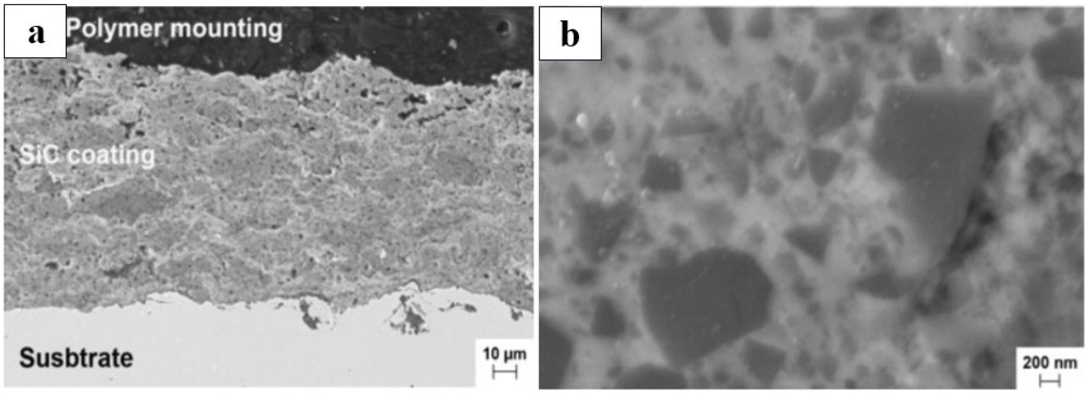

Figure 2.14 SEM images of SiC coating (a) Cross-section of as-sprayed silicon carbide-based coating, and (b) Silicon carbide particles embedded in yttrium aluminium garnet (YAG) matrix [77].

Recent advances have shown that suspension route is an interesting approach, worth exploring for the deposition of SiC coatings. However, achieving homogeneous distribution of binders in the suspension feedstock remains a challenge [79]. Moreover, research work to fully understand the mechanical and wear performance of suspension sprayed SiC coatings remains work in progress. Available study by Mubarok *et al*. uses different methods including mechanical mixing and co-precipitation, and crystalline-SiC method to deliver the binder into the SiC suspension feedstocks. The results show that, while the coating obtained are characterized by defects such as voids and porosity, the crystalline method produced the coating with the highest cohesion, thus resulting in a denser coating [79]. Thus, the study has shown that more improvements in needed to deposit high-quality SiC coatings using suspension route.

2.3.3.2 Friction and wear properties

The tribological behavior of bulk silicon carbide materials under various experimental testing conditions have been widely reported. Mubarok *et al*. investigations compared the sliding wear performance of thermally sprayed SiC coatings under dry, 3.5 wt.% NaCl solution and polyalphaolefin (PAO) lubricant. The results according to Fig. 2.15a-b indicate that PAO-lubricated sliding exhibits the lowest coefficient of friction (CoF) at a steady level of 0.10, whereas the highest CoF, obtained for SiC coatings in a 3.5 wt.% NaCl solution, reached 1.00 and 0.86, respectively, and characterized by erratic fluctuations. However, the dry sliding tests on the SiC coatings demonstrated a low coefficient of friction of approximately 0.20-0.23, with slight variations, suggesting that the rubbing contact interface is partially lubricated [77].

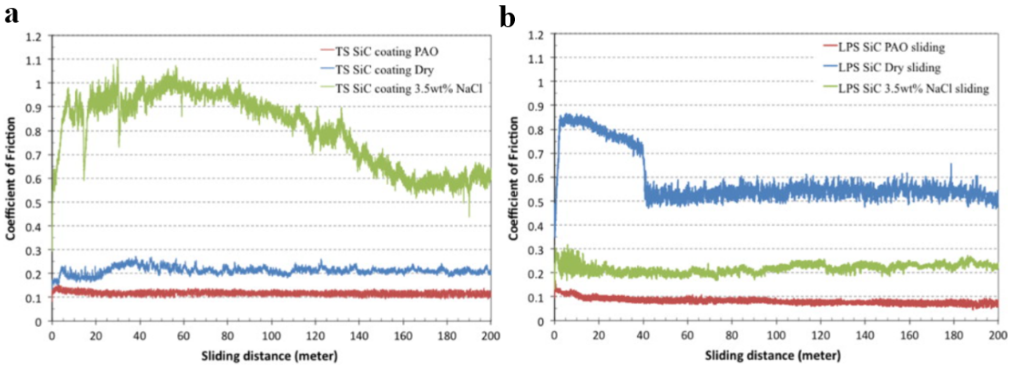

Figure 2.15 Coefficient of friction of (a) thermally sprayed SiC coatings and (b) LPS–SiC bulk materials against AISI 440C balls tested in the three different environments [77].

The wear rate results in Fig. 2.16 exhibit a similar trend as the friction results. The low COF observed for PAO-lubrication led to the lowest wear rates in both SiC coating and the counterface. In comparison to the LPS-SiC material, the SiC coating exhibits a higher specific wear rate. The wear rate of the SiC in dry sliding condition is significantly lower than that of bulk LPS-SiC material. The most significant wear rates are seen in a 3.5 wt.% NaCl solution for the SiC coating and under dry conditions for the bulk LPS-SiC. The experiments conducted in NaCl solution consistently yield the highest wear rate on the ball due to tribo-corrosion process affecting the stainless-steel balls, which accelerates wear due to corrosion. Another study by Venturi et al. reported the wear performance of SiC/YAG composite coatings produced by high velocity oxygen liquid-fuel (HVOLF) under different applied loads of 10, 20, 30 and 40 N. The results show that the coating exhibit lower coefficient of friction and improved wear performance at low load (≤ 10 N). The result is an indication that SiC coating can perform better and more suitable for low load applications, under 20 N [76].

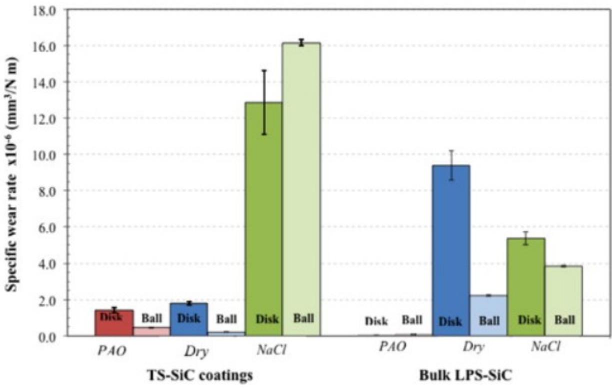

Figure 2.16 Specific wear rate of SiC coatings and bulk LPS–SiC against AISI 440C balls in three different sliding environments [77].

References

[1] J. Williams, “The Invention of Tribology: Peter Jost’s Contribution,” *Lubricants*, vol. 12, no. 3, 2024, doi: 10.3390/lubricants12030065.

[2] A. Stachowiak, G., and Batchelor, “Engineering Tribology. 4th Edition,” 2013. https://www.perlego.com/book/1857756/engineering-tribology-pdf.

[3] B. N. T. Persson, “History of Tribology,” in *Encyclopedia of Lubricants and Lubrication*, T. Mang, Ed. Berlin, Heidelberg: Springer Berlin Heidelberg, 2014, pp. 791–797.

[4] A. Abdelbary, *Extreme Tribology*. 2020.

[5] I. Hutchings, *Tribology: Friction and Wear of Engineering Materials*. Elsevier Science, 1992.

[6] J. Echávarri, E. de la Guerra, and E. Chacón, “Tribology: A Historical Overview of the Relation Between Theory and Application,” in *A Bridge between Conceptual Frameworks: Sciences, Society and Technology Studies*, R. Pisano, Ed. Dordrecht: Springer Netherlands, 2015, pp. 135–154.

[7] B. Bhushan, *Introduction to tribology–Second edition*. John Wiley & Sons, Ltd, 2013.

[8] P. J. Blau, “The significance and use of the friction coefficient,” *Tribol. Int.*, vol. 34, no. 9, pp. 585–591, 2001, doi: https://doi.org/10.1016/S0301-679X(01)00050-0.

[9] I.-J. Kim, “Frictional Behaviours and Mechanisms,” in *Engineering Metrology for Pedestrian Falls Prevention and Protection: Theories to Applications for Designing Safer Shoes and Floors*, Cham: Springer International Publishing, 2022, pp. 117–151.

[10] V. L. Popov, L. Voll, Q. Li, Y. S. Chai, and M. Popov, “Generalized law of friction between elastomers and differently shaped rough bodies,” *Sci. Rep.*, vol. 4, no. 1, p. 3750, 2014, doi: 10.1038/srep03750.

[11] G. Straffelini, “Friction,” in *Friction and Wear: Methodologies for Design and Control*, Cham: Springer International Publishing, 2015, pp. 21–60.

[12] A. S. Rathaur, J. K. Katiyar, and V. K. Patel, “Introduction and Applications of Tribology,” in *Tribology in Materials and Applications*, J. K. Katiyar, P. Ramkumar, T. V. V. L. N. Rao, and J. P. Davim, Eds. Cham: Springer International Publishing, 2020, pp. 1–14.

[13] K. Holmberg, A. Matthews, and H. Ronkainen, “Coatings tribology - Contact mechanisms and surface design,” *Tribol. Int.*, vol. 31, no. 1–3, pp. 107–120, 1998, doi: 10.1016/S0301-679X(98)00013-9.

[14] J. Gates and G. J. Gore, “Wear of metals: Philosophies and practicalities,” *Met. forum*, vol. 19, pp. 53–89, 1995.

[15] T. Murakami, “1 - Importance of biotribology,” in *Biotribology of Natural and Artificial Joints*, T. Murakami, Ed. Elsevier, 2023, pp. 1–27.

[16] A. Gåård, N. Hallbäck, P. Krakhmalev, and J. Bergström, “Temperature effects on adhesive wear in dry sliding contacts,” *Wear*, vol. 268, no. 7, pp. 968–975, 2010, doi: https://doi.org/10.1016/j.wear.2009.12.007.

[17] I.-J. Kim, “Wear Behaviours and Mechanisms,” in *Engineering Metrology for Pedestrian Falls*

Prevention and Protection: Theories to Applications for Designing Safer Shoes and Floors, Cham: Springer International Publishing, 2022, pp. 153–191.

[18] A. Horwood and N. Chockalingam, "Chapter 2 - Principles of materials science," in *Clinical Biomechanics in Human Locomotion*, A. Horwood and N. Chockalingam, Eds. Academic Press, 2023, pp. 91–174.

[19] H. Liao, B. Normand, and C. Coddet, "Influence of coating microstructure on the abrasive wear resistance of WC/Co cermet coatings," *Surf. Coatings Technol.*, vol. 124, no. 2, pp. 235–242, 2000, doi: https://doi.org/10.1016/S0257-8972(99)00653-2.

[20] A. T. Alpas, S. Bhattacharya, and I. M. Hutchings, "4.5 Wear of Particulate Metal Matrix Composites," in *Comprehensive Composite Materials II*, P. W. R. Beaumont and C. H. Zweben, Eds. Oxford: Elsevier, 2018, pp. 137–172.

[21] J. D. Gates, "Two-body and three-body abrasion: A critical discussion," *Wear*, vol. 214, no. 1, pp. 139–146, 1998, doi: https://doi.org/10.1016/S0043-1648(97)00188-9.

[22] F. Sadeghi, B. Jalalahmadi, T. S. Slack, N. Raje, and N. K. Arakere, "A Review of Rolling Contact Fatigue," *J. Tribol.*, vol. 131, no. 4, Sep. 2009, doi: 10.1115/1.3209132.

[23] W. D. C. HR and D. G. Rethwisch, *Materials Science and Engineering*. 2018.

[24] A. H. Yaghtin, E. Salahinejad, A. Khosravifard, A. Araghi, and A. Akhbarizadeh, "Corrosive wear behavior of chromium carbide coatings deposited by air plasma spraying," *Ceram. Int.*, vol. 41, pp. 7916–7920, 2015, doi: 10.1016/j.ceramint.2015.02.131.

[25] D. Zakrzewska and A. Krella, "Cavitation Erosion Resistance Influence of Material Properties," *Adv. Mater. Sci.*, vol. 19, pp. 18–34, 2019, doi: 10.2478/adms-2019-0019.

[26] H. W. Liu, X. J. Xu, M. H. Zhu, P. D. Ren, and Z. R. Zhou, "High temperature fretting wear behavior of WC–25Co coatings prepared by D-gun spraying on Ti–Al–Zr titanium alloy," *Tribol. Int.*, vol. 44, no. 11, pp. 1461–1470, 2011, doi: https://doi.org/10.1016/j.triboint.2011.01.002.

[27] J. J. Yao *et al.*, "Local Cellular Responses to Titanium Dioxide from Orthopedic Implants.," *Biores. Open Access*, vol. 6, no. 1, pp. 94–103, 2017, doi: 10.1089/biores.2017.0017.

[28] D. Arnell, "2 - Mechanisms and laws of friction and wear," in *Tribology and Dynamics of Engine and Powertrain*, H. Rahnejat, Ed. Woodhead Publishing, 2010, pp. 41–72.

[29] N. Jeyaprakash and C.-H. Yang, "Friction, Lubrication, and Wear," in *Tribology in Materials and Manufacturing*, A. Patnaik, T. Singh, and V. Kukshal, Eds. Rijeka: IntechOpen, 2020.

[30] D. M. Pirro, M. Webster, and E. Daschner, *Lubrication Fundamentals, Third Edition, Revised and Expanded*. 2017.

[31] R. Franz and C. Mitterer, "Vanadium containing self-adaptive low-friction hard coatings for high-temperature applications: A review," *Surf. Coatings Technol.*, vol. 228, pp. 1–13, 2013, doi: https://doi.org/10.1016/j.surfcoat.2013.04.034.

[32] W. J. Bartz, "Lubricants and the environment," *Tribol. Int.*, vol. 31, no. 1–3, pp. 35–47, 1998, doi: 10.1016/S0301-679X(98)00006-1.

[33] J. Luo, S. Wen, L. K. Y. Li, and P. L. Wong, *Progresses and problems in nano-tribology*, vol.

43, no. 5. Chinese science bulletin, 1998.

[34] A. Rezzoug, S. Abdi, A. Kaci, and M. Yandouzi, “Thermal spray metallisation of carbon fibre reinforced polymer composites: Effect of top surface modification on coating adhesion and mechanical properties,” *Surf. Coatings Technol.*, vol. 333, no. July 2017, pp. 13–23, 2018, doi: 10.1016/j.surfcoat.2017.10.066.

[35] J. D. Majumdar, *Thermal and cold spraying technology in manufacturing*. Handbook of Manufacturing Engineering and Technology, 2014.

[36] P. Vuoristo, “Thermal Spray Coating Processes,” *Compr. Mater. Process. Thirteen Vol. Set*, vol. 4, pp. V4-229-V4-276, 2014, doi: 10.1016/B978-0-08-096532-1.00407-6.

[37] S. Wu *et al.*, “Surface nano-architectures and their effects on the mechanical properties and corrosion behavior of Ti-based orthopedic implants,” *Surf. Coatings Technol.*, vol. 233, pp. 13–26, 2013, doi: https://doi.org/10.1016/j.surfcoat.2012.10.023.

[38] M. I. Boulos, P. L. Fauchais, and J. V. R. Heberlein, “Fundamentals of Combustion and Thermal Plasmas,” in *Thermal Spray Fundamentals: From Powder to Part*, Cham: Springer International Publishing, 2021, pp. 57–83.

[39] G. Graziani, M. Bianchi, E. Sassoni, A. Russo, and M. Marcacci, “Ion-substituted calcium phosphate coatings deposited by plasma-assisted techniques: A review,” *Mater. Sci. Eng. C*, vol. 74, pp. 219–229, 2017, doi: https://doi.org/10.1016/j.msec.2016.12.018.

[40] Y. Zhang *et al.*, “Microstructures and properties of high-entropy alloys,” *Prog. Mater. Sci.*, vol. 61, pp. 1–93, 2014, doi: https://doi.org/10.1016/j.pmatsci.2013.10.001.

[41] F. Miranda, F. Caliari, A. Essiptchouk, and G. Pertraconi, “Atmospheric Plasma Spray Processes: From Micro to Nanostructures,” in *Atmospheric Pressure Plasma*, A. Nikiforov and Z. Chen, Eds. Rijeka: IntechOpen, 2018.

[42] R. Unabia, R. Candidato, and L. Pawłowski, “Current Progress in Solution Precursor Plasma Spraying of Cermets: A Review,” *Metals (Basel).*, vol. 8, no. 6, 2018, doi: 10.3390/met8060420.

[43] P. Fauchais *et al.*, “Suspension and solution plasma spraying,” *J. Phys. D. Appl. Phys.*, vol. 46, no. 22, 2013, doi: 10.1088/0022-3727/46/22/224015.

[44] B. Pateyron, N. Calve, and L. Pawłowski, “Influence of water and ethanol on transport properties of the jets used in suspension plasma spraying,” *Surf. Coatings Technol.*, vol. 220, pp. 257–260, 2013, doi: https://doi.org/10.1016/j.surfcoat.2012.10.010.

[45] L. Pawlowski, *The Science and Engineering of Thermal Spray Coatings: Second Edition*. John Wiley & Sons, New York, 2008.

[46] H. Podlesak, L. Łatka, D. Dietrich, L. Pawłowski, B. Wielage, and T. Lampke, “Electron microscopy and diffraction studies of suspension-plasma-sprayed ZrO2 + 8 wt.\% Y2O3 coatings,” *Surf. \& Coatings Technol.*, vol. 220, pp. 67–73, 2013, https://api.semanticscholar.org/CorpusID:137298100.

[47] S. Goel *et al.*, “Axial Plasma Spraying of Mixed Suspensions: A Case Study on Processing, Characteristics, and Tribological Behavior of Al2O3-YSZ Coatings,” *Appl. Sci.*, vol. 10, no. 15, 2020, doi: 10.3390/app10155140.

[48] G. Bolelli *et al.*, “Sliding and abrasive wear behaviour of HVOF- and HVAF-sprayed Cr3C2–NiCr hardmetal coatings,” *Wear*, vol. 358–359, pp. 32–50, 2016, doi: https://doi.org/10.1016/j.wear.2016.03.034.

[49] X. Gao, C. Li, Y. Xu, X. Chen, and X. Han, “Effects of Fuel Types and Process Parameters on the Performance of an Activated Combustion High Velocity Air-Fuel (AC-HVAF) Thermal Spray System,” *J. Therm. Spray Technol.*, vol. 30, pp. 1–16, 2021, doi: 10.1007/s11666-021-01250-7.

[50] V. Matikainen, H. Koivuluoto, P. Vuoristo, J. Schubert, and Š. Houdková, “Effect of Nozzle Geometry on the Microstructure and Properties of HVAF-Sprayed WC-10Co4Cr and Cr3C2-25NiCr Coatings,” *J. Therm. Spray Technol.*, vol. 27, no. 4, pp. 680–694, 2018, doi: 10.1007/s11666-018-0717-z.

[51] E. Sadeghi, “Corrosion Behavior of HVAF-Sprayed Bi-Layer Coatings,” 2016.

[52] P. Poza and M. Á. Garrido-Maneiro, “Cold-sprayed coatings: Microstructure, mechanical properties, and wear behaviour,” *Prog. Mater. Sci.*, vol. 123, p. 100839, 2022, doi: https://doi.org/10.1016/j.pmatsci.2021.100839.

[53] R. E. Chupp, R. C. Hendricks, S. B. Lattime, and B. M. Steinetz, “Sealing in Turbomachinery,” *J. Propuls. Power*, vol. 22, pp. 313–349, 2006, https://api.semanticscholar.org/CorpusID:109015945.

[54] P. Stoyanov, K. M. Harrington, and A. Frye, “Insights into the Tribological Characteristic of Cu-Based Coatings Under Extreme Contact Conditions,” *Jom*, vol. 72, no. 6, pp. 2191–2197, 2020, doi: 10.1007/s11837-020-04087-7.

[55] W. Zhai *et al.*, “Recent Progress on Wear-Resistant Materials: Designs, Properties, and Applications,” *Adv. Sci.*, vol. 8, p. 2003739, 2021, doi: 10.1002/advs.202003739.

[56] T. Hoornaert, Z. K. Hua, and J. H. Zhang, “Hard Wear-Resistant Coatings: A Review,” in *Advanced Tribology*, 2010, pp. 774–779.

[57] C. Donnet and A. Erdemir, “Historical developments and new trends in tribological and solid lubricant coatings,” *Surf. Coatings Technol.*, vol. 180–181, pp. 76–84, 2004, doi: https://doi.org/10.1016/j.surfcoat.2003.10.022.

[58] Z. Marcano, J. Lesage, D. Chicot, G. Mesmacque, E. S. Puchi-Cabrera, and M. H. Staia, “Microstructure and adhesion of Cr3C2–NiCr vacuum plasma sprayed coatings,” *Surf. Coatings Technol.*, vol. 202, no. 18, pp. 4406–4410, 2008, doi: https://doi.org/10.1016/j.surfcoat.2008.04.017.

[59] D. I. Pantelis, P. Psyllaki, and N. Alexopoulos, “Tribological behaviour of plasma-sprayed Al2O3 coatings under severe wear conditions,” *Wear*, vol. 237, no. 2, pp. 197–204, 2000, doi: https://doi.org/10.1016/S0043-1648(99)00324-5.

[60] P. Ctibor and M. Prantnerová, “Plasma spraying and characterization of chromium carbide-nickel chromium coatings,” *Prog. Color. Color. Coatings*, vol. 9, no. 4, pp. 281–290, 2016.

[61] F. Rubino, D. Merino, A. T. Silvestri, C. Munez, and P. Poza, “Mechanical properties optimization of Cr3C2-NiCr coatings produced by compact plasma spray process,” *Surf. Coatings Technol.*, vol. 465, p. 129570, 2023, doi: https://doi.org/10.1016/j.surfcoat.2023.129570.

[62] M. Mrdak, “Influence of a powder feed rate on the properties of the plasma sprayed chromium carbide-25% nickel chromium coating,” *Vojnoteh. Glas.*, vol. 62, pp. 7–26, 2014, doi: 10.5937/vojtehg62-3793.

[63] P. Chhabra and M. Kaur, “Wear and friction characteristics of atmospheric plasma sprayed Cr3C2–NiCr coatings,” *Tribol. - Mater. Surfaces Interfaces*, vol. 14, no. 3, pp. 177 – 192, 2020, doi: 10.1080/17515831.2020.1720383.

[64] L. Lin, G.-L. Li, H.-D. Wang, J.-J. Kang, Z.-L. Xu, and H.-J. Wang, “Structure and wear behavior of NiCr–Cr3C2 coatings sprayed by supersonic plasma spraying and high velocity oxy-fuel technologies,” *Appl. Surf. Sci.*, vol. 356, pp. 383–390, 2015, doi: https://doi.org/10.1016/j.apsusc.2015.08.019.

[65] R. J. Alroy, M. Kamaraj, D. V. Lakshmi, K. Praveen, P. S. Babu, and G. Sivakumar, “Tailoring microstructural features of Cr3C2-25NiCr coatings through diverse spray variants and understanding the high-temperature erosion behavior,” *Tribol. Int.*, vol. 188, p. 108810, 2023, doi: https://doi.org/10.1016/j.triboint.2023.108810.

[66] W. Yinglong, “Friction and wear performances of detonation-gun- and plasma-sprayed ceramic and cermet hard coatings under dry friction,” *Wear*, vol. 161, no. 1, pp. 69–78, 1993, doi: https://doi.org/10.1016/0043-1648(93)90454-T.

[67] B. B. Mishra and H. Nautiyal, “Frictional and wear behavior of Cr3C2-NiCr coating on AISI-304 stainless steel,” *Adv. Mater. Process. Technol.*, vol. 8, no. 4, pp. 4007–4017, 2022, doi: 10.1080/2374068X.2022.2036508.

[68] J. F. Li, C. X. Ding, J. Q. Huang, and P. Y. Zhang, “Wear mechanism of plasma-sprayed Cr3C2□NiCr against TiO2 coating,” *Wear*, vol. 211, no. 2, pp. 177–184, 1997, doi: https://doi.org/10.1016/S0043-1648(97)00109-9.

[69] A. R. Govande, A. Chandak, B. R. Sunil, and R. Dumpala, “Carbide-based thermal spray coatings: A review on performance characteristics and post-treatment,” *Int. J. Refract. Met. Hard Mater.*, vol. 103, p. 105772, 2022, doi: https://doi.org/10.1016/j.ijrmhm.2021.105772.

[70] M. Xie, S. Zhang, and M. Li, “Comparative investigation on HVOF sprayed carbide-based coatings,” *Appl. Surf. Sci.*, vol. 273, pp. 799–805, 2013, doi: https://doi.org/10.1016/j.apsusc.2013.03.010.

[71] S. Mahade, A. Mulone, S. Björklund, U. Klement, and S. V Joshi, “Investigating Load-dependent Wear Behavior and Degradation Mechanisms in Cr3C2-NiCr coatings deposited by HVAF and HVOF,” *J. Mater. Res. Technol.*, 2021, https://api.semanticscholar.org/CorpusID:239953533.

[72] E. Gariboldi, L. Rovatti, N. Lecis, L. Mondora, and G. A. Mondora, “Tribological and mechanical behaviour of Cr3C2–NiCr thermally sprayed coatings after prolonged aging,” *Surf. Coatings Technol.*, vol. 305, pp. 83–92, 2016, doi: https://doi.org/10.1016/j.surfcoat.2016.07.087.

[73] V. Matikainen, G. Bolelli, H. Koivuluoto, P. Sassatelli, L. Lusvarghi, and P. Vuoristo, “Sliding wear behaviour of HVOF and HVAF sprayed Cr3C2-based coatings,” *Wear*, vol. 388–389, pp. 57–71, 2017, doi: 10.1016/j.wear.2017.04.001.

[74] S. Mahade, A. Mulone, S. Björklund, U. Klement, and S. Joshi, “Novel suspension route to

incorporate graphene nano-platelets in HVAF-sprayed Cr3C2–NiCr coatings for superior wear performance,” *J. Mater. Res. Technol.*, vol. 13, pp. 498–512, 2021, doi: https://doi.org/10.1016/j.jmrt.2021.04.096.

[75] S. Mahade, L. Baiamonte, E. Sadeghimeresht, S. Björklund, F. Marra, and S. Joshi, “Novel utilization of powder-suspension hybrid feedstock in HVAF spraying to deposit improved wear and corrosion resistant coatings,” *Surf. Coatings Technol.*, vol. 412, p. 127015, 2021, doi: https://doi.org/10.1016/j.surfcoat.2021.127015.

[76] F. Venturi, A. R. Romero, and T. Hussain, “SiC/YAG composite coatings by a novel liquid fuelled high velocity oxy-fuel suspension thermal spray,” *Surf. Coatings Technol.*, vol. 471, p. 129865, 2023, doi: https://doi.org/10.1016/j.surfcoat.2023.129865.

[77] F. Mubarok and N. Espallargas, “Tribological behaviour of thermally sprayed silicon carbide coatings,” *Tribol. Int.*, vol. 85, 2015, doi: 10.1016/j.triboint.2014.11.027.

[78] A. Rincón, Z. Pala, and T. Hussain, “A suspension high velocity oxy-fuel thermal spray manufacturing route for silicon carbide – YAG composite coatings,” *Mater. Lett.*, vol. 281, p. 128601, 2020, doi: https://doi.org/10.1016/j.matlet.2020.128601.

[79] F. Mubarok and N. Espallargas, “Suspension Plasma Spraying of Sub-micron Silicon Carbide Composite Coatings,” *J. Therm. Spray Technol.*, vol. 24, 2015, doi: 10.1007/s11666-015-0242-2.

Chapter

3. INFLUENCE OF DEPOSITION PROCESS AND BINDER CONTENT ON THE TRIBOLOGICAL BEHAVIOR OF CHROMIUM CARBIDE - BASED COATINGS: A COMPARISON BETWEEN APS AND HVAF PROCESSES

In this chapter…

The tribological studies between two different compositions of chromium carbide powders sprayed with atmospheric plasma spray (APS) and high velocity air-fuel (HVAF) technique have been provided. The testing, characterization and data analysis were performed to assess the friction and wear behavior of the as-sprayed coatings at room and elevated temperature conditions.

3.1 Abstract

Chromium carbide-based coatings have commonly been used for tribological applications due to their hardness, improved corrosion and oxidation resistance in harsh environments. This study focuses on the influence of deposition processes (i.e., APS and HVAF) and binder content (i.e., pure carbide vs cemented carbide) on the coatings microstructure, mechanical, and tribological properties at room temperature (RT) and 450 °C. Microstructural analysis revealed that both APS and HVAF coatings had a uniform and dense structure, while the APS coatings showed higher porosity and lower Cr_3C_2 content due to carbide dissolution, decarburization, and oxidation. The tribological tests showed that APS sprayed Cr_3C_2 coating (high power condition) had the highest friction and wear volume loss, possibly due to their high porosity and brittle nature. The HVAF sprayed Cr_3C_2-25NiCr coatings produced by 4L4 nozzle showed the lowest friction and wear loss at both room temperature and 450 °C.

Keywords: Carbides, Thermal Spray, APS, HVAF, Tribology, Gas Turbine

3.2 Introduction

Recent advances in mechanical systems in the aerospace and power generation sectors have placed increasingly demanding operating conditions on materials at their tribological interfaces [1]. In high temperature environments, these tribological contacts experience significant wear, which negatively impacts the lifespan and stability of the overall system. As a result, there is a need to develop durable coatings that can withstand these harsh conditions while maintaining optimum performance [2]–[4]. The focus is on innovative solutions that improve wear resistance and thermal stability, ensuring the reliability and longevity of critical components in demanding service applications [5]. For instance, thermally sprayed coatings are effective for providing adequate protection against wear degradation for critical components within a gas turbine. The coatings help to maintain the required performance level of the engines by lowering the friction between two surfaces in contact and promote durability of structural component. This has consequently driven a growing interest in the development of next-generation carbide-based coating materials capable of withstanding extreme environmental and contact conditions [6], [7].

Thermally sprayed Cr_3C_2-based coatings are widely employed as wear-resistant solutions in the cold section of jet engines, particularly within the low and high-pressure compressor (LPC and HPC) regions, to mitigate wear issues and extend the service life of critical components [3]. These coatings are renowned for their enhanced wear resistance, especially under high temperature conditions [8], [9]. Cr_3C_2-based coatings are typically processed as composite materials by co-deposition with nickel-chromium binder (i.e., Cr_3C_2-25NiCr). This combination improves toughness, ductility and facilitates effective load distribution between the carbides and the matrix phase [10]–[18]. Moreover, cemented chromium carbides possess good corrosion and oxidation resistance making them fit for use in harsh environments [20], [21]. However, research has indicated that some Cr_3C_2 phases dissolve into the NiCr matrix during spraying, leading to the formation of amorphous or nanocrystalline phases [19]. These phases are known to reduce the toughness of the matrix [8]. On the other hand, binder-free Cr_3C_2 particles pose a challenge during spraying due to their intrinsic hardness and lack of plastic deformation to allow coating build-up. However, the possibilities of fabricating binder-free Cr_3C_2 coatings have been demonstrated by several other authors using different spraying techniques. Brupbacher *et al.* [22] successfully deposited a thick binder-free Cr_3C_2 coating by the reducing plasma-sprayed Cr_2O_3 with methane-containing gas. The coating microstructure comprised of microporous Cr_3C_2 surface layer and considerable amount of Cr_2O_3 phases remains unconverted leading to insufficient carbide formation. Investigation by Förg *et al.* [23] demonstrated that Cr_3C_2 coatings can be achieved by high velocity suspension flame spraying (HVSFS). While partial oxidation and decarburization of Cr_3C_2 particles occur during spraying, the excess oxygen favors the coating's microhardness. In terms of tribological behavior, Umashanker *et al.* [24] studied the room temperature wear behavior of APS sprayed Cr_2O_3 and Cr_3C_2 coatings under different loading conditions. The results show that Cr_3C_2 coatings demonstrate the best wear performance due to low porosity and improved microhardness. Batraev *et al.* [21] study revealed that the mechanical and abrasive wear resistance of detonation sprayed Cr_3C_2 coatings were inferior to those of conventional Cr_3C_2-NiCr sprayed coatings. The reason was ascribed to the chemical interactions of Cr_3C_2 powder with the active components of the detonation product during spraying which led to formation of composite coatings as the oxygen and carbon ratio increases. The room temperature sliding and erosion wear behavior of suspension plasma sprayed Cr_3C_2 coatings were reported by Mahade *et al.* [25]. The improved tribological performance was attributed to the mechanical properties of nanostructured feedstocks, including higher hardness, increased cohesive strength, and high toughness. The available studies have demonstrated that binder-free Cr_3C_2 coatings deposited by plasma spray method exhibit improved sliding wear performance at room temperature. However, the details of the sliding wear behavior and wear mechanisms at high temperature conditions are still lacking. Thus, further research is needed to develop robust Cr_3C_2 coatings that can be compared with the well-established Cr_3C_2-25NiCr coatings.

Based on the preceding reviews, the aim of this present work was tailored towards assessing the microstructure, mechanical properties, and tribological behavior of binder-free Cr_3C_2 coatings. Plasma spray process was employed for the deposition of Cr_3C_2 particles due to the high melting temperature of chromium carbide measured at 2168 K [26]. Compared to other thermal spray processes, plasma spray methods can generate extremely high temperatures (exceeding 10,000°C), which are essential for melting refractory materials like chromium carbide [27]. Thus, it is anticipated that the high plasma temperature will ensure that Cr_3C_2 particles are sufficiently melted, resulting in improved adhesion and cohesion of the deposited coatings. The as-deposited Cr_3C_2 coatings were compared with the well-established Cr_3C_2-25NiCr powder deposited by APS and HVAF spray processes. The rationale for the comparison is to provide understanding of how different spray techniques and the presence of a binder influence the properties and performance of chromium carbide-based coatings. Moreover, HVAF process was selected because it is widely accepted for the deposition of Cr_3C_2-25NiCr powder due to lower temperatures and higher particle velocities which results in coatings with minimal oxidation and denser microstructures [12], [16], [28], [29]. The coating microstructures, compound phases, as well as the worn surfaces after sliding test were characterized using high resolution electron microscopy and X-ray diffraction. The wear mechanisms at room temperature and elevated temperature were analyzed based on *ex-situ* analysis. Finally, the observations from the *ex-situ* analysis were correlated to the differences in friction and wear behavior.

3.3 Experimental method

3.3.1 Feedstock material

The powders used in the study were commercially available sintered pure carbide (Cr_3C_2) powders and agglomerated and sintered cemented carbide (Cr_3C_2-25NiCr) supplied by Praxair Surface Technology, USA. The nominal powder size from the supplier was -45 µm for the pure chromium carbide, while that of cemented chromium carbide was -45 µm/+11 µm. In-house analysis of the powder particle size distribution was performed by dispersing the as-received powders in pure deionized water, using a particle size analyzer (Spraytec, Malvern Panalytical, UK) equipped with a wet dispersion accessory. The results are presented in (section 3.1).

3.3.2 Coating deposition

The APS spraying was performed using a Mettech Axial III plasma spray torch (Northwest Mettech Corp. Canada). The Mettech gun has three converging plasma jets which allow the axial injection of ceramic powder directly at the center of the plasma stream [30]. Furthermore, axial injection offers solutions to the problems that arise when attempting to penetrate the plasma radially with fine particles or droplets [31]. The deposition parameters used for spraying both powders are shown in Table 3.1 for APS and in Table 3.2 for HVAF. Two spray parameters designated as High power (HP), and Low power (LP) were used for the APS spraying processes. Investigation by Rotich *et al*. [32] reported that defects such as interlamellar cracks, oxide phases and porosity content decreased as the plasma power was increased. Similarly, Chang-Jiu *et al.* [33] study revealed that coatings with a comparable microstructure and properties to those deposited by conventional plasma spray can be achieved using a low-power spray torch. Based on the initial set of trials, a different plasma gas (Ar: 45%, N_2: 45%, H_2: 10%) was used for depositing APS Cr_3C_2-25NiCr (LP) to reduce the chances of overheating the particles [34].

On the other hand, the deposition of Cr_3C_2-25NiCr powder was performed using the commercial M3 HVAF torch (Uniquecoat Technologies LLC, USA), equipped with two types of convergent-divergent De Laval nozzles (4L2 and 4L4). These specific nozzle configurations have been previously employed by Kaveh *et al*. [35] for the successful deposition of WC-based coatings. According to

Matikainen *et al*. [36], the particle melting and subsequent carbide dissolution can be efficiently controlled by changing the nozzle geometry from cylindrical to convergent-divergent. In this study, similar nozzle configurations were used with the aim of optimizing the heating and melting degree of the particles, as well as the resulting carbide dissolution and decarburization. This approach offers a practical deposition process which is crucial for achieving the desired coating characteristics. Details of the nozzle setups and geometries can be found in the previously published article [36].

Table 3.1 APS parameters used for depositing chromium carbide-based coatings.

Deposition parameters	Spray condition	
	High power	Low power
Total plasma gas flow (l/min)	150	150
Current (A)	230	180
Power (kW)	112	73
Ar. (%)	0	50
N_2. (%)	80	20
H_2 (%)	20	30
Carrier (l/min)	8	12
Feed rate (g/min)	150	150
Spray Distance (mm)	100	100
Touch transverse speed (mm/s)	1000	1000
Number of passes	5	5

Table 3.2 HVAF parameters used for depositing chromium carbide-based coating.

Deposition parameters	Nozzles	
	4L2	4L4
Fuel type	Propylene	Propylene
Air pressure (psi)	96	96
Air Flow rate (NLPM)	7878	5584
Fuel 1 pressure (psi)	82	86
Fuel 1 flow rate (g/min)	393	359
Fuel 2 pressure (psi)	82	82
Fuel 2 flow rate (g/min)	287	266

Powder feed rate (g/min)	105	105
Carrier gas (L/min)	45	45
Torch traverse speed (mm/s)	1000	1000
Spray Distance (mm)	300	300
Number of passes	8	8

The powders were deposited on 304L stainless-steel substrate with dimensions of (25.4 × 25.4 × 4.3 mm). The steel substrate surfaces were grit-blasted using 20-grit alumina abrasive particles to increase the surface roughness and compressed air was used to remove grit residue from the surface. Thereafter, the substrates were preheated up to 150 °C before spraying to enhance adherence of the coatings to the substrates [5].

3.3.3 Characterization

The microstructural features of the chromium carbide powders were determined using Scanning Electron Microscopy (SEM) (SU8230, Hitachi, Japan) built with energy dispersive spectroscopy (EDS). The powder and coatings were prepared according to standard metallographic preparation (ASTM E03). The coating thicknesses were obtained from the prepared cross-section images. A confocal laser microscope (Olympus LEXT 4000, USA) was used to measure the coating surface roughness. Five readings were taken at different locations and averaged to determine the roughness value. The porosity and carbide retention were obtained with ImageJ software by considering ten backscattered SEM images at 2.00 k magnification (20 µm scale bar) in different locations of coating according to standard ASTM E2109-01 practice [37].

The phase analysis of powder and coatings was characterized by using Philips X'Pert Pro X-ray diffractometer system (Malvern Panalytical, UK) with Cu-Kα radiation (step size = 0.02°, time per step = 2 sec, $\lambda = 1.5406$ Å, scanning range 2Θ of 20° and 90°) was used and operated at a power of 40 kV and 40 mA. The obtained diffractograms were analyzed and indexed using the Rietveld analytical software built with the XRD system.

The Vickers microhardness was measured on a polished cross-section using a Micro combi tester-MCT^3 (Anton Paar, Switzerland) according to the EN ISO 4516 standard. A load of 3 N ($HV_{0.3}$) were selected with a dwell time of 10 s. For each load, 15 impressions were performed at different spots to average the microhardness of coatings.

3.3.4 Tribology testing and post-test characterization

The APS Cr_3C_2 (HP), APS Cr_3C_2-25NiCr (LP), and HVAF Cr_3C_2-25NiCr (4L4) coatings were selected for tribological assessment due to their relatively dense microstructure characterized by low porosity and high microhardness values. The wear test matrices are presented in Table 3.3, and the sliding wear tests were conducted with three repetitions for each coating. The coatings were subjected to wear testing at room (25 °C) and elevated temperature (450 °C) in dry sliding conditions without polishing the coating surface to replicate real-world conditions. A reciprocating ball-on-flat tribometer (Anton Paar TriTec SA, Switzerland) was used for the sliding wear testing of the coatings. The average wear volume and the standard deviation were determined by considering the area under the curve minus material pile-up of each profile. The applied 10 N load was chosen to enhance high contact stress and repeated sliding action (accelerated condition) on the coating surface. Furthermore, the alumina counter body was selected because of its hardness, high-temperature stability, and chemical inertness [38].

Prior to the high temperature wear test, the coatings and alumina counterball (Φ 6. 35 mm) was heated up to 450 °C. However, the measured temperature on the top side during sliding wear test was 340 °C. This is because the wear test was performed under room temperature atmosphere which resulted in significant heat loss at the top side of the heating stage. A total of three repeat tests were performed to average the friction value. The wear volume loss of the tested coatings was analyzed using a confocal laser microscope (Olympus LEXT 4000, USA). Thereafter, scanning electron microscope (SEM) and energy dispersive spectroscopy (EDS) were employed to interpret the wear surface morphologies and identify the tribolayers formed on the worn surface of the wear tracks. Raman measurements were performed on the worn surface using InVia spectrometer (Renishaw, UK) with radiation $\lambda = 514$ nm and Ar^+ laser source.

Table 3.3 The friction test parameters of the ball on flat tribometer.

Tribology testing parameters	Values
Applied load, N	10
Track length, mm	10
Frequency, Hz	1
Total sliding cycle	2500
Total sliding distance, m	50
Counter body (Al_2O_3) dia. mm	6.35
Test temperatures (°C)	25 and 450

3.4 Results

3.4.1 Feedstock and coating characteristics

The powder morphology of Cr_3C_2 and Cr_3C_2-25NiCr in the as-received condition are presented in Fig. 3.1a-b, respectively. The Cr_3C_2 powder (Fig. 3.1a) is characterized by angular morphology with irregular particle shapes and sizes [21]. The Cr_3C_2-25NiCr powder is composed of spherical morphology with a considerable amount of intragranular porosity as shown in Fig. 3.1b. Additionally, the Cr_3C_2-25NiCr particles showed adequate bonding with the surrounding binder which is a characteristic feature of commercial grade agglomerated and sintered powders [15].

The particle size distribution of Cr_3C_2 and Cr_3C_2-25NiCr powder values is presented in Fig. 3.1c-d. The particle size distribution of the Cr_3C_2 powder [i.e., Dv (10), Dv (50), and Dv (90)] was measured to be 8 µm, 18 µm, and 40 µm, while that of Cr_3C_2-25NiCr powder were 21 µm, 34 µm, and 54 µm, respectively. Comparing these results with those provided by the supplier, the Cr_3C_2-25NiCr particles appeared slightly agglomerated. Thus, it can be inferred that Cr_3C_2-25NiCr particle sizes are marginally larger than those of Cr_3C_2 particles.

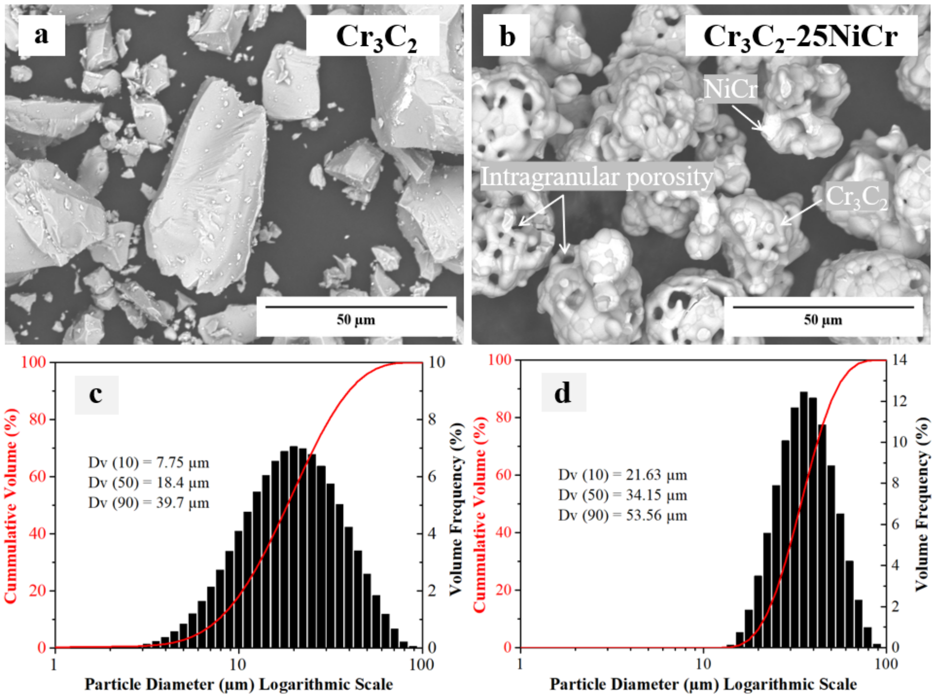

Figure 3.1 SEM morphology and particle size distribution of chromium carbide-based powder, (a-c) Cr_3C_2, (b-d) Cr_3C_2-25NiCr, [Dv: median for volume distribution].

The XRD diffraction pattern of APS coatings are presented in Fig. 3.2a. In all APS coatings, diffraction peaks corresponding to Cr_7C_3 and Cr_3O_2 appeared while Cr_3C_2 diffraction peaks were not detected. Also, the detected NiCr peak intensity of APS Cr_3C_2-25NiCr (LP) and APS Cr_3C_2-25NiCr (HP) coatings was lower compared to the initial feedstock powder. Therefore, it can be inferred that phase transformation and decomposition of Cr_3C_2 phase occur in APS coatings.

The XRD diffraction pattern of HVAF coatings are presented in Fig. 3.2b. The phase composition of HVAF coatings (i.e., 4L4 and 4L2 nozzles) comprise mainly of peaks corresponding to Cr_3C_2 and F.C.C NiCr, while phases such as (Cr_7C_3 and $Cr_{23}C_7$) or chromium oxides (Cr_3O_2) were not identified. This can be interpreted by the fact that HVAF process leads to less decarburization or oxidation compared to APS, due to lower processing temperatures. However, a broad peak between 42° and 45° was identified for both coatings. Additionally, a reduction in the F.C.C NiCr diffraction peak towards the lower 2ϴ was also observed and pronounced in 4L2 than 4L4 spray condition. The effects occur due to the presence of larger Cr solute atoms in the metallic phase [18].

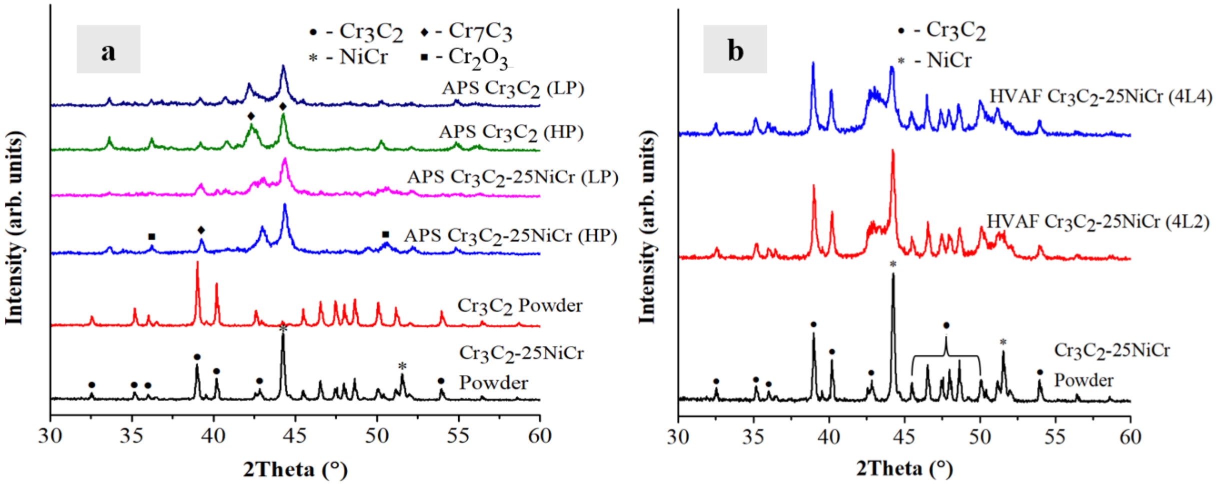

Figure 3.2 XRD diffraction patterns of chromium carbide-based feedstocks powder and as-sprayed coatings (a) APS, (b) HVAF

The cross-sections and EDS elemental mapping of APS sprayed coatings with high and low power are presented in Fig. 3.3a-d. The microstructure of all APS coating exhibits a typical lamellae structure characterized by porosities and microcracks between intersplat regions. The thickness, surface roughness, deposition efficiency and porosity are presented in Table 3.4. Among the Cr_3C_2 coatings, APS sprayed Cr_3C_2 (LP) coating exhibit a higher porosity content compared to the APS sprayed Cr_3C_2 (HP) coating. Whereas among the Cr_3C_2-25NiCr coatings, the APS sprayed Cr_3C_2-25NiCr (LP) coating demonstrated the lowest porosity content (i.e. compared to the APS Cr_3C_2-25NiCr (HP) coating), as well as exhibit the highest thickness, roughness, and deposition efficiency than all the APS sprayed coatings. While other APS coatings demonstrate complete melting of carbide phases, some considerable amount of carbide phases measured to be 19.3 ± 1.1 vol. % were retained in APS Cr_3C_2-25NiCr (LP) coating as shown in Fig. 3.3c and tabulated in Table 3.4. It is worth mentioning that the carbide retention in other APS coatings could not be determined due to significant melting. Also, all the APS coatings are characterized by different contrasts. In the APS Cr_3C_2 (LP) and APS Cr_3C_2 (HP) coatings, the dark grey contrast comprised of chromium, carbon, and oxygen while the light grey contrast is composed of chromium and carbon with negligible oxygen [23]. In the APS Cr_3C_2-25NiCr (LP) and APS Cr_3C_2-25NiCr (HP) coatings, the darkest grey contrast, mostly found in Fig. 3.3c comprised of chromium and carbon without nickel indicating the secondary Cr_7C_3 phases, as found in XRD analysis (Fig. 3.2a). The light grey contrast is composed of chromium, carbon and nickel representing dissolved carbides in supersaturated nickel solid solutions [38], [39]. The EDS mapping results revealed the presence of chromium, carbon, oxygen for all APS coatings, and nickel for Cr_3C_2-25NiCr coatings. The presence of oxygen agrees with the formation of Cr_2O_3 which has also been reported in previous study [11], [23].

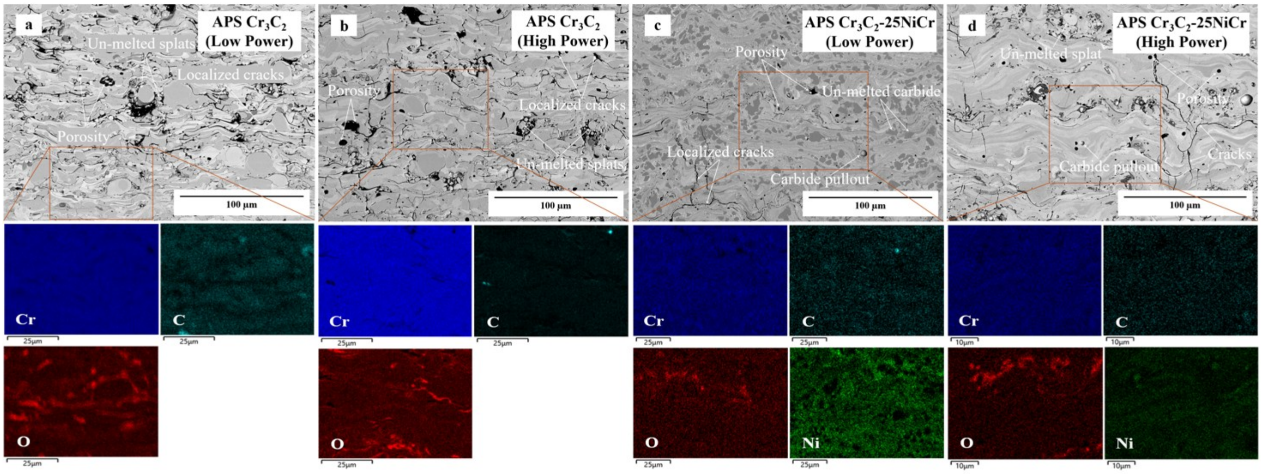

Figure 3.3 Cross-sectional SEM images and elemental map analysis of APS sprayed coatings (a) Cr_3C_2 (LP), (b) Cr_3C_2 (HP), (c) Cr_3C_2-25NiCr (LP), (d) Cr_3C_2-25NiCr (HP).

The cross-sections and EDS elemental mapping of HVAF sprayed Cr_3C_2-25NiCr coatings with 4L2 and 4L4 nozzles are presented in Fig. 3.4a-b. Both coatings exhibit a dense microstructure characterized by hard Cr_3C_2 phases bonded in NiCr matrix binder indicating minimal degradation of carbide particles. Moreover, carbide cracks with uniformly distributed fine porosities were also observed in both HVAF coatings. The coating thickness, surface roughness, deposition efficiency and porosity are presented in Table 3.4. Both HVAF spray coatings show comparable thickness, roughness, and deposition efficiency. However, the porosity content in HVAF Cr_3C_2-25NiC (4L2) spray coating is marginally higher than the HVAF Cr_3C_2-25NiCr (4L4) spray coating. The dark grey contrast is composed of chromium and carbon which represents the primary Cr_3C_2 phases while the light grey regions are composed of chromium, carbon and nickel which represents solute Cr_3C_2 in NiCr matrix [15] and correlated with the XRD findings in Fig. 3.2b. Meanwhile, the white contrast represents the Ni-rich regions. The carbide content for all HVAF spray coatings is presented in Table 3.4. The chromium carbide content of HVAF Cr_3C_2-25NiCr (4L2) and HVAF Cr_3C_2-25NiCr (4L4) coatings were measured to be 57.3 and 52.9%, respectively. It should be reminded that the nominal volume fraction of Cr_3C_2 in commercial 75Cr_3C_2-25NiCr powder is approximately 79% [17], [36]. Therefore, it can be inferred that 4L2 and 4L4 nozzle sprayed Cr_3C_2-25NiCr coatings exhibit lower Cr_3C_2 content than the initial feedstock powder. The EDS mapping results revealed the distributions of Cr, C and Ni with negligible O content. The EDS results are indications that HVAF method produced minimal in-flight oxidation of carbide particles compared to APS method.

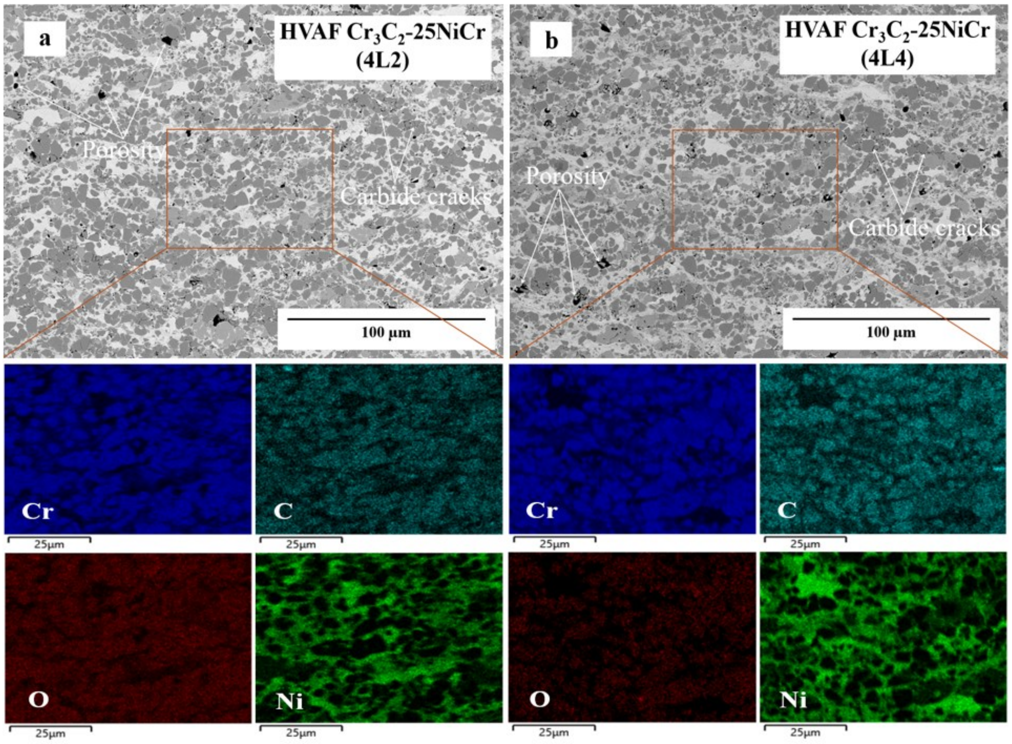

Figure 3.4 Cross-sectional SEM images and elemental map analysis of HVAF sprayed Cr3C2-25NiCr coatings, (a) 4L2 nozzle, (b) 4L4 nozzle.

Table 3.4 Microstructural parameters, carbide and matrix contents of all coatings (average ± standard deviation)

Sample designation	Thickness (µm)	Roughness (µm)	DE (%)	Porosity (%)	Carbide (vol.%)	Matrix (vol.%)
APS Cr_3C_2 (LP)	265 ± 10	9 ± 0.3	54	11.7 ± 1.0	–	–
APS Cr_3C_2 (HP)	245 ± 7	8 ± 0.3	57	10.3 ± 0.8	–	–

APS Cr_3C_2-25NiCr (LP)	350 ± 7	15 ± 2	87	2.5 ± 0.2	19.3 ± 1.1	78.2 ± 3.0
APS Cr_3C_2-25NiCr (HP)	250 ± 3	10 ± 0.2	62	7.1 ± 0.5	—	—
HVAF Cr_3C_2-25NiCr (4L2)	315 ± 9	8 ± 0.3	39	2.7 ± 0.2	57.3 ± 0.2	40.0 ± 1.0
HVAF Cr_3C_2-25NiCr (4L4)	320 ± 4	7 ± 0.3	35	1.8 ± 0.1	52.9 ± 0.8	45.3 ± 1.0

The average microhardness values are presented in Fig. 3.5. The APS Cr_3C_2 (LP) coating has lower microhardness values than the APS Cr_3C_2 (HP) coating. However, the APS Cr_3C_2-25NiCr (LP) coating has higher microhardness values than APS Cr_3C_2-25NiCr (HP) coating and even demonstrates the highest average microhardness value (960 $HV_{0.3}$) among the APS coatings. On the other hand, HVAF Cr_3C_2-25NiCr (4L4) coating demonstrates a higher microhardness than the HVAF Cr_3C_2-25NiCr (4L2) coating. The microhardness value of HVAF Cr_3C_2-25NiCr (4L4) coating is lower than all the APS sprayed coatings except APS Cr_3C_2 (LP) coating and even lower than those reported by other authors with similar chemical composition [16], [18].

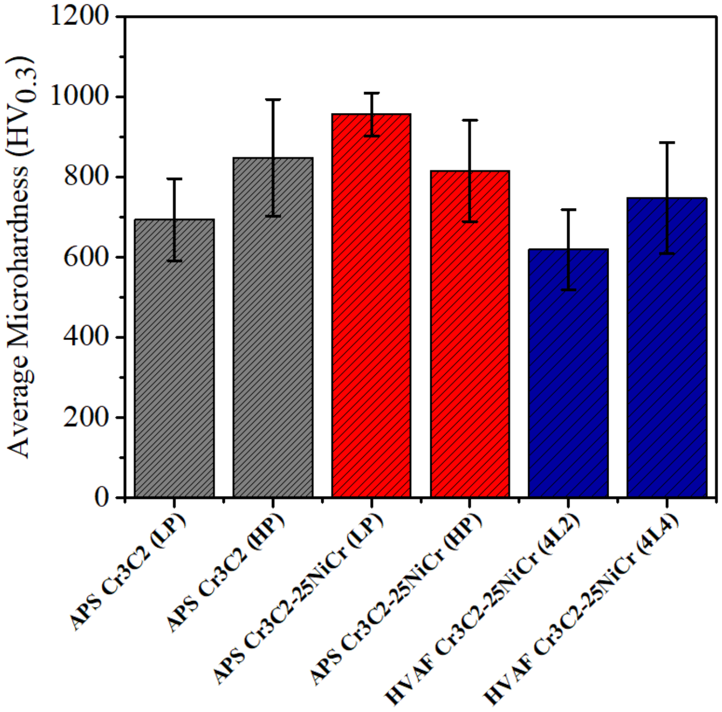

Figure 3.5 Vickers microhardness of Cr_3C_2 and Cr_3C_2-25NiCr coatings at room temperature

3.4.2 Sliding wear behavior

3.4.2.1 Friction coefficient and wear volume

The friction coefficient versus the number of sliding cycles for the RT tests is presented in Fig. 3.6a. The coefficient of friction of APS Cr_3C_2 (HP) coating increased from 0.38 to ~ 0.78 upon initial 250 sliding cycles and dropped sharply to 0.59. Subsequently, it increased again to ~ 0.76 and stabilized gradually at around ~ 0.68 up till the entire sliding test duration. On the other hand, both APS Cr_3C_2-25NiCr (LP) and HVAF Cr_3C_2-25NiCr (4L4) coating show extended running-in regime within 1000 sliding cycles. The friction coefficient of APS Cr_3C_2-25NiCr (LP) coating increased from ~ 0.36 to ~ 0.52, while that of HVAF Cr_3C_2-25NiCr (4L4) coating increased from ~ 0.24 to ~ 0.48. Both coatings attained a comparable steady state friction at around ~ 0.48.

Figure 3.6 b presents the friction coefficient versus number of cycles plot for all tested coatings at HT. It can be observed that the steady-state regime was attained after a short sliding cycle (250 cycles) compared to RT. The friction coefficient of APS Cr_3C_2 (HP) coating increased slightly from ~ 0.66 to ~ 0.78 and subsequently decreased to a steady-state value of ~ 0.66 with a fluctuating profile that lasted throughout the test duration. Similarly for APS Cr_3C_2-25NiCr (LP) coating, the friction coefficient decreased sharply from a peak of ~ 0.62 to ~ 0.42 but display increased variation around 0.44 towards the end of the test. On the other hand, HVAF Cr_3C_2-25NiCr (4L4) coating have an initial friction of ~ 0.3 which increased slightly to a steady-state regime that varies between ~ 0.38 and ~ 0.4 up till the entire sliding test.

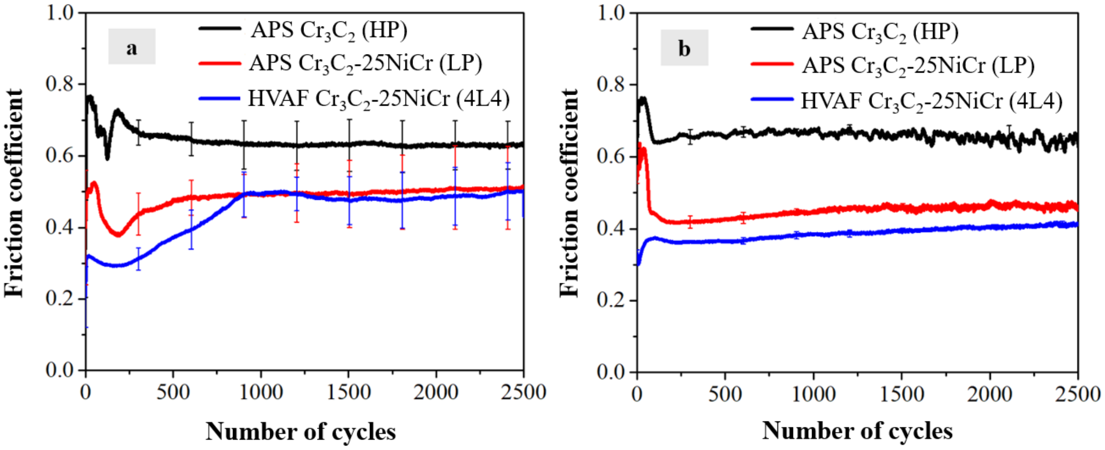

Figure 3.6 Variation of friction coefficient (COF) with sliding distance at load of 10 N for all as-sprayed chromium carbide coatings at (a) room temperature (b) elevated temperature

The specific wear volume plot of all tested coatings at RT are presented in Fig. 3.7. The wear volume loss for all tested coatings follows a descending trend. For the APS Cr_3C_2 (HP) coating, the wear volume was 12.7×10^{-2} mm^3, which is three times higher than the APS Cr_3C_2-25NiCr (LP) coating (4.2×10^{-2} mm^3), and eight times higher than the HVAF Cr_3C_2-25NiCr (4L4) coating (1.5×10^{-2} mm^3).

For the high temperature conditions, the wear volume loss was higher at 450 °C than at RT. The APS Cr_3C_2 (HP) coating volume was 14.0×10^{-2} mm^3, which is 38% more than APS Cr_3C_2-25NiCr (LP) coating (10.1×10^{-2} mm^3), and almost three times higher than that of HVAF Cr_3C_2-25NiCr (4L4) coating (4.6×10^{-2} mm^3).

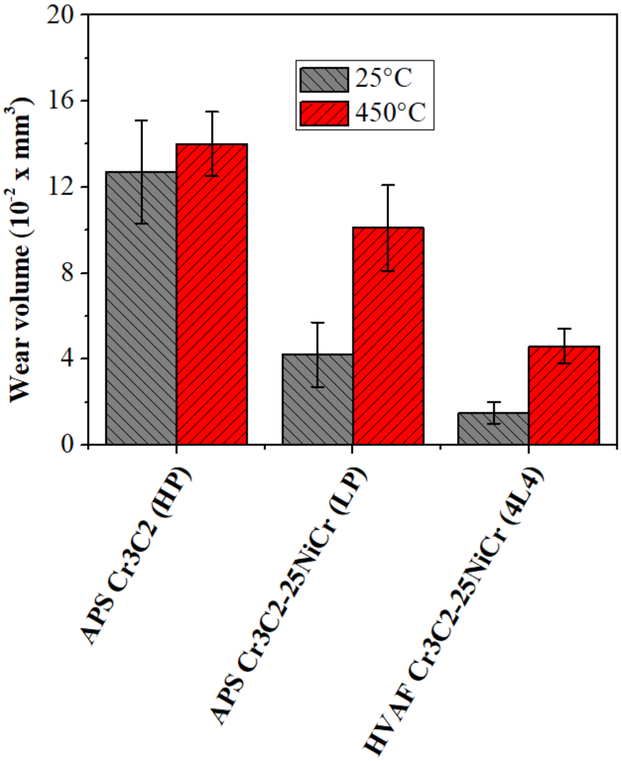

Figure 3.7 Specific wear volume of as-sprayed chromium carbide-based coatings.

3.4.3 Ex-situ analysis

3.4.3.1 Worn surface morphologies

The SEM micrographs of the worn surface for all tested coatings at room temperatures are presented in Fig. 3.8a-c. The SEM image of the worn APS Cr_3C_2 (HP) coating surface showed inherent pores, delaminated layer, and extended surface cracks, which propagated across the carbide grains. Similarly, the worn surface of APS Cr_3C_2-25NiCr (LP) coating in Fig. 3.8b also revealed significant crack regions as well as delaminated layer covered by loose and clustered debris. The HVAF Cr_3C_2-25NiCr (4L4) coating worn surface in Fig. 3.8c exhibits a homogeneous surface morphology characterized by smeared layer, pullout, and plastically deformed carbide particles. The SEM/EDS mapping confirmed that the dark phase on the worn-out surface of all tested coatings is rich in oxygen, indicating the formation of tribo-oxide layer. The worn surface of APS Cr_3C_2 (HP) and APS Cr_3C_2-25NiCr (LP) coatings had higher oxygen content than the HVAF Cr_3C_2-25NiCr (4L4).

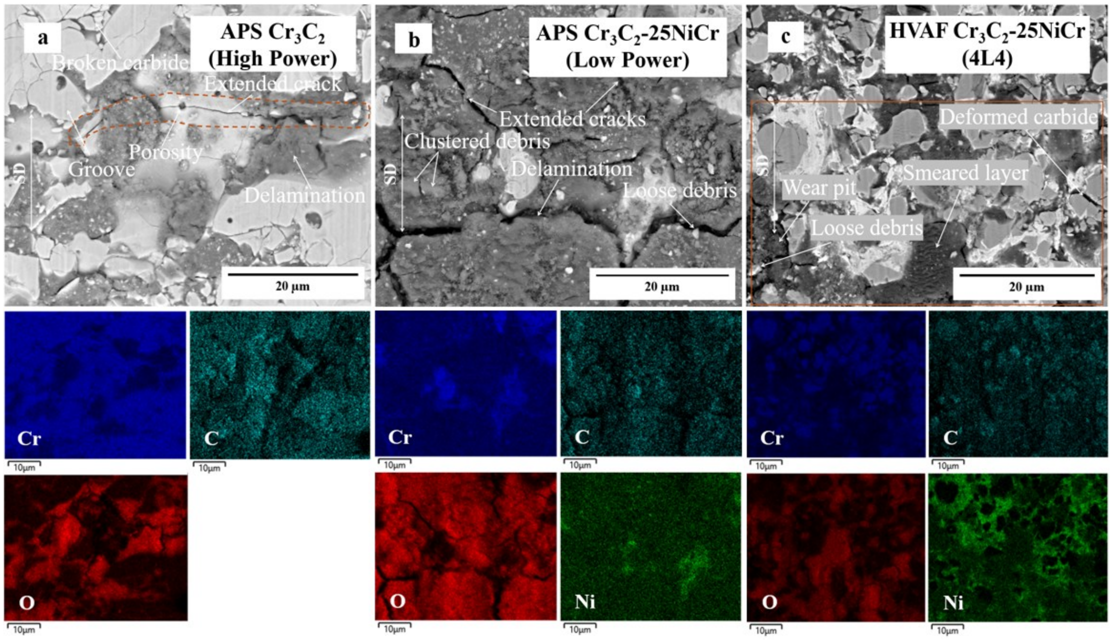

Figure 3.8 SEM worn surface morphologies and elemental map analysis of (a) APS Cr_3C_2 (HP) (b) APS Cr_3C_2-25NiCr (LP) (c) HVAF Cr_3C_2-25NiCr (4L4) at RT.

Similarly, the SEM micrographs of the worn surface for all tested coatings at 450 °C are presented in Figure 3.9a-c. It can be observed that APS Cr_3C_2 (HP) and APS Cr_3C_2-25NiCr (LP) coatings (Fig. 3.9a-b) undergo significant wear damage than at RT. Both surfaces are comprised of delaminated layer, extended surface cracking and high volume of fragmented wear debris covering the entire worn surface. Whereas the HVAF Cr_3C_2-25NiCr (4L4) coating worn-out surface in Fig. 3.9c exhibit features of embedded debris (adhesion) and plastically deformed carbides. Furthermore, visible wear pit containing debris particles possibly formed by continuous carbide pull-out were also observed. The SEM/EDS mapping presented showed homogeneous distribution of elements on the worn coating surface having high amount of oxygen content. The higher oxygen content observed for all tested coatings is an indicator that significant oxidation occurs at elevated temperature compared to room temperature.

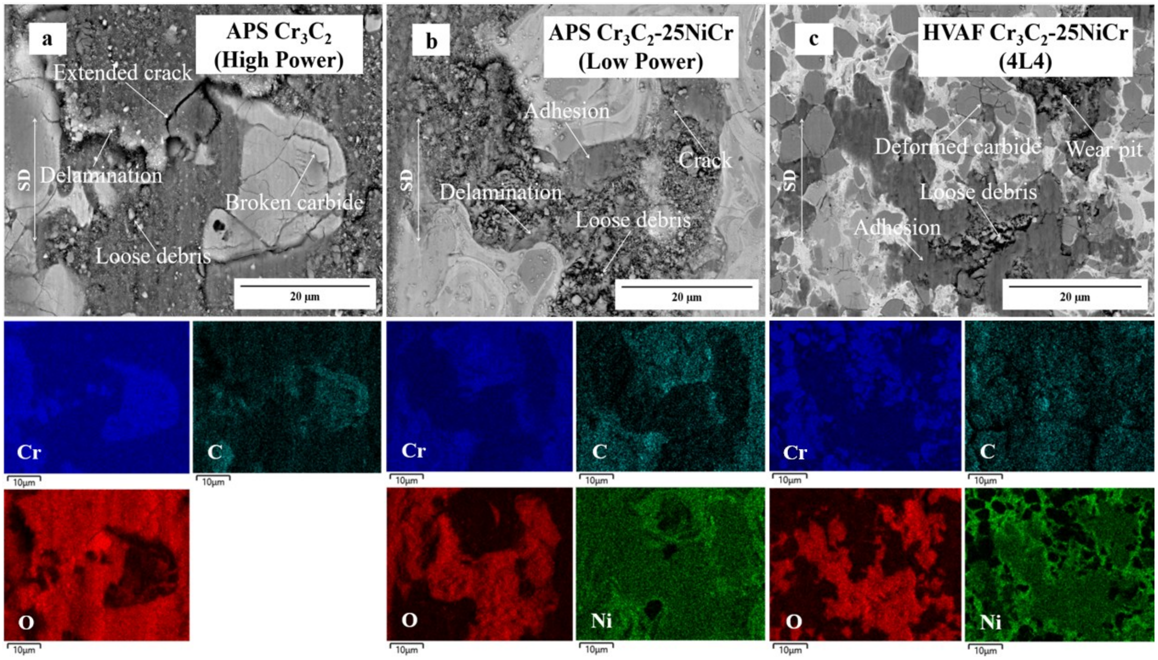

Figure 3.9 SEM worn surface morphologies and elemental map analysis of (a) APS Cr_3C_2 (HP) (b) APS Cr_3C_2-25NiCr (LP) (c) HVAF Cr_3C_2-25NiCr (4L4) at HT.

3.4.3.2 Raman analysis

Raman spectroscopy following the sliding tests at RT and 450 °C are shown in Fig. 3.10a-b. As observed, the characteristic peaks on the worn surface at 303 cm^{-1}, 348 cm^{-1}, and 548 cm^{-1} correspond to Cr_2O_3, while the peak at 691 cm^{-1} corresponds to amorphous CrO_2 [40]. The intensity of the oxide peaks for both APS coatings is higher compared to the oxide peak intensity for HVAF coating. Furthermore, characteristic broad bands of graphite peaks were also observed in all coatings around 1350 cm^{-1} and 1580 cm^{-1} at RT and 450 °C [18]. The Raman results also confirmed that a mixed composite of chromium oxide tribo-films was formed on the worn surface which supports the counterball EDS point analysis observations in Table 3.5.

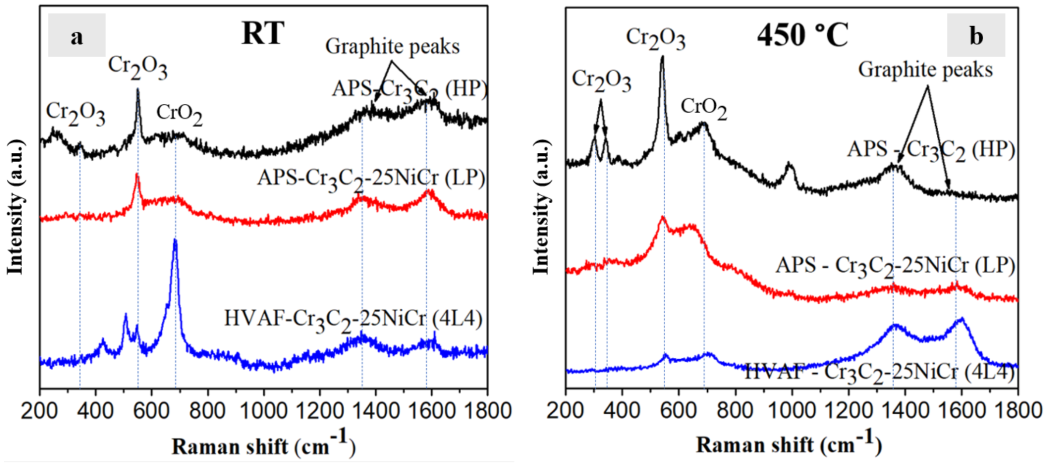

Figure 3.10 Raman spectrum of worn coatings at (a) 25 °C, and (b) 450 °C.

3.4.3.3 Cross-section of worn surfaces

Figure 3.11 presents the cross-section SEM micrographs of the worn coatings at RT and 450 °C. At RT, non-uniform tribo-film were formed on the surface of APS Cr_3C_2 (HP) and APS Cr_3C_2-25NiCr (LP) coatings (Fig. 3.11a and 3.11c). Furthermore, defects such as subsurface cracking were evident on the cross-section surface of both APS coatings. Whereas a uniform tribo-film of 3 ± 0.7 µm thick can be observed for HVAF Cr_3C_2-25NiCr (4L4) coating in Fig. 3.11e. At 450 °C, a small amount of tribo-film with significant subsurface cracking can be observed for APS Cr_3C_2 (HP) coating in Fig. 3.11b. APS Cr_3C_2-25NiCr (LP) coating shows no evidence of tribo-film formation (Fig. 3.11d). However, a slightly unform tribo-film of 1 ± 0.2 µm thick was formed on the sliding interface of HVAF Cr_3C_2-25NiCr (4L4) coating in Fig. 3.11f.

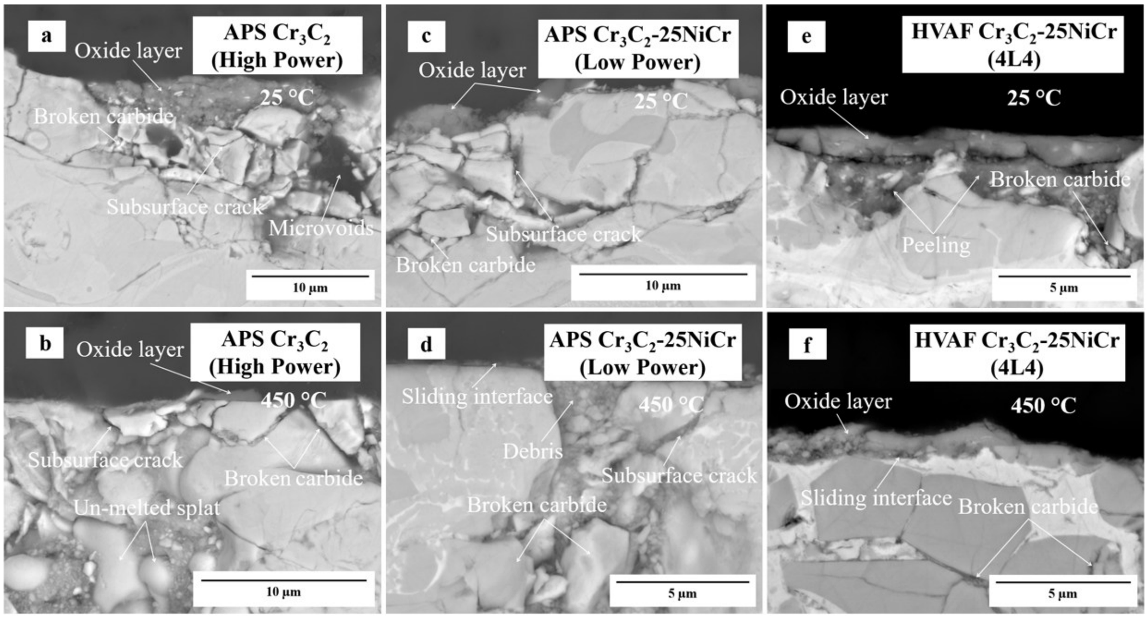

Figure 3.11 SEM wear track cross-sections of chromium carbide-based coatings at RT and 450 °C conditions (a and b) APS Cr_3C_2 (HP), (c and d) APS Cr_3C_2-25NiCr (LP), and (e and f) HVAF Cr_3C_2-25NiCr (4L4).

3.4.3.4 Sliding counterface

The SEM micrographs of the alumina counterball following sliding contact against the tested coatings at RT and 450 °C are presented in Fig. 3.12a-f. At RT, high material transfer to the alumina counterparts was observed for the APS Cr_3C_2 (HP) coating. Whereas low material transfer was observed on the APS Cr_3C_2-25NiCr (LP) coating counterball, while the HVAF Cr_3C_2-25NiCr (4L4) coating counterparts exhibit the lowest material transfer and lowest contact area. At 450 °C, a considerable amount of transferred materials was evident on the counterball of all tested coatings. The transferred materials are relatively smooth with less rupture morphology compared to those observed at RT. Overall, the APS Cr_3C_2 (HP) coating had the highest material transfer to the counterface with a relatively larger concentric contact area followed by APS Cr_3C_2-25NiCr (LP) counterball. On the other hand, HVAF Cr_3C_2-25NiCr (4L4) counterball displayed the lowest transfer layer with lowest concentric contact area.

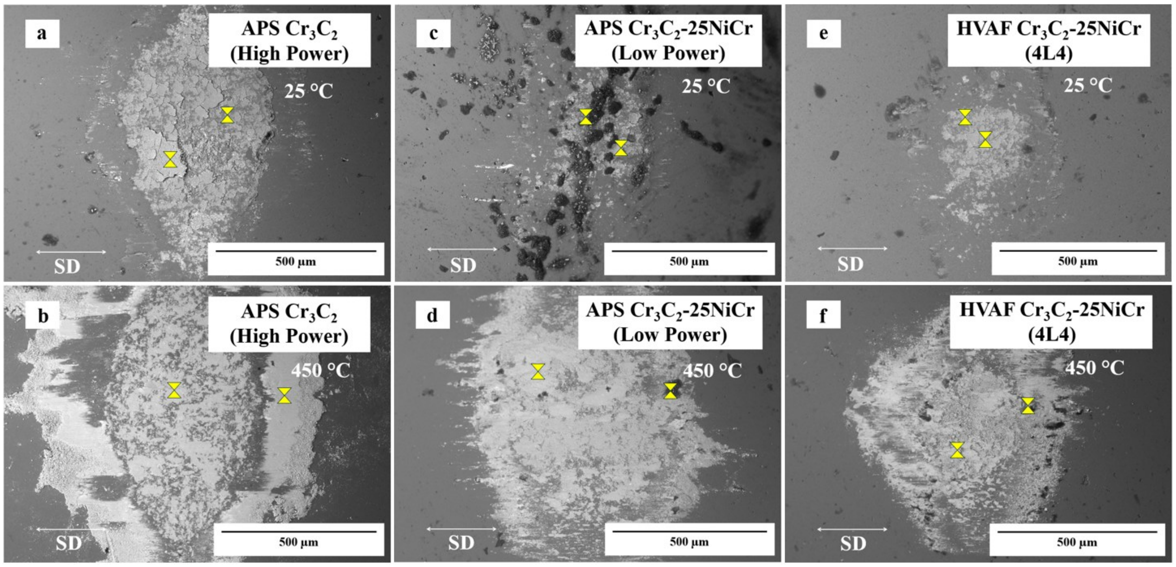

Figure 3.12 SEM images of the alumina counter balls sliding against chromium carbide-based coatings at RT and 450 °C conditions, (a and b) APS Cr_3C_2 (HP), (c and d) APS Cr_3C_2-25NiCr (LP), and (e and f) HVAF Cr_3C_2-25NiCr (4L4).

Table 3.5 presents the chemical compositions (wt.%) at two different locations on the alumina counterball. Elements found on the counterball of all tested coatings are predominantly C, O, Al, Cr, as well as Ni for Cr_3C_2-25NiCr coatings. As the Cr content increases, the Al content decreases for all tested coatings except HVAF Cr_3C_2-25NiCr coatings, when temperature increases from 25 °C to 450 °C. This observation can be interpreted by the fact that considerable amount of chromium oxide was formed at elevated temperatures than at room temperature.

Table 3.5 Chemical composition (average) of selected positions in Fig. 3.12 determined by EDS.

Elements	APS Cr_3C_2 (HP)		APS Cr_3C_2-25NiCr (LP)		HVAF Cr_3C_2-25NiCr (4L4)	
	RT	HT	RT	HT	RT	HT
C	5.0	4.0	35	37	12	27
O	50	40	35	28	46	24
Al	20	5	6	4	11	7
Cr	25	51	18	24	21	22
Ni	-	-	6	7	10	20

3.5 Discussions

3.5.1 Microstructure, Characterization, and Microhardness

The higher porosity content of the APS sprayed Cr_3C_2 coatings (Fig. 3.3a and 3.3b) when compared to the APS sprayed Cr_3C_2-25NiCr coatings (Fig. 3.3c and 3.3d) is ascribed to the significant amount of unmolten particles within the APS sprayed Cr_3C_2 coatings. Those unmolten particles form weak bonds with the surrounding molten particles, resulting in numerous intersplat zones characterized by oxide layers, microcracks and high porosity [42]. Oxide layers within intersplat zones also contribute to the increased oxidation of the APS sprayed Cr_3C_2 coatings. Moreover, previous research have shown Cr_3C_2 particles are sensitive to air and readily reacts with oxygen at 488 °C to form Cr_2O_3 than cemented carbide [43]. Whereas APS sprayed Cr_3C_2-25NiCr coatings (Fig. 3.3c and 3.3d) are mainly dominated by molten and flattened splats with fewer pore regions due to the presence of soft metallic (NiCr) phase. The metallic phases typically melt at (1,690 K) to form molten NiCr [44]. The resulting molten NiCr wet and increase cohesion with the carbides phase, thereby filling the micro-voids created by the hard carbide particles, while reducing the overall porosity content [11]. The presence of Cr_7C_3 and Cr_3O_2 phases observed for all APS coatings (Fig. 3.2a) is an indication that the APS method leads to decarburization and oxidation of Cr_3C_2 phase due to high processing temperature, which has been previously reported [11], [39]. On the other hand, both HVAF spray coatings (Fig. 3.4a-b) comprise of higher content of partially deformed/undeformed Cr_3C_2 particles when compared to the coatings produced by APS process. This implies that HVAF spraying of Cr_3C_2-25NiCr mainly undergoes plastic deformation with minimal degradation. The minimal carbide degradation can be attributed to the higher particle velocity and lower particle temperature in HVAF processes, which reduces the chances of carbide exposure to the combustion flame [15], [17], [44]. The XRD results in Fig. 3.2b also confirmed that the phase composition of HVAF sprayed Cr_3C_2-25NiCr coatings (4L2 and 4L4) were similar and comprised of minimal oxidation/decarburization. The broad peaks observed between 42° and 45° in the XRD patterns indicate the formation of amorphous or nanocrystalline phases resulting from rapid solidification during processing. Similar results have been reported by several authors [15], [17]. The porosity contents in both HVAF coatings seamlessly reveal the effects of pre-existing intergranular pores and carbide cracks in Fig. 3.1b, Fig. 3.4a and 3.4b, respectively. Carbide cracking are typical characteristics of agglomerated and sintered Cr_3C_2-25NiCr powder formed when particles impinges the substrate at high speeds, causing the fragmentation of carbides upon impact [36]. The general loss of carbide contents as shown in Table 4 largely depends on the rebounding of poorly adhered particles, selective deposition of particles, and carbide dissolution within the metallic phase [18], [36].

The microhardness measurements in Fig. 3.5 indicated that the APS sprayed Cr_3C_2-25NiCr (LP) coating was the hardest of the APS coatings. This higher hardness is attributed to the microstructural features of the coating. Firstly, the optimized parameters (refer to section 3.3.2) used for the deposition of the APS Cr_3C_2-25NiCr (LP) coating resulted in good interlamellar cohesion and low porosity compared to other APS coatings. In contrast, other APS spray coatings had high amount of porosity and decohesion which reduces coating density, lowers the elastic modulus, and hinders the uniform distribution of loads [11]. Besides the porosity effect, the effects of Cr_7C_3 phase are another key factor that determine APS hardness. Among the APS coatings, APS Cr_3C_2-25NiCr (LP) coating display retention of Cr_7C_3 phase as confirmed by the XRD analysis in Fig. 3.2a. These secondary phases provide solid solution strengthening of the soft NiCr phase [46]. It is likely that the indentation marks were made in areas of the matrix strengthened by Cr_7C_3 phases leading to increased hardness [8], [47]. HVAF Cr_3C_2-25NiCr (4L4) coating also demonstrates improved hardness compared to the 4L2 coating due to its lower porosity content. However, its hardness is lower when compared to the APS Cr_3C_2-25NiCr (LP) coating. The microhardness behavior in this context is largely influenced by the amount of oxides present, such that the higher the oxide content, the higher the microhardness [23].

3.5.2 Friction and Wear Behavior

At RT, all the tested coatings exhibit a low COF (Fig. 3.6a) during the initial running-in stage, possibly due to a low amount of adhesion and interaction between the surface asperities and the counterface [48]. However, the COF increases as the sliding test progresses, and that APS Cr_3C_2 (HP) coating demonstrates a higher COF than the other tested samples. The sudden increase in the COF may be attributed to higher adhesion resulting from interactions between surface asperities and the counterface [49], as well as ploughing formation due to the breakdown of cold weld zone [18]. Similar behavior was reported for HVOF sprayed WC-12Co coating [50], where increase in the amount of ploughing resulted in higher COF. Moreover, the high surface roughness for example APS Cr_3C_2-25NiCr (LP) coating, likely contributes to the high and unstable COF observed, particularly during the running-in stage of the sliding test. The roughness increases the real contact area between the mating surface resulting in high COF as the asperities interact [51]. The studies by Feng *et al.* [52] and Siu *et al.* [53] also revealed that friction coefficient tends to increase with increase in surface roughness. Following this initial increase, there was a sharp decrease in the COF observed for all tested coatings. The decease in COF was more pronounced for APS coatings and less pronounced for HVAF coating. The decreased COF could indicate the reduction of adhesion in the contact interfaces due to the formation of protective layers (i.e., oxide layers from the previously generated wear debris). However, when the oxide layer thickness reached a critical value and strain became too high, the oxide layers breakdown [54], [55]. This phenomenon led to an increase in the COF for all the tested coatings as the test proceeded and eventually reached the steady state conditions. At 450 °C, the friction behavior follows a similar trend to the RT with a lower starting friction value (Fig. 3.6b). However, all the tested coatings attained the steady-state regime faster due to oxides formation in the contact interfaces [50]. The sliding test proceeds with an increased COF for all the samples tested. While a sharp decrease in COF and subsequent steady-state regime was observed for all coatings, the lowest COF was observed for HVAF. This low COF could be due to the low adhesion between the interacting surfaces during sliding because of the formation of smeared smooth layer on the wear tracks [56].

Based on the *ex-situ analysis*, the proposed wear mechanism of thermally sprayed Cr_3C_2 and Cr_3C_2-NiCr coatings are illustrated in Fig. 3.13. At RT, the APS Cr_3C_2 (HP) coating exhibits the highest wear rate, likely due to its high porosity, low density and poorly bonded particles. Additionally, low hardness and brittle behavior of the coating could contribute to high wear. Researchers found that high porosity and high brittleness are assumed to promote crack propagation during repeated loading, promoting removal of carbide particles and delamination of the tribo-oxide film (Fig. 3.8a), leading to increased wear [50], [57]. Also, the significant transfer of materials to the counterface (Fig. 3.12a), correlated well with the reduced hardness and high wear of APS Cr_3C_2 (HP) coating. On the other hand, the APS Cr_3C_2-25NiCr (LP) coating exhibited a much lower wear rate (i.e., ~ 67% lower) compared to the APS Cr_3C_2 (HP) coating. The improved wear resistance is ascribed to its low porosity (Table 4) and high hardness (Fig. 3.5). While the worn surface is characterized by surface cracks and delaminated tribo-oxide layer (Fig. 3.8b), the counterface contain low transferred material compared to the APS Cr_3C_2 (HP) coating (Fig. 3.12c), which could be due to its high hardness [56]. The low wear due to high hardness was observed by Sikorski *et al.* [56] where they showed that the harder materials exhibit a low adhesion between the tribo-contacts. Moreover, the high temperatures deposition process (i.e., APS) facilitates carbide-matrix cohesion within the lamellae in Cr_3C_2-25NiCr (LP) coating and hence, improved the wear resistance [54]. Whereas the high velocity deposition processes (i.e., HVAF) Cr_3C_2-25NiCr (4L4) coating allowed the production of denser coatings with strong cohesion between the successive splats, eventually leading to low porosity. These characteristics of the coatings produce negligible wear and the lowest material transfer to the counter ball during sliding [15], [16]. Additionally, the presence of smooth smeared surface caused the lowest wear volume among three coatings [58]. The uniform lubricious tribo-film formation on the sliding surface of HVAF Cr_3C_2-25NiCr (4L4) coating (Fig. 3.11e) resulted in lowest wear volume when compared to the other two APS coatings by preventing direct contact between the coating and the counterface [59]. On the other hand, the higher amount of dispersed Cr_3C_2 phases facilitated by HVAF processes together with matrix toughness contributes to improved wear resistance by providing a barrier against material removal during sliding. This observation is in agreement with previously published results by Houdková *et al*. [8].

At 450 °C, the wear volume loss of all tested coatings is significantly higher (Fig. 3.7), than the room temperature conditions. Additionally, the material transferred to the counterfaces of all tested coatings seems higher at higher temperature when compared to the counterfaces at RT (Fig. 3.12b, 3.12d, and 3.12f). The wear volume of APS Cr_3C_2 (HP) coating increased slightly due to the oxidation and formation of abrasive and non-lubricious oxides (i.e., CrO_2 and Cr_2O_3) during sliding as shown in Fig. 3.10b. Borisov *et al*. reported that the high wear rate of binder-free chromium carbide coating was due to the formation of brittle Cr_2O_3 phases [60]. Moreover, lack of binder could have contributed to the coating's high brittleness and low fracture toughness, making it more susceptible to delamination and spallation [61]. Similarly, the reduced wear performance of APS Cr_3C_2-25NiCr (LP) coating at elevated temperatures may be attributed to oxidation of the metallic binder at elevated temperature. Similar results were reported by other author [62]. The oxidation of the NiCr binder leads to the formation of a brittle oxide layer characterized by low fracture toughness. The brittle oxide layer cracks and delaminates during sliding wear, leading to increased wear. Furthermore, binder oxidation reduces the splat bonding, resulting in carbide pull-out during sliding and exacerbating wear through increased debris generation and surface roughening [63]. On the other hand, the high wear volume of HVAF coating compared to RT is linked to the dissolution of hard carbide phases in the matrix, which adversely impacts the coating's toughness and reduces its wear resistance. These effects possibly weaken the carbide network, causing dislodging of cracked carbide grains during sliding (Fig. 3.9c) and significant transfer of materials to the counterpart at high temperature (Fig. 3.12f) than RT [8]. However, at high temperature, the APS Cr_3C_2-25NiCr (LP) coating still showed higher wear resistance than APS Cr_3C_2 (HP) due to the presence of binder. The HVAF Cr_3C_2-25NiCr (4L4) coating demonstrates the lowest wear volume loss among the tested coatings, attributed to the formation of stable and lubricious oxide layer, as illustrated in Fig. 3.11f. Additionally, the lowest wear volume of the HVAF Cr_3C_2-25NiCr (4L4) coating is associated with the low oxidation of coating produced by the HVAF processes. The low porosity and greater cohesion between the splats due to the presence of binder enhanced the overall wear performance both at room and elevated temperatures [12].

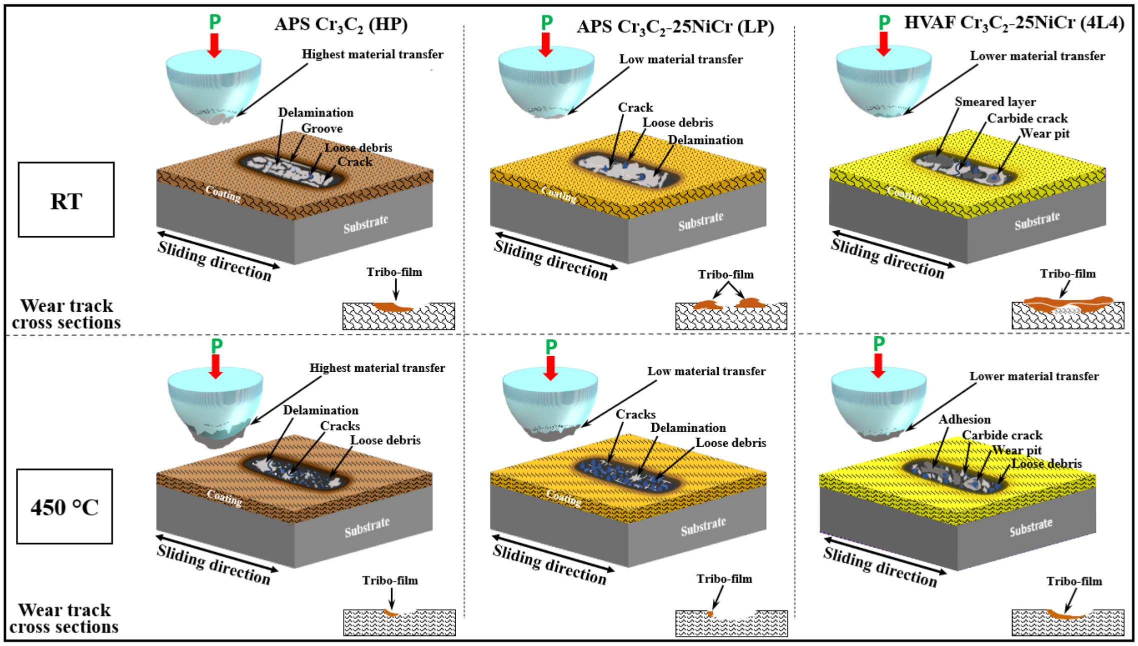

Figure 3.13 Schematic of wear mechanisms for chromium carbide-based APS and HVAF coatings at RT and 450 °C.

3.6 Conclusion

This study evaluated the tribological performance of pure chromium carbide (Cr_3C_2) and cemented chromium carbide (Cr_3C_2-25NiCr) deposited via APS and HVAF techniques at room and elevated temperatures. While both methods produced dense coatings, APS coatings (except APS Cr_3C_2-25NiCr LP) had higher porosity than HVAF coatings. The Cr_3C_2 content was lower in all as-sprayed coatings due to carbide dissolution and oxidation in APS, and carbide rebounding in HVAF. APS Cr_3C_2 (HP) coatings had higher friction and wear at room temperature and 450 °C, whereas HVAF Cr_3C_2-25NiCr (4L4) demonstrated the lowest friction. The APS coating also showed higher wear at both ambient and elevated temperatures due to its brittle nature and high oxidation during sliding. On the other hand, the HVAF sprayed coating outperformed the other two coatings in terms of wear resistance due to the presence or formation of a smeared, smooth and lubricious oxide layer. Future research should focus on optimizing HVAF deposited Cr_3C_2-25NiCr coatings by varying the binder composition in the coatings and improving wear resistance over a range of temperatures. In addition, investigating different feedstock compositions and testing performance under more severe conditions will help assess their long-term durability.

References

[1] E. A. Baskharone, “Introduction to Gas-Turbine Engines,” *Princ. Turbomach. Air-Breathing Engines*, pp. 1–8, 2010, doi: 10.1017/cbo9780511616846.002.

[2] R. E. Chupp, R. C. Hendricks, S. B. Lattime, and B. M. Steinetz, “Sealing in Turbomachinery,” *J. Propuls. Power*, vol. 22, pp. 313–349, 2006. Available: https://api.semanticscholar.org/CorpusID:109015945.

[3] P. Stoyanov, K. M. Harrington, and A. Frye, “Insights into the Tribological Characteristic of Cu-Based Coatings Under Extreme Contact Conditions,” *Jom*, vol. 72, no. 6, pp. 2191–2197, 2020, doi: 10.1007/s11837-020-04087-7.

[4] K. Holmberg, A. Matthews, and H. Ronkainen, “Coatings tribology - Contact mechanisms and surface design,” *Tribol. Int.*, vol. 31, no. 1–3, pp. 107–120, 1998, doi: 10.1016/S0301-679X(98)00013-9.

[5] A. Roy *et al.*, “Friction and wear behavior of suspension plasma sprayed tantalum oxide coatings at elevated temperatures,” *Surf. Coatings Technol.*, vol. 452, p. 129097, 2023, doi: https://doi.org/10.1016/j.surfcoat.2022.129097.

[6] A. Pauzi, M. Ghazali, W. F. H. W Zamri, and A. Rajabi, “Wear Characteristics of Superalloy and Hardface Coatings in Gas Turbine Applications-A Review,” *Metal*, vol. 10, pp. 2–14, 2020, doi: 10.3390/met10091171.

[7] A. Khitab, Z. U. Abdin, I. Ahmed, and T. Karim, “8 - Thermal insulation of buildings through classical materials and nanomaterials,” in *Recent Advances in Nano-Tailored Multi-Functional Cementitious Composites*, M. Şahmaran, F. Shaikh, and G. Yıldırım, Eds. Woodhead Publishing, 2022, pp. 277–303.

[8] Š. Houdková, Z. Česánek, E. Smazalová, and F. Lukáč, “The High-Temperature Wear and Oxidation Behavior of CrC-Based HVOF Coatings,” *J. Therm. Spray Technol.*, vol. 27, no. 1, pp. 179–195, 2018, doi: 10.1007/s11666-017-0637-3.

[9] M. Yang, Y. Liang, T. Huang, Q. Jin, D. Kong, and P. Song, “Oxidation behaviour and properties of carbide ceramic reinforced Ni-based composite coatings at 700 °C,” *Ceram. Int.*, 2024, doi: https://doi.org/10.1016/j.ceramint.2024.07.234.

[10] N. Vashishtha, R. K. Khatirkar, and S. G. Sapate, “Tribological behaviour of HVOF sprayed WC-12Co, WC-10Co-4Cr and Cr3C2−25NiCr coatings,” *Tribol. Int.*, vol. 105, pp. 55–68, 2017.

[11] F. Rubino, D. Merino, A. T. Silvestri, C. Munez, and P. Poza, “Mechanical properties optimization of Cr3C2-NiCr coatings produced by compact plasma spray process,” *Surf. Coatings Technol.*, vol. 465, p. 129570, 2023, doi: https://doi.org/10.1016/j.surfcoat.2023.129570.

[12] S. Mahade, A. Mulone, S. Björklund, U. Klement, and S V Joshi, “Investigating Load-dependent Wear Behavior and Degradation Mechanisms in Cr3C2-NiCr coatings deposited by HVAF and HVOF,” *J. Mater. Res. Technol.*, 2021. https://api.semanticscholar.org/CorpusID:239953533.

[13] S. Mahade, A. Mulone, S. Björklund, U. Klement, and S. Joshi, “Novel suspension route to incorporate graphene nano-platelets in HVAF-sprayed Cr3C2–NiCr coatings for superior wear performance,” *J. Mater. Res. Technol.*, vol. 13, pp. 498–512, 2021, doi: https://doi.org/10.1016/j.jmrt.2021.04.096.

[14] S. Matthews, B. James, and M. Hyland, “The Effect of Heat Treatment on the Oxidation Mechanism of Blended Powder Cr3C2-NiCr Coatings,” *J. Therm. Spray Technol.*, vol. 19, no. 1, pp. 119–127, 2010, doi: 10.1007/s11666-009-9381-7.

[15] R. J. Alroy, M. Kamaraj, and G. Sivakumar, “Influence of processing condition and post-spray heat treatment on the tribological performance of high velocity air-fuel sprayed Cr3C2-25NiCr coatings,” *Surf. Coatings Technol.*, vol. 463, p. 129498, 2023, doi: https://doi.org/10.1016/j.surfcoat.2023.129498.

[16] V. Matikainen, G. Bolelli, H. Koivuluoto, P. Sassatelli, L. Lusvarghi, and P. Vuoristo, “Sliding wear behaviour of HVOF and HVAF sprayed Cr3C2-based coatings,” *Wear*, vol. 388–389, pp. 57–71, 2017, doi: 10.1016/j.wear.2017.04.001.

[17] V. Matikainen *et al.*, “A Study of Cr3C2-Based HVOF- and HVAF-Sprayed Coatings: Microstructure and Carbide Retention,” *J. Therm. Spray Technol.*, vol. 26, no. 6, pp. 1239–1256, 2017, doi: 10.1007/s11666-017-0578-x.

[18] G. Bolelli *et al.*, “Sliding and abrasive wear behaviour of HVOF- and HVAF-sprayed Cr3C2-NiCr hardmetal coatings,” *Wear*, vol. 358–359, pp. 32–50, 2016, doi: 10.1016/j.wear.2016.03.034.

[19] E. Gariboldi, L. Rovatti, N. Lecis, L. Mondora, and G. A. Mondora, “Tribological and mechanical behaviour of Cr3C2–NiCr thermally sprayed coatings after prolonged aging,” *Surf. Coatings Technol.*, vol. 305, pp. 83–92, 2016, doi: https://doi.org/10.1016/j.surfcoat.2016.07.087.

[20] I. S. Batraev, V. Y. Ulianitsky, A. A. Shtertser, D. V Dudina, and A. V Ukhina, “Formation of Composite Coatings during Detonation Spraying of Cr3C2,” *J. Compos. Sci.*, vol. 7, no. 2, 2023, doi: 10.3390/jcs7020071.

[21] S. Matthews, “Development of high carbide dissolution/low carbon loss Cr3C2–NiCr coatings by shrouded plasma spraying,” *Surf. Coatings Technol.*, vol. 258, pp. 886–900, 2014, doi: https://doi.org/10.1016/j.surfcoat.2014.07.062.

[22] M. C. Brupbacher, D. Zhang, W. M. Buchta, Y.-R. Rhim, D. C. Nagle, and J. B. Spicer, “Post-treatment of Plasma-Sprayed Cr2O3 with Methane-Containing Gas for Conversion to Binder-Free Cr3C2,” *J. Therm. Spray Technol.*, vol. 24, no. 8, pp. 1513–1519, 2015, doi: 10.1007/s11666-015-0348-6.

[23] A. Förg, M. Blum, A. Killinger, J. A. Moreno Nicolás, and R. Gadow, “Deposition of chromium oxide-chromium carbide coatings via high velocity suspension flame spraying (HVSFS),” *Surf. Coatings Technol.*, vol. 351, pp. 171–176, 2018, doi: https://doi.org/10.1016/j.surfcoat.2018.07.072.

[24] R. U. L, T. P. Bharathesh, B. R. B, and S. R, “Transitional Wear of Plasma Spray Cr2O3 and Cr3C2 Coatings Deposited on Low Carbon Steel,” *Int. J. Emerg. Sci. Eng.*, vol. 10, no. 4, pp. 1–7, 2022, doi: 10.35940/ijese.d2524.0310422.

[25] S. Mahade, K. Narayan, S. Govindarajan, S. Bjorklund, N. Curry, and S. V Joshi, “Exploiting Suspension Plasma Spraying to Deposit Wear-Resistant Carbide Coatings,” *Materials (Basel).*, vol. 12, 2019, doi: 10.3390/ma12152344.

[26] N. V. Kobernik *et al.*, “Chromium Carbides in Abrasion-Resistant Coatings,” *Russ. Eng. Res.*, vol. 40, no. 12, pp. 1013–1016, 2020, doi: 10.3103/S1068798X20120084.

[27] P. Fauchais, R. Etchart-Salas, V. Rat, J. F. Coudert, N. Caron, and K. Wittmann-Ténèze, "Parameters Controlling Liquid Plasma Spraying: Solutions, Sols, or Suspensions," *J. Therm. Spray Technol.*, vol. 17, no. 1, pp. 31–59, 2008, doi: 10.1007/s11666-007-9152-2.

[28] V. Matikainen, H. Koivuluoto, and P. Vuoristo, "A study of Cr3C2-based HVOF- and HVAF-sprayed coatings: Abrasion, dry particle erosion and cavitation erosion resistance," *Wear*, vol. 446–447, p. 203188, 2020, doi: https://doi.org/10.1016/j.wear.2020.203188.

[29] L. Janka, J. Norpoth, R. Trache, S. Thiele, and L.-M. Berger, "HVOF- and HVAF-Sprayed Cr3C2-NiCr Coatings Deposited from Feedstock Powders of Spherical Morphology: Microstructure Formation and High-Stress Abrasive Wear Resistance Up to 800 °C," *J. Therm. Spray Technol.*, vol. 26, no. 7, pp. 1720–1731, 2017, doi: 10.1007/s11666-017-0621-y.

[30] F. Arhami and F. Ben Ettouil, "As-Sprayed Highly Crystalline Yb2Si2O7 Environmental Barrier Coatings (EBCs) by Atmospheric Plasma Spray (APS)," *J. Therm. Spray Technol.*, vol. 32, 2023, doi: 10.1007/s11666-022-01526-6.

[31] Z. Tang, H. Kim, I. Yaroslavski, G. Masindo, Z. Celler, and D. Ellsworth, "Novel Thermal Barrier Coatings Produced by Axial Suspension Plasma Spray," *Therm. Spray 2011 Proc. from Int. Therm. Spray Conf.*, vol. 83713, pp. 571–575, 2011, doi: 10.31399/asm.cp.itsc2011p0571.

[32] S. Rotich, N. Kipkirui, T.-T. Lin, and S.-H. Chen, "Effect of Varying Plasma Powers on High-Temperature Applications of Plasma-Sprayed Al0.5CoCrFeNi2Ti0.5 Coatings," *Materials (Basel).*, vol. 15, p. 7198, 2022, doi: 10.3390/ma15207198.

[33] C.-J. Li and B. Sun, "Effects of spray parameters on the microstructure and property of Al2O3 coatings sprayed by a low power plasma torch with a novel hollow cathode," *Thin Solid Films*, vol. 450, no. 2, pp. 282–289, 2004, doi: https://doi.org/10.1016/j.tsf.2003.11.166.

[34] M. Lorenzo-Bañuelos, A. Díaz, D. Rodríguez, I. I. Cuesta, A. Fernández, and J. M. Alegre, "Influence of Atmospheric Plasma Spray Parameters (APS) on the Mechanical Properties of Ni-Al Coatings on Aluminum Alloy Substrate," *Metals (Basel).*, vol. 11, no. 4, 2021, doi: 10.3390/met11040612.

[35] K. Torkashvand, M. Gupta, S. Björklund, F. Marra, L. Baiamonte, and S. Joshi, "Influence of nozzle configuration and particle size on characteristics and sliding wear behaviour of HVAF-sprayed WC-CoCr coatings," *Surf. Coatings Technol.*, vol. 423, p. 127585, 2021, doi: https://doi.org/10.1016/j.surfcoat.2021.127585.

[36] V. Matikainen, H. Koivuluoto, P. Vuoristo, J. Schubert, and Š. Houdková, "Effect of Nozzle Geometry on the Microstructure and Properties of HVAF-Sprayed WC-10Co4Cr and Cr3C2-25NiCr Coatings," *J. Therm. Spray Technol.*, vol. 27, no. 4, pp. 680–694, 2018, doi: 10.1007/s11666-018-0717-z.

[37] ASTM, "ASTM E-2109-14 Standard Test Methods for determining area percentage porosity in thermal sprayed coatings," vol. 04, no. Reapproved 2014, pp. 4–7, 1999, doi: 10.1520/E2109-01R21.

[38] C. Bidmeshki *et al.*, "Microstructural, Mechanical, and Tribological Evaluation of Cu-Al-based Coatings Deposited by APS and HVOF," *J. Therm. Spray Technol.*, vol. 32, no. 8, pp. 2321–2335, 2023, doi: 10.1007/s11666-023-01665-4.

[39] F. Otsubo, H. Era, K. Kishitake, and T. Uchida, "Properties of Cr3C2-NiCr cermet coating sprayed by high power plasma and high velocity oxy-fuel processes," *J. Therm. Spray Technol.*, vol. 9, no. 4, pp. 499–504, 2000, doi: 10.1007/BF02608553.

[40] Y. Zhang *et al.*, “High-temperature tribological behavior of thermally-treated supersonic plasma sprayed Cr3C2-NiCr coatings,” *Int. J. Refract. Met. Hard Mater.*, vol. 95, p. 105456, 2021, doi: https://doi.org/10.1016/j.ijrmhm.2020.105456.

[41] M. Mohammadtaheri, Q. Yang, Y. Li, and J. Corona-Gomez, “The Effect of Deposition Parameters on the Structure and Mechanical Properties of Chromium Oxide Coatings Deposited by Reactive Magnetron Sputtering,” *Coatings*, vol. 8, no. 3, 2018, doi: 10.3390/coatings8030111.

[42] A. Ranjan, A. Islam, M. Pathak, M. K. Khan, and A. K. Keshri, “Plasma sprayed copper coatings for improved surface and mechanical properties,” *Vacuum*, vol. 168, p. 108834, 2019, doi: https://doi.org/10.1016/j.vacuum.2019.108834.

[43] M. Mahajan, S. Rajpoot, and O. P. Pandey, “Int . Journal of Refractory Metals and Hard Materials In-situ synthesis of chromium carbide (Cr3C2) nanopowders by chemical-reduction route,” *Rmhm*, vol. 50, pp. 113–119, 2015. Available: http://dx.doi.org/10.1016/j.ijrmhm.2014.12.010.

[44] C. Shi, S. Liu, Irfan, Q. Gong, H. Wang, and M. Hu, “Deposition mechanisms and characteristics of nano-modified multimodal Cr3C2–NiCr coatings sprayed by HVOF,” *Rev. Adv. Mater. Sci.*, vol. 61, no. 1, pp. 526–538, 2022, doi: doi:10.1515/rams-2022-0042.

[45] M. I. Boulos, P. L. Fauchais, and J. V. R. Heberlein, “Fundamentals of Combustion and Thermal Plasmas,” in *Thermal Spray Fundamentals: From Powder to Part*, Cham: Springer International Publishing, 2021, pp. 57–83.

[46] D. Dzhurinskiy, A. Babu, P. Pathak, A. Elkin, S. Dautov, and P. Shornikov, “Microstructure and wear properties of atmospheric plasma-sprayed Cr3C2-NiCr composite coatings,” *Surf. Coatings Technol.*, vol. 428, p. 127904, 2021, doi: https://doi.org/10.1016/j.surfcoat.2021.127904.

[47] H.-B. Zhu, J. Shen, F. Gao, Y. Yu, and C. Li, “Microstructure and Sliding Wear Performance of Cr7C3-(Ni,Cr)3(Al,Cr) Coating Deposited from Cr7C3 In Situ Formed Atomized Powder,” *J. Therm. Spray Technol.*, vol. 26, no. 1, pp. 254–264, 2017, doi: 10.1007/s11666-016-0498-1.

[48] P. Schwingenschlögl, P. Niederhofer, and M. Merklein, “Investigation on basic friction and wear mechanisms within hot stamping considering the influence of tool steel and hardness,” *Wear*, vol. 426–427, pp. 378–389, 2019, doi: https://doi.org/10.1016/j.wear.2018.12.018.

[49] Y. Liu, G. Yang, Z. Hang, H. Fu, N. Xi, and H. Chen, “Elevated temperature wear behaviour of CeO2 modified WC-12Co coating,” *J. Rare Earths*, vol. 37, no. 6, pp. 673–678, 2019, doi: https://doi.org/10.1016/j.jre.2018.11.007.

[50] A. R. Govande, S. Tailor, B. R. Sunil, and R. Dumpala, “Effect of inert environment on the sliding wear behaviour of the HVOF sprayed WC-12Co coating,” *Int. J. Refract. Met. Hard Mater.*, vol. 111, p. 106109, 2023, doi: https://doi.org/10.1016/j.ijrmhm.2023.106109.

[51] M. Federici, C. Menapace, A. Moscatelli, S. Gialanella, and G. Straffelini, “Effect of roughness on the wear behavior of HVOF coatings dry sliding against a friction material,” *Wear*, vol. 368, pp. 326–334, 2016. https://api.semanticscholar.org/CorpusID:138018108.

[52] D. Feng, M. Shen, X. Peng, and X. Meng, “Surface Roughness Effect on the Friction and Wear Behaviour of Acrylonitrile–Butadiene Rubber (NBR) Under Oil Lubrication,” *Tribol. Lett.*, vol. 65, no. 1, p. 10, 2016, doi: 10.1007/s11249-016-0793-5.

[53] J. H. W. Siu and L. K. Y. Li, “An investigation of the effect of surface roughness and coating

thickness on the friction and wear behaviour of a commercial MoS2-metal coating on AISI 400C steel," *Wear*, vol. 237, no. 2, pp. 283–287, 2000, doi: 10.1016/S0043-1648(99)00349-X.

[54] T. F. J. Quinn, "Review of oxidational wear: Part I: The origins of oxidational wear," *Tribol. Int.*, vol. 16, no. 5, pp. 257–271, 1983, doi: https://doi.org/10.1016/0301-679X(83)90086-5.

[55] M. Vardavoulias, "The role of hard second phases in the mild oxidational wear mechanism of high-speed steel-based materials," *Wear*, vol. 173, no. 1, pp. 105–114, 1994, doi: https://doi.org/10.1016/0043-1648(94)90262-3.

[56] M. E. Sikorski, "Correlation of the Coefficient of Adhesion With Various Physical and Mechanical Properties of Metals," *J. Basic Eng.*, vol. 85, no. 2, pp. 279–285, 1963, doi: 10.1115/1.3656577.

[57] Y. Liu, T. E. Fischer, and A. Dent, "Comparison of HVOF and plasma-sprayed alumina/titania coatings—microstructure, mechanical properties and abrasion behavior," *Surf. Coatings Technol.*, vol. 167, no. 1, pp. 68–76, 2003, doi: https://doi.org/10.1016/S0257-8972(02)00890-3.

[58] M. Asuquo, R. B. Nair, M. Fotoohinezhadkhales, A. Akbarnozari, P. Stoyanov, and C. Moreau, "Tribological Behavior of Atmospheric Plasma-Sprayed Cu-Ni Coatings," *J. Therm. Spray Technol.*, 2024, doi: 10.1007/s11666-024-01843-y.

[59] S. Rukhande, W. S. Rathod, and D. Bhosale, "Sliding Wear Investigation of Ni-based Coating for High-Temperature Application," *Tribol. Ind.*, vol. 43, pp. 247–258, 2021, doi: 10.24874/ti.945.08.20.11.

[60] Y. S. Borisov, Y. G. Tkachenko, I. N. Gorbatov, G. A. Avtonomov, D. Z. Yurchenko, and V. V Rishin, "Wear behavior of plasma-sprayed chromium-carbide-base coatings at temperatures of 20–1000°C," *Sov. Powder Metall. Met. Ceram.*, vol. 17, no. 10, pp. 801–804, 1978, doi: 10.1007/BF00796371.

[61] P. Ru *et al.*, "Effects of SiC on Microstructure and Properties of Coatings Prepared by Plasma Spraying Cr2O3-Al-SiC Powder," *J. Therm. Spray Technol.*, vol. 32, no. 5, pp. 1350–1361, 2023, doi: 10.1007/s11666-023-01568-4.

[62] Y. G. Tkachenko, A. P. Épik, A. P. Garda, I. N. Gorbatov, and V. M. Litvin, "Wear resistance of detonation-deposited chromium-carbide-base coatings at temperatures of 20–1000°C," *Sov. Powder Metall. Met. Ceram.*, vol. 17, no. 8, pp. 619–622, 1978, doi: 10.1007/BF00797338.

[63] N. Behera, M. R. Ramesh, and M. R. Rahman, "Elevated temperature wear and friction performance of WC-CoCr/Mo and WC-Co/NiCr/Mo coated Ti-6Al-4V alloy," *Mater. Charact.*, vol. 215, p. 114207, 2024, doi: https://doi.org/10.1016/j.matchar.2024.114207.

Chapter

4. SUSPENSION PLASMA SPRAYING OF PURE SILICON CARBIDE COATINGS

In this chapter…

The microstructural study of pure silicon carbide (SiC) powders sprayed with suspension plasma spray (SPS) technique have been provided. The testing, characterization and data analysis was performed to understand the coating structure

4.1 Abstract

Silicon carbide-based (SiC) coatings have become potential candidates for high-temperature tribological applications due to their high chemical and structural stability. Researchers believed that SiC coatings cannot be deposited by thermal spray process due to its decomposing nature at high temperatures. However, this study achieved the deposition of pure SiC coatings by low power (LP) and high power (HP) suspension plasma spray (SPS) process. Microstructural observations showed that the LP coating exhibited a dense dome-shape columnar structure characterized by low porosity, while the HP coating exhibited a feathery columnar structure characterized by intra-columnar pores and inter-columnar gaps. Although the EDS analysis revealed that SiC particles undergo some oxidation, the LP spray process was effective in producing SiC coatings with minimal oxidation compared to the HP spray process. It is expected that this preliminary study will open a pathway for future research and optimization in this area.

Keywords: Silicon carbides, Suspension plasma spray, Thermal spray process, Gas turbine engine

4.2 Introduction

Silicon carbide (SiC) is a ceramic material that possesses unique physical properties such as high thermal and chemical stability, high strength, high thermal conductivity, and low coefficient of linear expansion [1]. Due to these excellent properties, SiC is widely finding applications as protective coating in numerous industries including and not limited to the aerospace, nuclear and offshore sectors [2]–[6]. Moreover, SiC materials are recommended for applications where low density and high temperature capabilities are required [4].

Despite the attractive properties, the main drawback of SiC material lies in its decomposing nature as it tends to sublimates at 2500-2600 °C under atmospheric spraying condition, making deposition challenging [7], [8]. Moreover, the oxidation kinetics of SiC materials are usually influenced by several factors such as nature of the substrate, moisture in the environment, particle size, and the sintering additives used [1]. Recent approach to prevent SiC particles from decomposition during spraying usually involve the co-depositon with a metallic or ceramic binders to facilitate the bonding of SiC particles, allowing SiC composite coating to be deposited [9]. For instance, Kang *et al*. [10] sucessfully fabricated a functionally graded SiC/Cu metal matrix composite (MMC) by plasma spray methods. However, the results shows that decomposition of the SiC and thermal expansion mismatch between SiC and Cu during rapid solidification occur. Arrabal *et al*. [11] investigation reported a high porosity content with poor contact between the splats of aluminium and SiC particles deposited by flame spray process. Mubarok *et al*. [9] study reveals that the fabrication of SiC composites coatings using yttrium aluminum garnet (YAG) as sintering aids did not result in an homogeneous distribution of oxide binder between the SiC particles. As a results, the coating obtained were characterized by poor mechanical performance due to low cohesive strength, high porosity, and powdery structure making the coatings vulnerable to grain pull-out. Mubarok and Espallargas [8] also reported the successful deposition of silicon carbide coatings using thermal spray detonation technique. However, the coating shows lack of sintering and characterized by fine pores formed during spraying and metallographic processing. Tului *et al*. [7] reported the deposition of compact and homogeneous coating with a low porosity content containing up to 66 vol.% of silicon carbide deposited by plasma spray process. While different grades of successful deposition of SiC coatings were reported in all the methods stated above, the available findings are below the desired expectations for SiC ceramic materials.

Recognizing the above research gaps, the present research explores the possibility of developing pure SiC coatings. To the authors knowledge, no research has been done to produce pure silicon carbide coatings. Suspension plasma spray (SPS) process was employed for the deposition of SiC nanoparticles. Plasma spraying process offer advantages such as high deposition rate, better cohesion and bonding of the coating with the substrate, high temperature and energy density, making this process unique for producing dense coatings [12]. Notably, suspension plasma spraying (SPS) is an advancement in air plasma spray (APS) process that enables the spraying of fine feedstock (100 nm - 5 µm diameter) [13]. Moreover, the SPS process can achieve fine and dense coating microstructures of few tenths to a few hundreds of micrometres thick coatings [9], [14]. The axial injection of nano or microns size particles into the core of the high-temperature plasma jet will ensure that particles are well melted and accelerated towards the substrates to form a coating [15], [16].

In the present study, deposition of pure SiC coatings were achieved using low power (LP) and high power (HP) spray mode. Thereafter, the microstructural analysis were performed using the high-resolution electron microscopy and X-ray diffraction. This preliminary study will open a pathway for future research and optimization in this area.

4.3. Experimental method

4.3.1 Feedstock material

The coating feedstock powder used in this research was sub-micron size silicon carbide (SiC) powder, supplied by Shanghai Luju Polymer Technology, China. The nominal powder size from the supplier was 500 nm. In-house analysis of the powder particle size distribution was performed by dispersing the as-received powder in ethanol using a particle size analyzer (Spraytec, Malvern Panalytical, UK) equipped with a wet dispersion accessory. The results are presented in section 4.4.

4.3.2 Suspension preparation

The present work utilized ethanol as the liquid carrier for the submicrometric feedstock into the plasma jet. The decision to use ethanol as a solvent is driven by the fact that a lower amount of heat is required to vaporize ethanol than that of other common solvents like water [17]. Moreover, the break-ups of suspension droplets are achieved faster when ethanol is used as a solvent [18]. The composition of the SiC loading in the suspension was 20 wt.%. This composition promotes good viscosity [19], production of smaller suspension droplets [14], and improves the flowability [20] of the suspension. A poly (acrylic acid sodium salt) dispersant with an average molecular weight ~ 360,000 (Sigma Aldrich, UK) was used and added in the range of 0 to 6 wt.% of the solid to achieve a stable slurry and dispersion of particles by electrostatic, steric or electro-steric repulsions [21]. The colloidal stability was monitored, and the sedimentation rate was measured after 48 h. Finally, the suspension with 4 wt.% of PVP and sedimentation lower than 1 mm after 1 h was selected as the optimal stable suspension. After establishing the colloidal stability, suspensions with the optimized dispersant (4 wt.%) were prepared in ethanol and the carbide powder was gradually dispersed in the solution. The mixture was stirred simultaneously by magnetic stirrer (ThermoFisher Scientific, USA) and sonication (Qsonica, USA) at 50 kW for 30 min before spraying. Thereafter, the prepared suspension was fed into the plasma pressurized container with a mechanically powered propeller for the continuous stirring of the suspension during spraying to avoid sedimentation or agglomeration of the solid particles.

4.3.3 Coating deposition

The suspension spraying was performed using Mettech Axial III plasma spray torch (Northwest Mettech Corp. Canada). The Mettech gun has three converging plasma jets which allow the axial injection of ceramic powder directly at the center of the plasma stream [22]. Furthermore, the axial injection offers solutions to the difficulties that arise when attempting to feed the plasma radially with fine particles or droplets [23]. The deposition parameters used for spraying both powders are tabulated in Table 4.1. Two spraying conditions designated as low power (LP) and high power (HP) were employed for the deposition of submicron SiC feedstock powder. Available studies have shown that low plasma power causes moderate melting of suspension droplets, resulting in low stress evolution [24]. Moreover, high plasma power mode increases plasma enthalpy, which enhances the proper melting and particle adhesion with the substrate [25]. Therefore, by utilizing different spraying conditions, we aim to gain a better understanding of how different spraying conditions influence the microstructural properties and to identify the optimal conditions for depositing pure SiC coatings. The silicon carbide powder was deposited on 304 L stainless-steel substrate of dimensions (25.4 × 25.4 × 4.3 mm). The steel substrate surfaces were grit-blasted using 20-grit alumina abrasive particles to increase the surface roughness and compressed air was used to remove grit residue from the substrate surface. Thereafter, the substrates were preheated up to 150 °C before spraying to enhance adherence of the coatings to the substrates [26].

Table 4.1 SPS parameters used for depositing silicon carbide coating.

Deposition parameters	Spray mode	
	Low power	High power
Total plasma gas flow (l/min)	245	210
Solid loading (wt.%)	20	20
Solvent	Ethanol	Ethanol
Power (kW)	92.3	111.3
Enthalpy (kJ/l)	8	13.5
Ar (%)	75	45
N_2 (%)	10	45
H_2 (%)	15	10
Suspension feed rate (ml/min)	45	45
Spray distance (mm)	75	75
Number of passes	70	35

4.3.4 Characterization

The microstructural features of SiC powder was determined by scanning electron microscopy (SEM) (SU8230, Hitachi, Japan) built with energy dispersive spectroscopy (EDS). The powder and coatings were prepared (mounted, sectioned, and polished) according to standard metallographic preparation (ASTM E03). The average coating thickness was determined and reported from the prepared cross-section images. The phase analysis of powder and coatings were determined using Philips X'Pert Pro X-ray diffractometer system (Malvern Panalytical, Malvern, UK) with Cu-Kα radiation (step size = 0.02°, time per step = 2 sec, $\lambda = 1.5406$ Å, scanning range 2Θ of 20° and 90°) was used and operated at a power of 40 kV and 40 mA. The obtained diffractograms were analyzed and indexed using the Rietveld analytical software built with the XRD system. Raman spectra measurements were performed using an InVia spectrometer (Renishaw, UK). An optical microscope with a 50 × lens was used to focus the excitation radiation $\lambda = 514.5$ nm from an Ar + ion laser source.

4.4 Results

4.4.1 Feedstock powder and coating

The powder morphology and particle size distribution of SiC powder in the as-received condition are presented in Fig. 4.1a-b. The SiC powder morphology in Fig. 4.1a comprised of agglomerated particles of random shapes (round, oblong, individual and coalesced particles sizes ranging between few tens of nanometers to a few micrometers). The particle size distribution (Fig. 4.1b), i.e., Dv (10), Dv (50), and Dv (90) was measured to be 0.63 µm, 1.06 µm, and 1.92 µm, respectively. Comparing these results with those provided by the supplier in section 4.3.1, it appears that the sub-micron size SiC particles form agglomerates of a few microns in size.

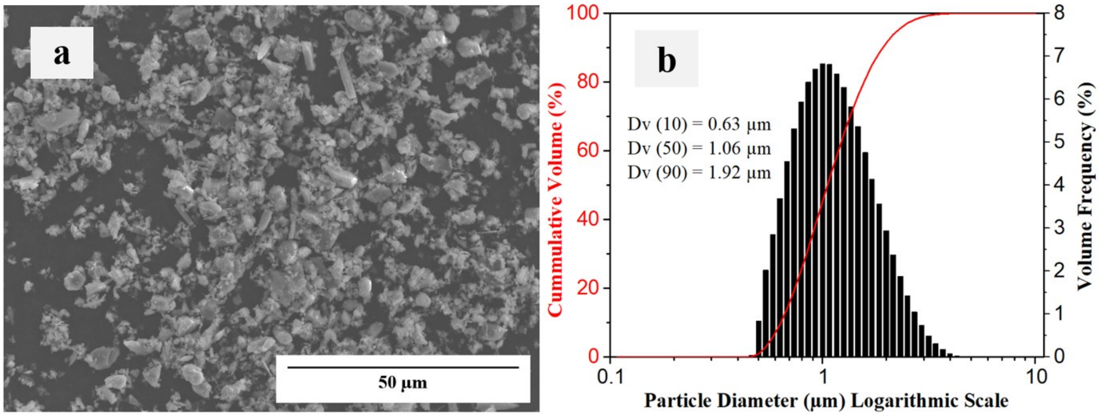

Figure 4.1 SEM image of SiC powder morphology (a), and particle size distribution (PSD) of SiC powder (b).

The SEM cross-sections and EDS mapping of SiC coatings with low power (LP) and high power (HP) are presented in Fig. 4.2a-b. The LP coating cross-section (Fig. 4.2a) exhibit a dense dome-shaped or bumpy microstructure which is similar to the those described in other investigations [26], [27]. Whereas the HP coating in Fig. 4.2b exhibit a feathery columnar structure characterized by inter-columnar gaps and intra-columnar pores, which were also reported by other authors [28]. Moreover, it can be observed that both LP and HP coatings were built on the crests of the undulated substrate surface, indicating that the coatings morphology strongly rely on the grit blasting effect of the substrate [29]. The average thickness value for coatings produced LP and HP spraying conditions were measured to be 46 ± 20 µm and 33 ± 22 µm, respectively. This difference in coating thickness can be attributed to the higher number of passes used in the LP process, which is twice that of the HP coating (Table 4.1). The EDS mapping analysis of the coatings confirms the presence of silicon, carbon, and oxygen content. Notably, the distribution of oxygen is marginally lower for LP spray coating and higher for HP spray coatings.

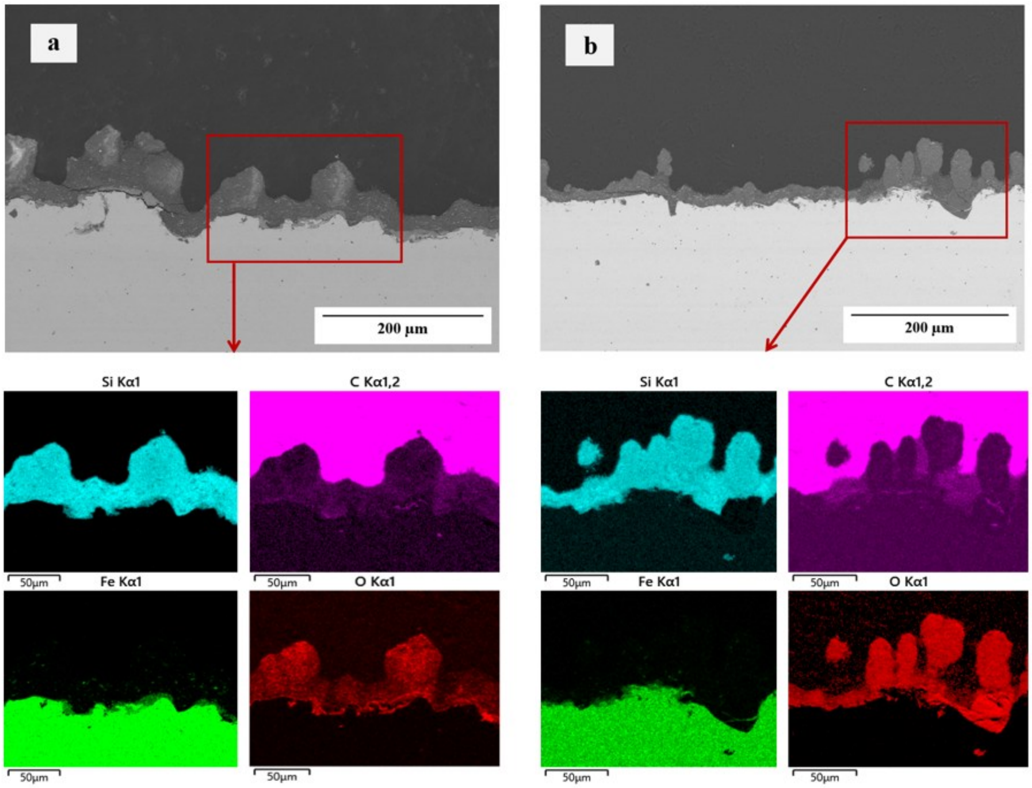

Figure 4.2 SEM/EDS images of the cross-section microstructure of SPS sprayed silicon carbide coating (a) low power, and (b) high power.

The XRD patterns of the pure SiC powder and the as-sprayed coatings are presented in Fig. 4.3a-b. The SiC powder phases (Fig. 4.3a) are mainly β-type (3C) structure observed around 35.6° (111), 41.4° (200), 60.0° (220), and 72.0° (311) [30]. Whereas in the as-sprayed coatings (Fig. 4.3b), a reduction in the SiC peaks were observed, and it appears that only a single phase is detected by the XRD for both coatings. Moreover, diffraction peaks corresponding to Fe - austenite were observed in both coatings around 43.5°, 50.5° and 74.3° [31], which is associated with the low thickness and/or non-uniformity of both coatings. No evidence of decomposition or oxidation into silica (SiO_2) was found within the detectable range of the XRD.

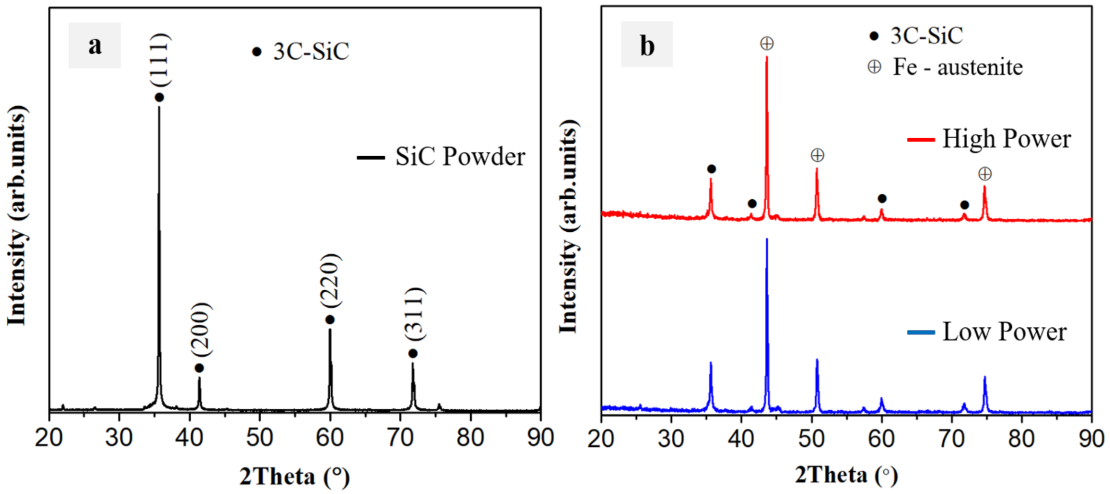

Figure 4.3 XRD data (a) SiC powder, and (b) As-sprayed low and high power coatings.

Raman spectroscopy in Fig. 4.4a-b presents the surface state of LP and HP coatings in the as-sprayed condition. Raman analysis of both coatings also confirmed the presence SiC peaks around ∼794 cm^{-1} which consists mainly of a cubic polytype structure [32]. It also appears that the SiC peak intensity observed for LP coating in Fig. 4.4a is higher than the those observed in HP coating (Fig. 4.4b). The presence of amorphous and crystalline peaks at ∼523 cm^{-1} corresponding to Si phases were detected in both coatings. Moreover, at Raman shift of 1600 °C, a broad peak corresponding to carbon was detected for both coatings, and that LP coating demonstrated the highest carbon signal. Similar findings was also reported by other authors that utilized suspension plasma fluidized bed CVD techniques for deposition of SiC coatings [33]. Therefore, the Raman spectra results correlate with the XRD observation in Fig. 4.3, which also shows no evidence of silica (SiO_2).

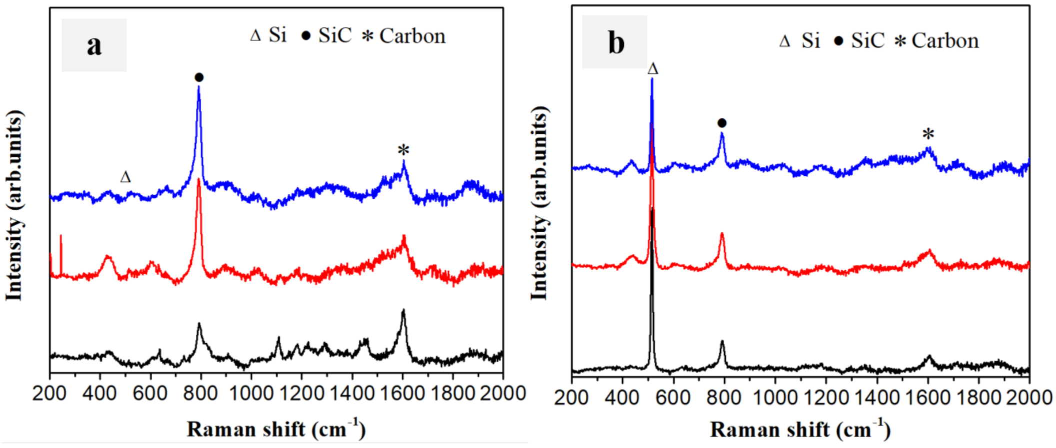

Figure 4.4 Raman spectrum of (a) low power (b) high power sprayed silicon carbide (SiC) coatings.

4.5 Discussions

Based on the microstructural analysis of the as-sprayed coatings represented in Fig. 4.2a-b, it was evident that low power (LP) and high power (HP) spray mode produced a columnar coating structure. Columnar microstructure in suspension plasma processes are associated with the stacking defects that occur due to larger surface asperities in relation to the average diameter of the particles impinging the surface [34]. Moreover, the columnar behavior has been correlated to the shadowing effect, which occur due to the interaction between surface asperities and the angular directions of impinging particles [35]. VanEvery *et al*. [36] reported the fundamental mechanisms which are responsible for the formation of columnar structures in SPS processes. The mechanisms were correlated with the numerical modeling work of Berghaus *et al*. [37], as shown in Fig. 4.5. When the suspension droplet size is less than 1 μm (submicron), plasma drag forces dominate over the particle inertia and redirect particle velocities from normal to parallel towards the surface, leading to significant shadowing effect and formation of columnar microstructure. Whereas when the suspension droplets size ranges between 1 μm and 5 μm, it may lead to the formation of feathery columnar structure having porosity bands within the columns given that the particles size range are still influenced by plasma drag forces. On the other hand, suspension droplets larger than 5 μm generally form a lamellar structure, as these larger particles directly impact the substrate with minimal influence from plasma drag forces. The present study employed submicron sized SiC particles (see section 4.3). It is hypothesized that the plasma drag force influenced the suspension droplets, making particles impact on the column asperities. The growing columns steadily shadow the surrounding area, thereby making incoming particles to impact the surface of the growing column, hence hindering the formation of a uniform coating microstructure [26].

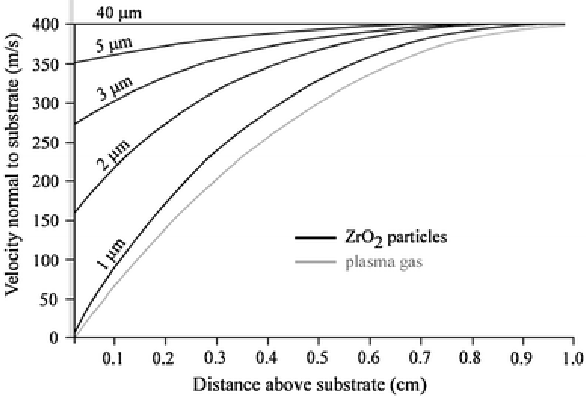

Figure 4.5 Effect of plasma flow on a trajectory of the droplets before the final impact as a function of droplet momentum [37].

The particle size behavior can be better understood by considering the Stokes number (*St*), given by the below equation:

$$St = \frac{\rho_p d_p^2 v_p}{\mu_g l_{BL}} \qquad (1)$$

Where the indices ρ_p is the density of the particle, d_p is the diameter of the particle, v_p is the velocity of the particle, μ_g is the dynamic viscosity of the gas, l_{BL} thickness of the flow boundary layer.

Submicron particles, measuring less than 1 µm usually exhibit low Stokes numbers and inertia, indicating that they will likely follow the plasma flow trajectory. Consequently, these particles may either generate defects by impacting the surface protrusions or get carried away by the gas, thereby failing to contribute to coating deposition [19], [34]. Thus, it can be inferred that the microstructural characteristics of LP and HP sprayed coatings are significantly influenced by the size of the suspension droplets and the resulting plasma drag forces.

A comparative analysis of the microstructure revealed that the LP spray mode produced a relatively dense microstructure with minimal porosity (Fig. 4.2a), while HP spray mode produce less dense microstructure due to the presence of inter-columnar pores and gaps (Fig. 4.2b). The enhanced microstructure of the LP sprayed coating is attributed to the influence of gas flow ratio, as illustrated in Table 4.1. Argon, as an inert gas, stabilizes the plasma arc and creates a non-reactive environment, thereby decreasing the risk of oxidation during spraying. On the other hand, hydrogen improves heat transfer and facilitates particle melting [38]. The mixture of Ar-H_2 plasma gas is commonly used in plasma spray processes to provide more enthalpy due to the diatomic structure of hydrogen [12]. Consequently, it can be deduced that the high Ar–H_2 gas flow ratio in LP conditions produced more energetic plasma jet, resulting in better particle melting and improved coating density with minimal porosity [39]. These findings contradict the results reported by other authors indicating that low plasma power leads to the formation of a porous microstructure characterized by larger and partially melted suspension droplets [25]. The detection of silicon and carbon by the EDS mapping (Fig. 4.2) agrees with the formation of SiC coating. Notably, the formation of SiC coating is more evident in LP spray mode compared to HP spray mode. This finding correlates with the XRD analysis (Fig. 4.3) and Raman characterization (Fig. 4.4), which indicate a greater SiC peak intensity for LP spray mode compared to the HP spray mode. At the same time, peaks associated with silica (SiO_2) were not detected by the XRD and Raman spectra, possibly because it is present in amorphous form with a weak signal that is easily overshadowed by the predominant XRD patterns. The underlying mechanism for SiC decomposition remains unclear. However, investigation by Darut *et al.* suggested that oxidation may occur due to reduced surrounding atmosphere and the rarefaction effect associated with small particle size [40]. In the present study, SiC decomposition is hypothesized to involve in-flight oxidation of SiC particles due to higher particle temperatures in plasma spray processes, longer dwell times (due to low particle velocity), and oxygen entrainment within the core of plasma spray system, where oxygen is completely transformed into highly reactive atomic oxygen [41]. Moreover, the higher oxide content in HP spray mode (Fig. 4.2b) showcases the influence of extremely high temperatures in the plasma jet, which can accelerate the oxidation of particles during spraying. Recent study by Niu *et al.* also confirmed that an increase in plasma power leads to an increase in heat flux and total enthalpy generated by the plasma, which in turn facilitates the complete melting of suspension droplets, and as well increase the chance of decomposition or oxidization of particles during spraying. On the other hand, the low thermal energy in LP spray mode ensures that particles are sufficiently melted without significant oxidation or decomposition [42]. Thus, it can be concluded that the oxides content in LP spray mode is relatively lower than the HP spray mode.

4.6 Conclusion

In this study, silicon carbide (SiC) coatings were produced using the suspension plasma spray (SPS) methods without the addition of matrix binder. An optimized suspension feedstock was achieved by regulating dispersant content, and the resulting suspension was deposited by low and high plasma power spray processes. The LP spray coating exhibits a dense dome-shape columnar structure containing minimal porosity while the HP spray coating exhibits a feathery columnar structure characterized by intra-columnar pores and inter-columnar gaps. Furthermore, the study finding also emphasizes that while both LP and HP spray processes result in oxidation of SiC particles, the LP spray mode was effective in producing SiC coatings with minimal oxidation compared to HP spray mode. The present study has shown that it is possible to deposit pure SiC coating by suspension plasma spray (SPS) process and open a pathway for the development of ceramic materials which are prone to decomposition. Future research should focus on optimizing SPS parameters to achieve a uniform and dense pure SiC coatings with minimal decomposition. Moreover, more detailed microstructural studies are needed to assess the actual composition and crystalline/amorphous characteristics of the SiC-O deposited layers.

References

[1] J. Roy, S. Chandra, S. Das, and S. Maitra, “Oxidation behaviour of silicon carbide - A review,” in *Reviews on Advanced Materials Science*, 2014, vol. 38, no. 1, pp. 29–39, https://api.semanticscholar.org/CorpusID:44418440.

[2] R. Yanaoka, Y. Ichikawa, K. Ogawa, T. Masuda, and K. Sato, “Fundamental study of suspension plasma sprayed silicate coatings,” *Mater. Trans.*, vol. 61, no. 7, pp. 1390–1395, 2020, doi: 10.2320/matertrans.T-M2020826.

[3] A. Rincon Romero, A. Lynam, H. Memon, F. Venturi, and T. Hussain, “Development of Thermal Sprayed Silicon Carbide Coatings by an Innovative Suspension/Solution Precursors Approach,” in *Thermal Spray 2022: Proceedings from the International Thermal Spray Conference*, 2022, vol. 84369, pp. 268–271, doi: 10.31399/asm.cp.itsc2022p0268.

[4] A. Rincón, Z. Pala, and T. Hussain, “A suspension high velocity oxy-fuel thermal spray manufacturing route for silicon carbide – YAG composite coatings,” *Mater. Lett.*, vol. 281, p. 128601, 2020, doi: https://doi.org/10.1016/j.matlet.2020.128601.

[5] P. Stoyanov, K. M. Harrington, and A. Frye, “Insights into the Tribological Characteristic of Cu-Based Coatings Under Extreme Contact Conditions,” *Jom*, vol. 72, no. 6, pp. 2191–2197, 2020, doi: 10.1007/s11837-020-04087-7.

[6] S. N. Perevislov, M. A. Markov, Y. A. Kuznetsov, I. N. Kravchenko, and A. V Krasikov, “Study of Thermal Conductivity of Materials Based on Silicon Carbide and Silicon Nitride,” *Steel Transl.*, vol. 53, no. 9, pp. 752–760, 2023, doi: 10.3103/S0967091223090115.

[7] M. Tului, B. Giambi, S. Lionetti, G. Pulci, F. Sarasini, and T. Valente, “Silicon carbide based plasma sprayed coatings,” *Surf. Coatings Technol.*, vol. 207, pp. 182–189, 2012, doi: 10.1016/j.surfcoat.2012.06.062.

[8] F. Mubarok and N. Espallargas, “Tribological behaviour of thermally sprayed silicon carbide coatings,” *Tribol. Int.*, vol. 85, 2015, doi: 10.1016/j.triboint.2014.11.027.

[9] F. Mubarok and N. Espallargas, “Suspension Plasma Spraying of Sub-micron Silicon Carbide Composite Coatings,” *J. Therm. Spray Technol.*, vol. 24, 2015, doi: 10.1007/s11666-015-0242-2.

[10] H.-K. Kang and S. B. Kang, “Thermal decomposition of silicon carbide in a plasma-sprayed Cu/SiC composite deposit,” *Mater. Sci. Eng. A*, vol. 428, no. 1, pp. 336–345, 2006, doi: https://doi.org/10.1016/j.msea.2006.05.054.

[11] R. Arrabal, A. Pardo, M. C. Merino, M. Mohedano, P. Casajús, and S. Merino, “Al/SiC thermal spray coatings for corrosion protection of Mg–Al alloys in humid and saline environments,” *Surf. Coatings Technol.*, vol. 204, no. 16, pp. 2767–2774, 2010, doi: https://doi.org/10.1016/j.surfcoat.2010.02.030.

[12] A. R. Govande, A. Chandak, B. R. Sunil, and R. Dumpala, “Carbide-based thermal spray coatings: A review on performance characteristics and post-treatment,” *Int. J. Refract. Met. Hard Mater.*, vol. 103, p. 105772, 2022, doi: https://doi.org/10.1016/j.ijrmhm.2021.105772.

[13] S. Mahade, K. Narayan, S. Govindarajan, S. Bjorklund, N. Curry, and S. V Joshi, “Exploiting Suspension Plasma Spraying to Deposit Wear-Resistant Carbide Coatings,” *Materials (Basel).*,

vol. 12, 2019, doi: 10.3390/ma12152344.

[14] R. Rampon, O. Marchand, C. Filiatre, and G. Bertrand, “Influence of suspension characteristics on coatings microstructure obtained by suspension plasma spraying,” *Surf. Coatings Technol.*, vol. 202, no. 18, pp. 4337–4342, 2008, doi: https://doi.org/10.1016/j.surfcoat.2008.04.006.

[15] D. Zhou, O. Guillon, and R. Vaßen, “Development of YSZ Thermal Barrier Coatings Using Axial Suspension Plasma Spraying,” *Coatings*, vol. 7, no. 8, 2017, doi: 10.3390/coatings7080120.

[16] J. Oberste Berghaus, J.-G. Legoux, C. Moreau, F. Tarasi, and T. Chráska, “Mechanical and Thermal Transport Properties of Suspension Thermal-Sprayed Alumina-Zirconia Composite Coatings,” *J. Therm. Spray Technol.*, vol. 17, no. 1, pp. 91–104, 2008, doi: 10.1007/s11666-007-9146-0.

[17] E. Alebrahim, A. Akbarnozari, F. Ben Ettouil, and C. Moreau, “Tailoring the porosity level of the suspension plasma sprayed coatings using a dual suspension injection system,” *Surf. Coatings Technol.*, vol. 478, p. 130401, 2024, doi: https://doi.org/10.1016/j.surfcoat.2024.130401.

[18] P. Fauchais, M. Vardelle, S. Goutier, and A. Vardelle, “Specific Measurements of In-Flight Droplet and Particle Behavior and Coating Microstructure in Suspension and Solution Plasma Spraying,” *J. Therm. Spray Technol.*, vol. 24, no. 8, pp. 1498–1505, 2015, doi: 10.1007/s11666-015-0319-y.

[19] N. Curry, K. VanEvery, T. Snyder, J. Susnjar, and S. Bjorklund, “Performance Testing of Suspension Plasma Sprayed Thermal Barrier Coatings Produced with Varied Suspension Parameters,” *Coatings*, vol. 5, no. 3, pp. 338–356, 2015, doi: 10.3390/coatings5030338.

[20] A. Roy *et al.*, “Friction and wear behavior of suspension plasma sprayed tantalum oxide coatings at elevated temperatures,” *Surf. Coatings Technol.*, vol. 452, p. 129097, 2023, doi: https://doi.org/10.1016/j.surfcoat.2022.129097.

[21] P. Fauchais *et al.*, “Suspension and solution plasma spraying,” *J. Phys. D. Appl. Phys.*, vol. 46, no. 22, 2013, doi: 10.1088/0022-3727/46/22/224015.

[22] F. Arhami and F. Ben Ettouil, “As-Sprayed Highly Crystalline Yb2Si2O7 Environmental Barrier Coatings (EBCs) by Atmospheric Plasma Spray (APS),” *J. Therm. Spray Technol.*, vol. 32, 2023, doi: 10.1007/s11666-022-01526-6.

[23] Z. Tang, H. Kim, I. Yaroslavski, G. Masindo, Z. Celler, and D. Ellsworth, “Novel Thermal Barrier Coatings Produced by Axial Suspension Plasma Spray,” *Therm. Spray 2011 Proc. from Int. Therm. Spray Conf.*, vol. 83713, pp. 571–575, 2011, doi: 10.31399/asm.cp.itsc2011p0571.

[24] C.-J. Li and B. Sun, “Effects of spray parameters on the microstructure and property of Al2O3 coatings sprayed by a low power plasma torch with a novel hollow cathode,” *Thin Solid Films*, vol. 450, no. 2, pp. 282–289, 2004, doi: https://doi.org/10.1016/j.tsf.2003.11.166.

[25] R. Chidambaram Seshadri, G. Dwivedi, V. Viswanathan, and S. Sampath, “Characterizing Suspension Plasma Spray Coating Formation Dynamics through Curvature Measurements,” *J. Therm. Spray Technol.*, vol. 25, no. 8, pp. 1666–1683, 2016, doi: 10.1007/s11666-016-0460-2.

[26] V. Jalilvand *et al.*, “Study on the Formation of (Co,Ni)O Solid Solution and Metallic Ni Phases During Suspension Plasma Spraying of CoO and NiO Powders,” *J. Therm. Spray Technol.*, vol.

32, no. 4, pp. 1167–1181, 2023, doi: 10.1007/s11666-022-01505-x.

[27] P. Sokołowski, S. Kozerski, L. Pawłowski, and A. Ambroziak, "The key process parameters influencing formation of columnar microstructure in suspension plasma sprayed zirconia coatings," *Surf. Coatings Technol.*, vol. 260, pp. 97–106, 2014, doi: https://doi.org/10.1016/j.surfcoat.2014.08.078.

[28] Z. Zou *et al.*, "A comparative study on the performance of suspension plasma sprayed thermal barrier coatings with different bond coat systems," *Surf. Coatings Technol.*, vol. 275, pp. 276–282, 2015, doi: https://doi.org/10.1016/j.surfcoat.2015.05.006.

[29] X. Chen, S. Kuroda, T. Ohnuki, H. Araki, M. Watanabe, and Y. Sakka, "Effects of Processing Parameters on the Deposition of Yttria Partially Stabilized Zirconia Coating During Suspension Plasma Spray," *J. Am. Ceram. Soc.*, vol. 99, 2016, doi: 10.1111/jace.14393.

[30] Z. Hu *et al.*, "Structural Controlling of Highly-Oriented Polycrystal 3C-SiC Bulks via Halide CVD," *Materials (Basel).*, vol. 12, no. 3, 2019, doi: 10.3390/ma12030390.

[31] Y. Chen, B. Gou, X. Ding, J. Sun, and E. Salje, "Real-time Monitoring Dislocations, Martensitic Transformations and Detwinning in Stainless Steel: Statistical Analysis and Machine Learning," *J. Mater. Sci. Technol.*, vol. 92, 2021, doi: 10.1016/j.jmst.2021.04.003.

[32] F. Cherif, I. Baba Ahmed, A. Abderrahmane, and S. Hamzaoui, "Effect of pellet size and additive on silica carbothermic reduction in microwave furnace for solar grade silicon," *Mater. Sci.*, vol. 37, 2019, doi: 10.2478/msp-2019-0014.

[33] E. López-Honorato, P. J. Meadows, J. Tan, and P. Xiao, "Control of stoichiometry, microstructure, and mechanical properties in SiC coatings produced by fluidized bed chemical vapor deposition," *J. Mater. Res.*, vol. 23, pp. 1785–1796, 2008, doi: 10.1557/JMR.2008.0220.

[34] G. Mauer and R. Vaßen, "Coatings with Columnar Microstructures for Thermal Barrier Applications," *Adv. Eng. Mater.*, vol. 22, no. 6, p. 1900988, 2020, doi: https://doi.org/10.1002/adem.201900988.

[35] A. Ganvir, S. Joshi, N. Markocsan, and R. Vassen, "Tailoring columnar microstructure of axial suspension plasma sprayed TBCs for superior thermal shock performance," *Mater. Des.*, vol. 144, pp. 192–208, 2018, doi: https://doi.org/10.1016/j.matdes.2018.02.011.

[36] K. VanEvery *et al.*, "Column Formation in Suspension Plasma-Sprayed Coatings and Resultant Thermal Properties," *J. Therm. Spray Technol.*, vol. 20, no. 4, pp. 817–828, 2011, doi: 10.1007/s11666-011-9632-2.

[37] J. O. Berghaus, S. Bouaricha, J. G. Legoux, and C. Moreau, "Injection Conditions and In-Flight Particle States in Suspension Plasma Spraying of Alumina and Zirconia Nano-Ceramics," *Therm. Spray 2005 Proc. from Int. Therm. Spray Conf.*, 2005, https://api.semanticscholar.org/CorpusID:251963969.

[38] J. R. Davies, *Introduction to thermal spray processing*. ASM International, 2004.

[39] S. Matthews, "Development of high carbide dissolution/low carbon loss Cr3C2–NiCr coatings by shrouded plasma spraying," *Surf. Coatings Technol.*, vol. 258, pp. 886–900, 2014, doi: https://doi.org/10.1016/j.surfcoat.2014.07.062.

[40] G. Darut, F. Ben-Ettouil, A. Denoirjean, G. Montavon, H. Ageorges, and P. Fauchais, "Dry

Sliding Behavior of Sub-Micrometer-Sized Suspension Plasma Sprayed Ceramic Oxide Coatings," *J. Therm. Spray Technol.*, vol. 19, no. 1, pp. 275–285, 2010, doi: 10.1007/s11666-009-9415-1.

[41] S. Milan Shahana, S. R. Bakshi, and M. Kamaraj, *High-Temperature Oxidation and Hot Corrosion of Thermal Spray Coatings*. Springer Singapore, 2022.

[42] Y. Niu, W. Bao, D. Liu, X. Li, and Y. Liu, "Analysis of enthalpy and energy conversion efficiency in high-power inductively coupled plasma," *Vacuum*, vol. 225, p. 113220, 2024, doi: https://doi.org/10.1016/j.vacuum.2024.113220.

Chapter

5. CONCLUSIONS & FUTURE WORK

In this chapter…

The overall conclusions of the thesis have been summarized and proposed future work has been presented

5.1 Conclusions

Thermal spray coatings are cutting-edge surface engineering methods designed to improve the durability and performance of aerospace components. Several studies have explored the impact of various deposition techniques, such as plasma and combustion spraying, on the wear resistance of carbide-based coatings, particularly in elevated temperature applications. This thesis successfully demonstrates the deposition of chromium carbide (pure carbide and cemented carbide) and silicon carbide coatings. Moreover, the tribological properties of chromium carbide coatings were evaluated at room and elevated temperatures. The findings from each investigation are presented in detail in their respective chapters, with the overall conclusions summarized in this final chapter.

- Among the APS coatings, cemented chromium carbide (Cr_3C_2-25NiCr) coatings deposited by low plasma power demonstrated the lowest porosity content, highest thickness, highest deposition efficiency, and overall improved hardness properties. While HVAF Cr_3C_2-25NiCr coating deposited 4L4 nozzle is fully dense with low level of oxygen and porosity content.
- Although, the friction and wear volume loss of HVAF Cr_3C_2-25NiCr (4L4) coating increased when exposed to high temperatures (i.e. 450°C), it exhibits the lowest CoF and wear volume loss at room and elevated temperatures compared to other tested coatings. The formation of stable and uniform tribofilm-layer at the sliding interface helps in reducing the coefficient of friction and protecting the surface from significant wear damage.
- The worn surface of the HVAF Cr_3C_2-25NiCr (4L4) coating at room temperature exhibited features such as plastically deformed carbides, a smeared layer, and wear pits containing loose debris, indicating that abrasive wear was the dominant mechanism. Whereas at 450°C, the worn surface revealed adhered materials and wear debris, suggesting that oxidative wear, with contributions from both adhesive and abrasive wear, governed the wear mechanism at elevated temperatures.
- Silicon carbide coatings deposited with low power exhibit a bumpy microstructure, whereas the high power sprayed SiC coating show a feathery columnar structure. The microstructural features of both coatings are strongly affected by the size of the suspension droplets and the plasma drag forces acting on them during deposition.
- The low power spray SiC coating demonstrated high coating thickness, low oxide content, and minimal porosity than the high plasma power coating. The low oxide content in low power SiC coating is associated with the lower thermal energy in low plasma power system, ensuring that particles are adequately melted without undergoing significant oxidation or decomposition.

5.2 Future work

1. While the present study has shown that APS can produce chromium carbide (Cr_3C_2-25NiCr) coatings with lower porosity and higher hardness, further research should explore a broader range of deposition parameters. Specifically, varying the plasma power, feedstock particle size, and nozzle design to optimize coating properties for tribological applications at elevated operating conditions.
2. The friction and wear behavior of HVAF Cr_3C_2-25NiCr (4L4) coatings at elevated temperatures (450°C) suggests that while these coatings perform well at room temperature, they are susceptible to wear at higher temperatures. Future work should focus on improving the high-temperature wear resistance by modifying the HVAF parameters to further enhance oxidation and thermal stability.
3. The microstructural features observed in the SiC coatings-bumpy microstructure in low-power coating and feathery columnar structure in high-power coating, suggest that further research is desirable. Therefore, future work should focus on optimizing SPS parameters such as adjusting the plasma power, suspension feed rate, and varying the feedstock particle sizes to achieve a uniform and dense pure SiC coatings with minimal decomposition. Moreover, more detailed microstructural studies are needed to assess the actual composition and crystalline/amorphous characteristics of the SiC-O deposited layers.
4. Also, advanced *ex-situ* methods such as transmission electron microscopy (TEM) or X-ray photoelectron spectroscopy (XPS) should be utilized for the worn surfaces analysis to understand the surface state wear mechanisms.